Eur. Phys. J. C (2016) 76:516
DOI 10.1140/epjc/s10052-016-4349-5

THE EUROPEAN PHYSICAL JOURNAL C

Special Article - Tools for Experiment and Theory

Precision tools and models to narrow in on the 750 GeV diphoton resonance

Florian Staub[1,a], **Peter Athron**[2,b], **Lorenzo Basso**[3,c], **Mark D. Goodsell**[4,d], **Dylan Harries**[5,e], **Manuel E. Krauss**[6,f], **Kilian Nickel**[6,g], **Toby Opferkuch**[6,h], **Lorenzo Ubaldi**[7,i], **Avelino Vicente**[8,j], **Alexander Voigt**[9,k]

[1] Theoretical Physics Department, CERN, Geneva, Switzerland
[2] ARC Centre of Excellence for Particle Physics at the Terascale, School of Physics, Monash University, Melbourne, VIC 3800, Australia
[3] CPPM, Aix-Marseille Université, CNRS-IN2P3, UMR 7346, 163 avenue de Luminy, 13288 Marseille Cedex 9, France
[4] LPTHE, UMR 7589, CNRS and Université Pierre et Marie Curie, Sorbonne Universités, 75252 Paris Cedex 05, France
[5] Department of Physics, ARC Centre of Excellence for Particle Physics at the Terascale, The University of Adelaide, Adelaide, SA 5005, Australia
[6] Bethe Center for Theoretical Physics and Physikalisches Institut der Universität Bonn, Nussallee 12, 53115 Bonn, Germany
[7] Raymond and Beverly Sackler School of Physics and Astronomy, Tel-Aviv University, 69978 Tel Aviv, Israel
[8] Instituto de Física Corpuscular (CSIC-Universitat de València), Apdo. 22085, 46071 Valencia, Spain
[9] Deutsches Elektronen-Synchrotron DESY, 22607 Hamburg, Germany

Received: 18 May 2016 / Accepted: 29 August 2016

Abstract The hints for a new resonance at 750 GeV from ATLAS and CMS have triggered a significant amount of attention. Since the simplest extensions of the standard model cannot accommodate the observation, many alternatives have been considered to explain the excess. Here we focus on several proposed renormalisable weakly-coupled models and revisit results given in the literature. We point out that physically important subtleties are often missed or neglected. To facilitate the study of the excess we have created a collection of 40 model files, selected from recent literature, for the `Mathematica` package `SARAH`. With `SARAH` one can generate files to perform numerical studies using the tailor-made spectrum generators `FlexibleSUSY` and `SPheno`. These have been extended to automatically include crucial higher order corrections to the diphoton and digluon decay rates for both CP-even and CP-odd scalars. Additionally, we have extended the `UFO` and `CalcHep` interfaces of `SARAH`, to pass the precise information about the effective vertices from the spectrum generator to a Monte-Carlo tool. Finally, as an example to demonstrate the power of the entire setup, we present a new supersymmetric model that accommodates the diphoton excess, explicitly demonstrating how a large width can be obtained. We explicitly show several steps in detail to elucidate the use of these public tools in the precision study of this model.

[a] e-mail: florian.staub@cern.ch
[b] e-mail: peter.athron@coepp.org.au
[c] e-mail: basso@cppm.in2p3.fr
[d] e-mail: goodsell@lpthe.jussieu.fr
[e] e-mail: dylan.harries@adelaide.edu.au
[f] e-mail: mkrauss@th.physik.uni-bonn.de
[g] e-mail: nickel@th.physik.uni-bonn.de
[h] e-mail: toby@th.physik.uni-bonn.de
[i] e-mail: ubaldi.physics@gmail.com
[j] e-mail: avelino.vicente@ific.uv.es
[k] e-mail: alexander.voigt@desy.de

Contents

Published online: 23 September 2016

1 Introduction

The first data from the 13 TeV run of the large hadron collider (LHC) contained a surprise: ATLAS and CMS reported a resonance at about 750 GeV in the diphoton channel with local significances of 3.9σ and 2.6σ, respectively [1,2]. When including the look-elsewhere-effect, the deviations from standard model (SM) expectations drop to 2.3σ and 1.2σ.[1]

This possible signal caused a lot of excitement, as it is the largest deviation from the SM which has been seen by both experiments. This in turn led to an avalanche of papers, released very quickly, which analysed the excess from various perspectives [5–359].

It is hard to explain the excess within the most commonly considered frameworks for physics beyond the standard model (BSM), like two-Higgs-doublet models (THDM) or the minimal supersymmetric standard model (MSSM) [360], to mention a couple of well-known examples. Thus, many alternative ideas for BSM models have been considered, some of which lack a deep theoretical motivation and are rather aimed at just providing a decent fit to the diphoton bump. Most of the papers in the avalanche were written quickly, some in a few hours, many in a few days, so the analyses of the new models are likely to have shortcomings. Some effects could be missed in the first attempt and some statements might not hold at a second glance. Indeed we have found a wide range of mistakes or unjustified assumptions, which represented the main motivation that prompted this work.

Now that the dust has settled following the stampede caused by the presentation of the ATLAS and CMS data, the time has come for a more detailed and careful study of the proposed ideas. In the past few years several tools have been developed which can be very helpful in this respect. In the context of renormalisable models, the Mathematica package SARAH [361–366] offers all features for the precise study of a new model: it calculates all tree-level properties of the model (mass, tadpoles, vertices), the one-loop corrections to all masses as well as the two-loop renormalisation group equations, and it can be interfaced with the spectrum generators SPheno [367,368] and FlexibleSUSY [369]. These codes, in turn, can be used for a numerical analysis of any model, which can compete with the precision of state-of-the-art spectrum generators dedicated just to the MSSM and NMSSM [370]. The RGEs are solved numerically at the two-loop level and the mass spectrum is calculated at one loop. Both codes have the option to include the known two-loop corrections [371–376] to the Higgs masses in the MSSM and NMSSM, which may, depending on the model,

[1] We note, however, that the most recent measurements including data collected in 2016 do not confirm the excess [3,4].

provide a good approximation of the dominant corrections. SPheno can also calculate the full two-loop corrections to the Higgs masses in the gaugeless limit at zero external momentum [377,378]. FlexibleSUSY has an extension to calculate the two-loop Higgs mass corrections using the complementary effective field theory approach, which is to be released very soon. SPheno makes predictions for important flavour observables, which have been not yet implemented in FlexibleSUSY. Of particular importance for the current study is that SPheno and FlexibleSUSY calculate the effective vertices for the diphoton and digluon couplings of the scalars, which can then be used by Monte-Carlo (MC) tools like CalcHep [379,380] or MadGraph [381,382]. Other numerical tools like MicrOmegas [383], HiggsBounds [384,385], HiggsSignals [386] or Vevacious [387] can easily be included in the framework.

These powerful packages provide a way to get a thorough understanding of the new models. The main goal of this work is to support the model builders and encourage them to use these tools. We provide several details about the features of the packages in the spirit of making this paper self-contained and bringing the reader unfamiliar with the tools to the level of knowledge necessary to use them. More information can be found in the manuals of each package. We have created a database of diphoton models in SARAH, by implementing 40 among those proposed in recent literature, which is now available to all interested researchers. For each model we have written model files to interface SARAH with SPheno and FlexibleSUSY.

Although in each case we have tried to check very carefully that we implement the model which has been proposed in the literature, it is of course possible that some details have been missed. The original authors of these models are encouraged to check the implementation themselves to satisfy that what we have implemented really does correspond to the model they proposed. In the description of some of the models we state cases where the model has problems or where we find difficulties for the proposed solution. This helps inform potential users about what they may see when running these models through the tools we are discussing here. *However especially in these cases we encourage the original authors to check what we have written and let us know if they disagree with any claim we make.*

The aim of this paper is to give a self-consistent picture of how – and why – the diphoton excess can be studied with the above mentioned public tools and the provided model files. For this purpose, we do not only summarise the implementation and validation of the models, but we also give a short introduction to the tools and explain their basic usage. In addition, we present the example of an $U(1)$ extended model and how this can be studied in all detail. This should enable the interested reader to directly make use of these powerful packages without the need to consult other references or manuals. However, before we start we also summarise common shortcomings of too simplified analyses and emphasise how they are easily avoided by using the tools. This provides the main motivation of this paper and we hope that other model builders will also see the necessity of using these packages. Of course, we do not intend to present a thorough study of all the models which we have implemented. However, we comment on some observations concerning the motivation or validity of a model regarding the diphoton excess which came to our mind during the implementation.

This paper is long but modular, and each section is to a large extent self contained, so the reader can easily jump to the section of greater interest. We have structured it as follows:

- In Sect. 2, we give a list of common mistakes we have found in the literature.
- In Sect. 3, we discuss at some length the implementation of the diphoton and digluon effective vertices.
- In Sect. 4, we give an overview of the models which we have implemented in SARAH.
- In Sect. 5, we provide an explicit example of how to quickly work out the details of a model, analytically with SARAH and numerically with the other tools. For this purpose we extended a natural supersymmetric (SUSY) model to accommodate the 750 GeV resonance.
- We conclude in Sect. 6.

2 Motivation

Precision studies in high energy physics have reached a high level of automation. There are publicly available tools to perform Monte-Carlo studies at LO or NLO [388–393], many spectrum generators [367,368,394–405] for the calculation of pole masses including important higher order corrections, codes dedicated only to Higgs [406–409] or sparticle decays [410–412], and codes to check flavour [413–417] or other precision observables [418]. This machinery has been used in the past mainly for detailed studies of some promising BSM candidates, like the MSSM, NMSSM or variants of THDMs. There are two main reasons why these tools are usually the preferred method to study these models: (i) it has been shown that there can be large differences between the exact numerical results and the analytic approximations; (ii) writing private routines for specific calculations is not only time consuming but also error prone. On the other hand, the number of tools available to study the new ideas proposed to explain the diphoton excess is still limited. Of these tools, many are not yet widely used largely due to the community's reluctance in adopting new codes. However, we think it is beneficial to adopt this new generation of generic tools like SARAH.

We noticed that several studies done in the context of the 750 GeV excess have overlooked important subtleties in some models, neglected important higher order corrections, or made many simplifying assumptions which are difficult to justify. Using generic software tools in this context can help address these issues: many simplifications will no longer be necessary and important higher order corrections can be taken into account in a consistent manner. In order to illustrate this we comment, in the following subsections, on several issues we became aware of when revisiting some of the results in the literature.

2.1 Calculation of the diphoton and digluon widths

2.1.1 The diphoton and digluon rates beyond leading order

A precise calculation of the diphoton rate is of crucial importance. In the validation process of this work, we identified several results in the literature that deviate, often by an order of magnitude or more, in comparison to our results [106,304,336]. Additionally we observed that in many cases there are important subtleties which we think are highly relevant.

First of all, the choice of the renormalisation scale of the running couplings appearing in the calculation. The majority of recent studies use the electromagnetic coupling at the scale of the decaying particle. However, one should rather use $\alpha_{em}(0)$, i.e. the Thompson limit (see for instance Refs. [419,420]), in order to keep the NLO corrections under control. Taking this into account already amounts to an $\mathcal{O}(10\,\%)$ change of the diphoton rate compared to many studies in the literature. In addition, as we will discuss in Sect. 2.2.3, an important prediction of a model is the ratio $\mathrm{Br}(S \to gg)/\mathrm{Br}(S \to \gamma\gamma)$, where S is the 750 GeV scalar resonance. It is well known that the digluon channel receives large QCD corrections. If one neglects these corrections the ratio will be severely underestimated.

To demonstrate these effects we show in Fig. 1 the total decay width[2] of the singlet S as a function of the mass M_{F_1} and coupling Y_{F_1} for a simple toy model containing only the vector-like fermions Ψ_{F_1} as presented in Ref. [276]. Table 1 contains benchmark points for the partial widths of the digluon and diphoton channels as well as the ratio of these two channels for both CP-even and CP-odd scalar resonances. This table contains the LO calculations performed using `SPheno` as a comparison to results previously shown in the literature [276]. We also show the partial widths including NLO corrections for the diphoton channel[3] and N^{3}LO QCD corrections to the gluon fusion production as implemented in Sect. 3.5. The discrepancies between the LO calculations arise purely through the choice of the renormalisation scale for the gauge couplings. However, the NLO results clearly emphasise that loop corrections at the considered mass scales are the dominant source of errors. To our knowledge, these uncertainties have thus far not received a sufficiently careful treatment in the literature; we give further discussion of this (and the remaining uncertainty in the `SARAH` calculation) in Sect. 3.7.

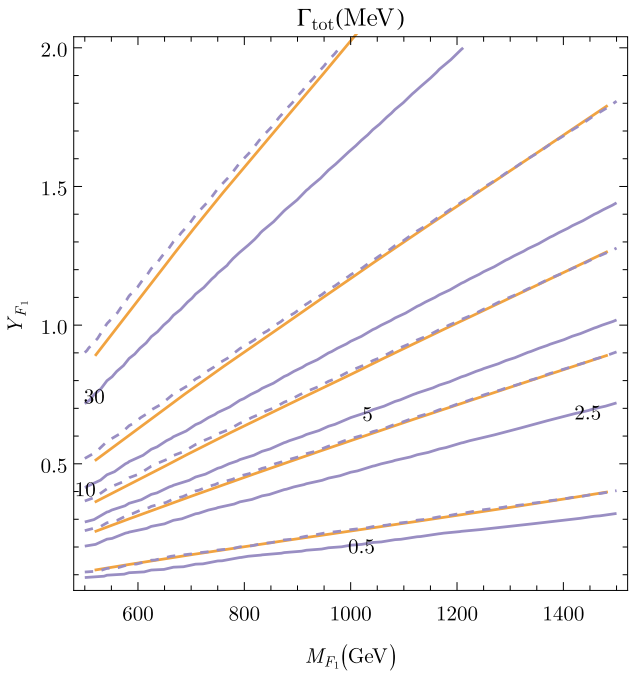

Fig. 1 The approximate total width (sum of the diphoton and digluon channels) of S as a function of the coupling Y_{F_1} and the mass m_{F_1} of the vector-like particle F_1, calculated using `SPheno` (*blue*) at LO (*dashed*) and NLO (*solid*). The *orange contours* are the results of the LO calculation from Ref. [276]. Here we assume a single generation of vector-like quarks

2.1.2 Constraints on a large diphoton width

In order to explain the measured signal, one needs a large diphoton rate of $\Gamma(S \to \gamma\gamma)/M_S \simeq 10^{-6}$ assuming a narrow width for S, while for a large width one requires $\Gamma(S \to \gamma\gamma)/M_S \simeq 10^{-4}$ [192]. In weakly-coupled models there are three different possibilities to obtain such a large width:

1. Assuming a large Yukawa-like coupling between the resonance and charged fermions

[2] Here, the total width is simply the sum of the diphoton and digluon channels ignoring small contributions from other sub-dominant channels.

[3] NLO corrections in the case of a CP-odd vanish in the limit $m_f \gg m_S$, see Sect. 3.5 for more detail.

Table 1 Branching fraction ratio, as well as the partial decay widths for the digluon and diphoton channels for a toy model containing only the relevant vector-like fermion pair Ψ_{F_i}. The above values are for the benchmark points $Y_{F_i} = 1$ and $m_{F_i} = 1$ TeV, where the values are for a CP-even/CP-odd scalar resonance, respectively. The SPheno NLO calculation includes N^{3}LO corrections for the digluon channel, while the diphoton decay width is calculated at NLO and LO for a CP-even and odd scalar respectively

Model	Br $(gg/\gamma\gamma)$	$\Gamma_{S\to gg}$ (MeV)	$\Gamma_{S\to\gamma\gamma}$ (MeV)
Ψ_{F_1}			
Ref. [276] LO	11.62/–	6.74/–	0.58/–
SPheno LO	13.47/12.22	6.78/14.27	0.50/1.17
SPheno NLO	23.27/20.27	11.04/23.71	0.47/1.17
Ψ_{F_2}			
Ref. [276] LO	24.42/–	15.14/–	0.62/–
SPheno LO	28.32/25.70	15.26/32.12	0.54/1.25
SPheno NLO	48.93/42.67	24.85/52.34	0.51/1.25
Ψ_{F_3}			
Ref. [276] LO	33.80/–	6.76/–	0.20/–
SPheno LO	39.20/35.56	6.78/14.27	0.17/0.40
SPheno NLO	67.72/59.06	11.04/23.71	0.16/0.40
Ψ_{F_4}			
Ref. [276] LO	49.84/–	14.95/–	0.30/–
SPheno LO	57.80/52.44	15.26/32.12	0.26/0.61
SPheno NLO	99.85/87.09	24.85/53.34	0.25/0.61
Ψ_{F_5}			
Ref. [276] LO	150.0/–	1.50/–	10.0×10^{-3}/–
SPheno LO	177.0/160.6	1.70/3.57	9.58×10^{-3}/22.22×10^{-3}
SPheno NLO	305.8/266.7	2.76/5.93	9.03×10^{-3}/22.22×10^{-3}
Ψ_{F_6}			
Ref. [276] LO	390.0/–	7.80/–	2.00×10^{-2}/–
SPheno LO	453.2/411.1	6.78/14.27	1.50×10^{-2}/3.47×10^{-2}
SPheno NLO	782.8/682.8	11.04/23.71	1.41×10^{-2}/3.47×10^{-2}

2. Assuming a large cubic coupling between the resonance and charged scalars
3. Using a large multiplicity and/or a large electric charge for the scalars and/or fermions in the loop

However, all three possibilities are also constrained by very fundamental considerations, which we briefly summarise in the following.

2.1.2.1 Large couplings to fermions A common idea to explain the diphoton excess is the presence of vector-like states which enhance the loop-induced coupling of a neutral scalar to two photons or two gluons. This led some authors to consider Yukawa-like couplings of the scalar to the vector-like fermions larger than $\sqrt{4\pi}$, which is clearly beyond the perturbative regime.[4] Nevertheless, a one-loop calculation is used in these analyses to obtain predictions for the partial widths [353], despite being in a non-perturbative region of parameter space.

[4] This diphoton excess could be triggered by strong interactions. Of course, in this case one cannot use perturbative methods to understand it.

Moreover, even if the couplings are chosen to be within the perturbative regime at the scale $Q = 750$ GeV, they can quickly grow at higher energies. This issue of a Landau pole has been already discussed to some extent in the literature [40,68,192,212,343,346], and one should ensure that the model does not break down at unrealistic small scales.

2.1.2.2 Large couplings to scalars One possibility to circumvent large Yukawa couplings is to introduce charged scalars, which give large loop contributions to the diphoton/digluon decay. A large cubic coupling between the charged scalar and the 750 GeV one does not lead to a Landau pole for the dimensionless couplings because of dimensional reasons. However, it is known that large cubic couplings can destabilise the scalar potential: if they are too large, the electroweak vacuum could tunnel into a deeper vacuum where $U(1)_{\rm em}$ gauge invariance is spontaneously broken, depending on the considered scenario. The simplest example with such a scenario is the SM, extended by a real scalar S and a complex scalar X with hypercharge Y. The scalar potential of this example is

$$V \supset \kappa\, S|X|^2 + \frac{1}{2}M_S S^2 + M_X|X|^2 + \cdots . \tag{2.1}$$

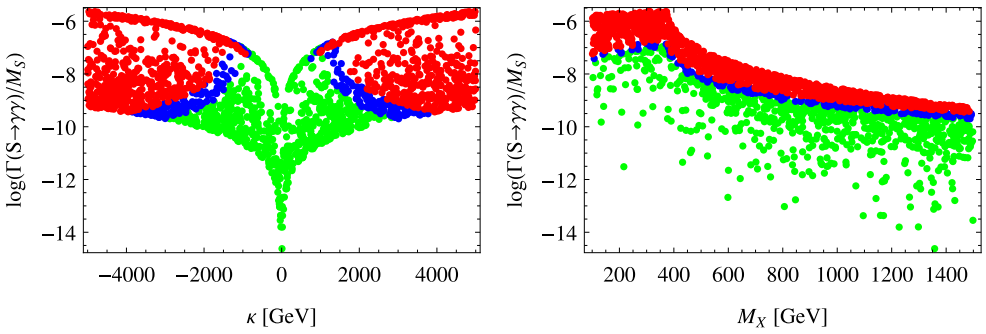

Fig. 2 $\Gamma(S \to \gamma\gamma)/M_S$ as a function of κ (*left*) and M_X (*right*). *Green points* have a stable vacuum, *blue points* have a meta-stable but long-lived vacuum, while for the *red* ones it decays in a short time, in comparison to cosmological time scales, with a survival probability below 10 %. The hypercharge of X was set to $Y = 1$

In Fig. 2 the dependence of the diphoton partial width as a function of κ and M_X is shown, and the stability of the electroweak potential as well as the life-time of its ground state is checked with `Vevacious` and `CosmoTransitions`. For more details about vacuum stability in the presence of large scalar cubic terms, we refer to Ref. [343]. The overall conclusion of [343] is that the maximal possible diphoton width, even when allowing for a meta-stable but sufficiently long-lived electroweak vacuum, is not much larger than in the case of vector-like fermions when requiring that the model is perturbative up to the Planck scale. It is therefore essential to perform these checks when studying a model that predicts large cubic scalar couplings. An example of the importance of these checks is demonstrated in Ref. [176]. Here it is shown that vacuum stability demands rule out an explanation in the constrained MSSM, proposed in Ref. [120], where the diphoton signal is produced through stop bound states. Moreover, vacuum stability also places stringent constraints on the pMSSM explanation of the excess [171]. Thus far no valid parameter point has been found which is in agreement with both the diphoton rate and vacuum stability constraints. Similar issues were observed in models with trilinear R-parity violation [12,165] which are disfavoured by these constraints and might work only in very fine-tuned parameter regions.

2.1.2.3 Large multiplicities To circumvent large Yukawa or cubic couplings, other models require a large number of generations of new BSM fields and/or large electric charges. As a consequence the running of the $U(1)_Y$ gauge coupling, g_1, gets strongly enhanced well below the Planck scale. Moreover, even before reaching the Landau pole, the model develops large (eventually non-perturbative) gauge couplings. This implies an enhancement of Drell–Yan processes at the LHC, with current data already setting stringent constraints and potentially excluding some of the models proposed to explain the diphoton excess [216,421]. For general studies on running effects in the context of the diphoton excess see [40,68,192,212,346]. We briefly discuss dramatic examples of this class of models proposed in Refs. [264] and

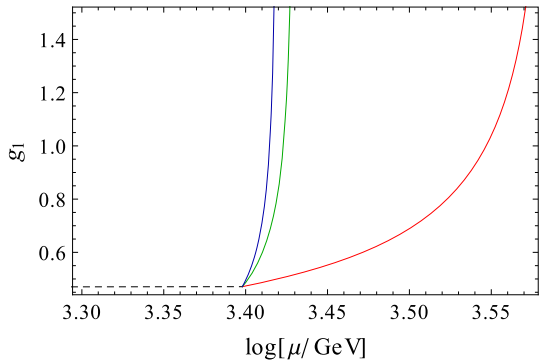

Fig. 3 Running of the $U(1)_Y$ gauge coupling, g_1, in the model presented in [325] for $N_k = 1000$ (*red*), $N_k = 6000$ (*green*) and $N_k = 9000$ (*blue*). The *black dashed line* corresponds to the SM running below $\mu_{NP} = 2.5$ TeV

[325], which feature approximately ∼100 and 6000–9000 generations of doubly-charged scalar fields respectively. In the model of Ref. [325] the SM particle content is enlarged by a vector-like doubly-charged fermion E, a Majorana fermion N_R, a singlet scalar S, a singly-charged scalar h^+ and N_k generations of the doubly-charged scalar field k^{++}. At the one-loop level the running of g_1 is governed by the renormalisation group equation (RGE)

$$\frac{dg_1}{dt} = \beta_{g_1} = \frac{1}{16\pi^2}\beta^{(1)}_{g_1}, \tag{2.2}$$

where $t = \log \mu$, μ being the renormalisation scale, and

$$\beta^{(1)}_{g_1} = \frac{g_1^3}{10}\,(75 + 8\,N_k) \tag{2.3}$$

is the one-loop β function. It is clear from Eq. 2.3 that a large value of N_k necessarily leads to a very steep increase of g_1 with the renormalisation scale, soon reaching a Landau pole. This is shown in Fig. 3, obtained by setting the masses of all the charged BSM states to $\mu_{\rm NP} = 2.5$ TeV, which is already the largest mass considered in this analysis. The

Table 2 Energy scale at which a Landau pole in g_1 appears as a function of N_k in the model of Ref. [325]

N_k	μ_{Landau}
10	2×10^{13} GeV
100	1.2×10^5 GeV
1000	3.8 TeV
6000	2.7 TeV
9000	2.6 TeV

running up to μ_{NP} is governed by the SM RGEs, and the result for g_1 is displayed with a black dashed line. For scales above $\mu_{\text{NP}} = 2.5$ TeV, the contributions from BSM fields become effective. Figure 3 shows that a Landau pole can be reached at relatively low energies once we allow for such large values of N_k. In fact, for $N_k = 9000$, we find that a Landau pole appears already at $\mu \simeq 2.6$ TeV. In this specific example the appearance of a Landau pole below 10^{16} GeV is unavoidable as soon as $N_k > 10$, as shown in Table 2.

2.1.3 How do the tools help?

The tools which we describe in more detail in the following sections can help to address all the above issues:

1. `FlexibleSUSY` and `SPheno` can calculate the diphoton and digluon rate including important higher order corrections.
2. Using the effective vertices calculated by `FlexibleSUSY/SPheno` and the interface to `CalcHep` or `MadGraph`, the gluon-fusion production cross-section of the 750 GeV mediator can be calculated numerically and one does not have to rely on analytical (and sometimes erroneous[5]) approximations.
3. `SARAH` calculates the RGEs for a model which can be used to check for the presence of Landau pole.
4. `Vevacious` can be used to check the stability of the scalar potential.

2.2 Properties of the 750 GeV scalar

2.2.1 Mixing with the SM Higgs

It is often assumed that S, although it is a CP-even scalar, does not mix with the SM-like Higgs h. However, if this is done in a very ad hoc way and not motivated by any symmetry, this assumption will not hold when radiative corrections are taken into account. To see this, one can consider, for example, the scalar potential

$$V = \frac{1}{2} M_S S^2 + M_X |X|^2 + \mu^2 |H|^2 + \kappa S |X|^2 + \lambda_S S^4 + \lambda_{SX} S^2 X^2 + \lambda_{HX} |H|^2 |X|^2 + \lambda |H|^4, \quad (2.4)$$

where H is the SM Higgs $SU(2)_L$ doublet, which contains the SM Higgs h. This potential in principle has all ingredients to get a large diphoton decay of S via a loop involving the charged scalar X. Note, however, that the potentially dangerous term $\kappa_H\, S|H|^2$ has been omitted. One can see immediately that this term would be generated radiatively by the diagram below.

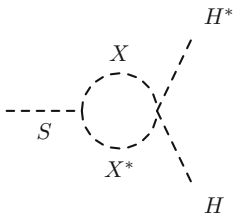

Note that it is also not possible to circumvent this decay by forbidding the λ_{HX} term: since H and X are charged under $SU(2)_L \times U(1)_Y$, also the $\lambda_{HX}|H|^2|X|^2$ term would be generated radiatively via diagrams like

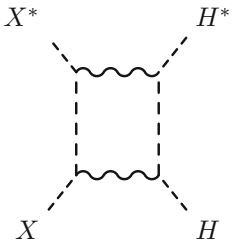

A mixing between the singlet and SM-like Higgs state has important consequences, since the mass eigenstate state would have additional tree level couplings to W and Z from the SM Higgs component. For a singlet dominated mass eigenstate, s, this would open up the decay channels $s \to hh$ and $s \to ZZ$, $s \to W^+W^-$, which are tightly constrained.

Another possibility is that all terms allowed by symmetries are taken into account, but very special relations among them are imposed like in Ref. [313]. When these relations hold, the above-mentioned tree-level decays in SM particles would cancel. However, as long as there is no symmetry behind these relations, they will not be invariant under RGE running. Therefore, immediately the question arises how large the tuning among the parameters must be to have a point that fulfils all constraints. To illustrate this issue, we make small variations in the couplings λ_{H3} and λ_{36},[6] which cause

[5] It is straightforward to see that the analytical estimate of the production cross section in Eq. (10) of Ref. [336] is wrong by orders of magnitude: consider the production of a SM-like scalar H with $m_H = 750$ GeV via top-loops. Then, the factor $h_F^2 m_t^2 / m_F^2$ drops out and one obtains $\sigma = 1440$ pb which is too large by roughly three orders of magnitude [422]. The authors of Ref. [304] (which originally made use of this analytic estimate) have revised their results in an updated version of their paper.

[6] This model assumes the 750 GeV boson to be a linear combination of two scalar fields χ_3 and χ_6. The quoted couplings arise in the scalar

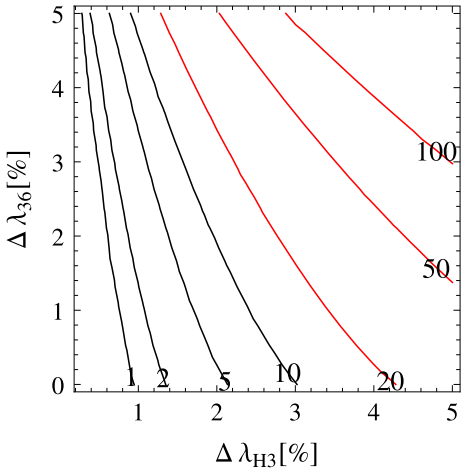

Fig. 4 The impact on small deviations from the parameter relations assumed in Ref. [313]. Specifically, the y-axis axis represents the deviation in the coupling λ_{36}, while the x-axis represents deviations in the coupling λ_{H3}. The *contour lines* show the ratio $\mathrm{Br}(S \to W^+W^-)/\mathrm{Br}(S \to \gamma\gamma)$. The *red line* indicates where the model would already be in conflict with current collider limits

non-vanishing tree-level couplings between S and the massive vector bosons, and check for which size of the deviations the condition $\mathrm{Br}(S \to W^+W^-)/\mathrm{Br}(S \to \gamma\gamma) < 20$ holds. The result is shown in Fig. 4. Here, the diphoton rate was maximised by setting the masses of the vector-like fields to 375 GeV and using a Yukawa coupling of $O(1)$. In principle, one could try to check what this means for the scale dependence of these ratios by calculating the RGEs. However, this cannot really be done for this setup since one obtains the following condition from the relations which have been imposed: $\lambda_{H3} = f_Y^2 \frac{M_S^2}{M_F^2}$, i.e. $\lambda_{H3} = 4 f_Y^2$ is needed to maximise the diphoton branching ratio. Thus, f_Y of $\mathcal{O}(1)$ immediately leads to a huge quartic coupling.

Thus, in general, it is very difficult to justify the assumption that the 750 GeV particles do not mix with the SM-like Higgs if there is no fundamental symmetry to forbid this mixing. However, this can already be forbidden using the CP symmetry: the mentioned problems can be circumvented in models where the diphoton excess stems from a CP-odd particle. In the case of a CP-even particle, it is crucial to include the mixing effects and to check at least how large the tuning in parameters must be.

2.2.2 To VEV or not to VEV?

The possibility that the new scalar receives a vacuum expectation value (VEV) is also often neglected. However, as we have just discussed, it often occurs that a H–S mixing will be induced, at least radiatively, in many models. Such radiative effects would immediately lead to a non-zero VEV for the new scalar. Even in cases where there is a symmetry which prevents a mixing with the SM Higgs, the 750 GeV particle will still receive a VEV if it is a CP-even scalar. This arises due to the introduced couplings to charged particles which are necessary to allow diphoton and digluon decays. More specifically, these introduced couplings will generate one-loop tadpole diagrams for S as shown in Fig. 5. Thus, the tadpole equation reads at the one-loop level

Fig. 5 Tadpole terms for S generated at one-loop level

$$\frac{\partial V^{(1L)}}{\partial v_S} = T^{(1L)} = T^{(T)} + \delta T = 0, \tag{2.5}$$

where $T^{(T)}$ is the tree-level tadpole, given by

$$\frac{\partial V^{(T)}}{\partial v_S} = T^{(T)} = c_1 v_S + c_2 v_S^2 + c_3 v_S^3 = 0. \tag{2.6}$$

Here, we have parametrised the tree-level expression so that the general form has the solution $v_S = 0$. One finds in general that the one-loop corrections are

$$\delta T = \begin{cases} \kappa A(M_X^2) & \text{for a scalar loop,} \\ 2Y M_\Psi A(M_\Psi^2) & \text{for a fermion loop,} \end{cases} \tag{2.7}$$

with $A(x^2) = \frac{1}{16\pi^2} x^2 [1 + \log(Q^2/x^2)]$. Taking M_Ψ, κ, M_X of the order 1 TeV, results in a VEV which is naturally of order $1\,\mathrm{TeV}^3/(16\pi^2 c_1)$. As a result, the simplifying assumption that v_S vanishes is in general hard to justify – apart from the rare case in which S is a complete singlet under all local and global symmetries; under this circumstance the VEV can always be rotated away. Therefore, it is important to check how the conclusions made about the model depend on this assumption. Here, the tools discussed in the following sections can really help, as including the non-vanishing v_S is no more difficult than assuming the VEV vanishes.

2.2.3 Additional decay channels

Many analyses concentrate only on the decay $S \to \gamma\gamma$ and completely neglect other potential decay channels. However,

potential as $\lambda_{H3}|\chi_3|^2|H|^2 + \lambda_{36}|\chi_3|^2|\chi_6|^2$, with H being the usual Higgs doublet. The couplings of χ_3 to vector-like quarks are given by the Yukawa couplings f_Y and f_X.

Table 3 Limits on $\Gamma(S \to X)/\Gamma(S \to \gamma\gamma)$ assuming a production of S via gluon fusion or heavy quarks. Values are taken from Ref. [192]

$e^+e^- + \mu^+\mu^-$	$\tau^+\tau^-$	$Z\gamma$	ZZ	Zh	hh	W^+W^-	$t\bar{t}$	$b\bar{b}$	jj	Inv.
0.6	6	6	6	10	20	20	300	500	1300	400

there are stringent constraints on the branching ratios of S into other SM final states, which are summarised in Table 3.

Thus, any model which tries to explain the excess via additional coloured states in the loop must necessarily worry about limits from dijet searches [423]. Therefore, an accurate calculation of the digluon decay rate is a necessity. As an example that illustrates why both additional channels and the diphoton/digluon width calculation are important we consider the model presented in Refs. [89,166] and considered in more detail here in Sect. 4.2.1.

This model extends the SM with a singlet and a scalar $SU(2)$-doublet colour octet. As an approximation the ratio of the singlet decays to gluons and to photons is

$$\frac{\Gamma(S \to gg)}{\Gamma(S \to \gamma\gamma)} \simeq \frac{9}{2}\frac{\alpha_s^2}{\alpha^2}. \tag{2.8}$$

In [89] this is quoted as $\simeq$750; before any NLO corrections are applied, we find 700. However, once we include all of the N^{3}LO corrections this is enhanced to 1150, near the bound for constraints on dijet production at 8 TeV and significantly squeezing the parameter space of the model.

Additionally in many works we observed that potential decay channels of the resonance were missed. For instance in Ref. [184], the authors, who considered the Georgi-Machacek model [424], missed the decay of the scalar into $W^\pm H^\mp$, which can be the dominant mode when kinematically allowed.

2.2.4 How do the tools help?

Many of the assumptions which we criticised were made to keep the study simple. However, when using the public tools presented in the next two section, there is no need for these simplifying assumptions:

1. `SARAH` automatically calculates all expressions for the masses and vertices in any renormalisable model, no matter how complicated they are.
2. `FlexibleSUSY` and `SPheno` give numerical predictions for the mass spectrum and the mixing among all states including higher order corrections.

Thus, for users the study becomes no more difficult when they drop all simplifying assumptions, and instead consider the model in full generality. Moreover, there is no chance to miss important effects in the decays of the new scalar:

1. As outlined above, `FlexibleSUSY` and `SPheno` calculate the diphoton and digluon rate very accurately
2. `SPheno` calculates all other two body decays[7] of the scalar. This makes it impossible to miss any channel.

2.3 Considering a full model

2.3.1 Additional constraints in a full model

There are several studies which extend an already existing model by vector-like states and then assume that this part of the model is decoupled from the rest. When this assumption is made it is clear that the results from toy models, with the minimal particle content will be reproduced. However, it is often not clear if this decoupling can be done without invoking specific structures in the choice of parameters, and if these assumptions hold at the loop level.

On the other hand, if model-specific features are used to explain the diphoton excess, it is likely that there will be important constraints on the model coming from other sectors. For instance, there might be bounds from flavour observables, dark matter, Higgs searches, neutrino mixing, electroweak precision observables, searches for BSM particles at colliders, and so on. All of that has to be checked to be sure that any benchmark point presented is indeed a valid explanation for all observations. Such a wide range of constraints is much easier to address by making exhaustive use of tools which provide a high level of automation.

2.3.2 Theoretical uncertainties of other predictions

Even if attempts are made to include the effects of the new states on other sectors of the model, it is important to be aware that there are large uncertainties involved in certain calculations. If the level of uncertainty is underestimated, this can have an impact on what is inferred from the calculation. The large uncertainty in a LO calculation of the diphoton and digluon rate has already been addressed in Sect. 2.1.1. However, there are also other important loop corrections especially in SUSY models: the accurate calculation of the Higgs mass is a long lasting endeavour where for the simplest SUSY models even the dominant three-loop corrections are partially tackled [425]. The current ball-park of the remaining uncertainty is estimated to be 3 GeV.

[7] Even three-body decays into another scalar and two fermions can be calculated with `SPheno`.

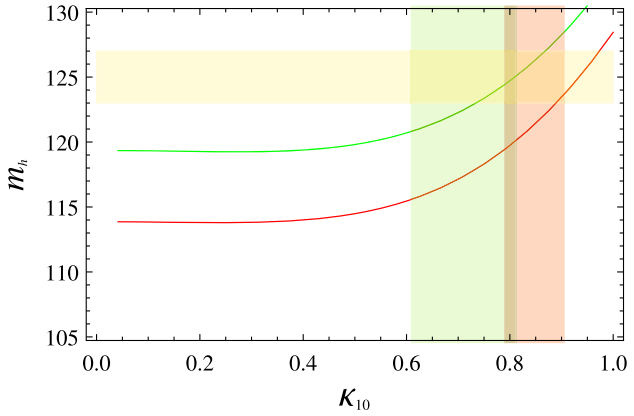

Fig. 6 Comparison of the two-loop Higgs mass calculation of Ref. [180] with the results obtained by SPheno. The parameters are those of Fig. 7 in Ref. [180] and we fixed $X_{\kappa_{10}} = 0$. The *lines* are the results from SPheno, while the *green* and *red shades* areas are the ranges of κ_{10} which predict $m_h = [123, 127]$ GeV according to Ref. [180]. *Red* takes $X_t = 4$ and *green* $X_t = 2$, where X_t is defined in Eq. (9) of the reference

However, most likely the MSSM cannot explain the excess, hence it would have to be extended. A common choice is to add additional pairs of vector-like superfields together with a gauge singlet, see Sect. 5. These new fields can also be used to increase the SM-like Higgs mass. However, this will in general also increase the theoretical uncertainty in the Higgs mass prediction, because these new corrections are not calculated with the same precision as the MSSM corrections. For instance, Ref. [180] has taken into account the effect of the new states on the SM-like Higgs. There, they use a one-loop effective potential approach considering the new Yukawa couplings to be $\mathcal{O}(1)$ or below, while also including the dominant two-loop corrections from the stop quark. They assumed that including these corrections is sufficient in order to achieve an uncertainty of 2 GeV in the Higgs mass prediction. One can compare their results encoded in Fig. 7 of Ref. [180] with a calculation including, in addition to the corrections taken into account in the paper, momentum dependence and electroweak corrections at the one-loop level, as well as the additional two-loop corrections arising from all the newly introduced states. These corrections can be important, as was shown for instance in Ref. [426]. The result of the comparison is shown in Fig. 6. We find a similar behaviour, but still there are several GeV difference between both calculations. For $\kappa_{10} = 0.8$ and $X_t = 4$, the point would be within the interesting range for $m_h = [123, 127]$ GeV, while the more sophisticated calculation predicts a mass below 120 GeV. Thus, the assumed uncertainty of 2 GeV in Ref. [180], which would even be optimistic in the MSSM, is completely unrealistic without including all the aforementioned higher order corrections.

2.3.3 How do the tools help?

The tools help to ensure that one really considers all aspects of a full model:

1. All masses of the model are calculated with high accuracy: FlexibleSUSY and SPheno include the full one-loop contribution to all pole masses in a model, while SPheno covers even the dominant two-loop corrections introduced by adding new states.
2. SPheno makes predictions for all important flavour observables in the model.
3. A link to MicrOmegas provides the possibility to calculate the dark matter relic density.
4. The interface to HiggsBounds and HiggsSignals offers the possibility to check all constraints from Higgs searches and to check if the results for the SM-like Higgs can be reproduced.

3 The SARAH framework and its diphoton extension

3.1 SARAH

One of the reasons that makes high energy particle physics an exciting field is the vast amount of experimental data available. When proposing a model one first has to check its self consistency, checking for instance the particle mass spectrum and vacuum stability requirements. Then it has to be tested against data related to collider searches, flavour observables, dark matter observations and Higgs measurements. A lot of effort has been devoted to developing an arsenal of specific tools to explore these quantities with high precision for specific classes of models, such as the MSSM, the THDM and the NMSSM to some extent. However, it is often very difficult – if not impossible – to explain the excess in the simplest versions of these models.[8] For the time being there is no specific model which is clearly preferred over others as an explanation of the excess, as reflected by the large variety of models that different authors have proposed, and it would be impractical to repeat the process of developing a code for each one of them. In the absence of a dedicated tool, the alternative is often to resort to approximations or just to leading order

[8] The MSSM with and without trilinear R-parity violation is disfavoured by the constrains from vacuum stability, see Sect. 2.1.2. In the NMSSM one can explain this excess by assuming the presence of additional final states via four-body decays like $\Phi \to (\phi_a)(\phi_a) \to 4\gamma\gamma$ [173,183]. This explanation requires the mass of ϕ_a to be tiny and very close to the pion mass. In the absence of a specific approximate $U(1)$ symmetry (either Peccei-Quinn or R-symmetry), a very delicate fine-tuning would be needed, rendering this possibility less attractive. Another possibility was presented in Ref. [37] where the diphoton signal originates from a parent resonance decay in very finely-tuned parameter regions with a low UV cutoff.

expressions, as described in the previous section, in which case the analysis (in particular for more complicated models) is of limited value.

Luckily, a dedicated powerful tool already exists. It is the Mathematica package SARAH [361–366], which can perform the most advanced quantum field theory computations and apply them generically to any given model. SARAH has been optimised for an easy, fast, and exhaustive study of renormalisable BSM models. Within a given model SARAH analytically calculates the following:

- All tree-level masses, vertices and tadpole equations
- The two-loop RGEs for a general quantum field theory and a softly broken SUSY theory using generic results of [427–436]
- The one-loop corrections to all one- and two-point functions

In addition SARAH also provides routines to export the derived information in order to use it for numerical calculations with dedicated tools. We give in the following a brief overview about the different possibilities.

3.2 SPheno

SARAH writes Fortran source code for SPheno [367,368] using the derived information about the mass matrices, tadpole equations, vertices, loop corrections and RGEs for the given model. With this code the user gets a fully functional spectrum generator for the model of their choice. The features of a spectrum generator created in this way are

- Full two-loop running of all parameters
- One-loop corrections to all masses
- Two-loop corrections to Higgs masses
- Complete one-loop thresholds at M_Z
- Calculation of the $h\gamma\gamma$ and hgg effective couplings at N^{3}LO, see Sect. 3.5
- Calculation of flavour and precision observables at full one-loop level
- Calculation of decay widths and branching ratios for two– and three body decays
- Interface to HiggsBounds and HiggsSignals
- Estimate of electroweak fine-tuning
- Prediction for LHC cross sections for all neutral scalars

3.3 FlexibleSUSY

FlexibleSUSY is a Mathematica package which uses the SARAH-generated expressions for the mass matrices, self-energies, tadpole equations, vertices and RGEs to create a C++ spectrum generator for both SUSY and non-SUSY models. The spectrum generators created with FlexibleSUSY have the following features:

- Full two-loop running of all parameters
- Three-loop running of all parameters in the SM and MSSM, except for the VEVs
- Calculation of the pole mass spectrum at the full one-loop level
- Partial two-loop corrections to the Higgs masses in the SM, Split-MSSM, MSSM, NMSSM, UMSSM and E$_6$SSM and partial three-loop corrections to the Higgs mass in the Split-MSSM
- Complete one-loop and partial two-loop and three-loop threshold corrections to the Standard Model at the scale $Q = M_Z$ or $Q = M_t$
- Calculation of the $h\gamma\gamma$ and hgg effective couplings at N^{3}LO, see Sect. 3.5
- An interface to GM2Calc [418] in the MSSM without flavour violation

FlexibleSUSY aims to generate spectrum generators which are modular such that components can be easily reused or replaced. This means that it is quite easy to re-use the precision calculations in FlexibleSUSY spectrum generators for other purposes or add additional routines.

3.4 Mass spectrum calculation: SUSY vs. non-SUSY

We have outlined that FlexibleSUSY and SPheno can include the radiative corrections to all particles up to the two-loop level in the $\overline{\text{DR}}'$ scheme. These corrections are included by default for supersymmetric models. It is known that loop corrections, in particular to the Higgs mass, are crucial. Typically the $\overline{\text{DR}}'$ and on-shell calculations are in good agreement. Consequently, the remaining difference between both calculations is often a good estimate for the theoretical uncertainty.

The treatment of non-supersymmetric models in FlexibleSUSY and SPheno is very similar to the treatment of supersymmetric models. The main difference is, that in non-supersymmetric models the parameters are defined in the $\overline{\text{MS}}$ scheme, while in supersymmetric ones the parameters are defined in the $\overline{\text{DR}}'$ scheme. In this paper we perform only tree-level mass calculations (if not stated otherwise), in which the definition of the renormalisation scheme is irrelevant. Thus, in the mass spectrum calculations performed in the following, one is allowed to use input parameters which are defined in the on-shell scheme. This is for instance the standard approach in the large majority of studies of the THDM: there are in general enough free parameters to perform a full on-shell renormalisation keeping all masses and mixing angles fixed. We find that the one-loop corrections in the $\overline{\text{MS}}$ scheme can give huge corrections to the tree-level

masses in nearly all models presented in the following. Therefore large fine-tuning of the parameters is necessary once the loop corrections are taken into account. A detailed analysis using a full on-shell renormalisation scheme is possible for each model, but is beyond the scope of this work. Of course, for models where it turns out to be unavoidable that shifts in the masses and mixings appear at the loop-level, the user can simply turn on the loop corrections in `FlexibleSUSY` and `SPheno` via a flag in the Les Houches input file.

3.5 Calculation of the effective diphoton and digluon vertices in `SPheno` and `FlexibleSUSY`

For the calculation of the partial width of a neutral scalar Φ decaying into two gluons or two photons we follow closely [419] for the LO and NLO contributions. The partial widths at LO are given by

$$\begin{aligned}\Gamma(\Phi\to\gamma\gamma)_{\rm LO} = \frac{G_F\alpha^2(0)m_\Phi^3}{128\sqrt{2}\pi^3}\Big|&\sum_f N_c^f Q_f^2 r_f^\Phi A_f(\tau_f)\\ &+\sum_s N_c^s r_s^\Phi Q_s^2 A_s(\tau_s)\\ &+\sum_v N_c^v r_v^\Phi Q_v^2 A_v(\tau_v)\Big|^2, \end{aligned}\tag{3.1}$$

$$\begin{aligned}\Gamma(\Phi\to gg)_{\rm LO} = \frac{G_F\alpha_s^2(\mu)m_\Phi^3}{36\sqrt{2}\pi^3}\Big|&\sum_f \frac{3}{2} D_2^f r_f^\Phi A_f(\tau_f)\\ &+\sum_s \frac{3}{2} D_2^s r_s^\Phi A_s(\tau_s)\\ &+\sum_v \frac{3}{2} D_2^v r_v^\Phi A_v(\tau_v)\Big|^2. \end{aligned}\tag{3.2}$$

Here, the sums are over all fermions f, scalars s and vector bosons v which are charged or coloured and which couple to the scalar Φ. Q is the electromagnetic charges of the fields, N_c are the colour factors and D_2 is the quadratic Dynkin index of the colour representation which is normalised to $\frac{1}{2}$ for the fundamental representation. We note that the electromagnetic fine structure constant α must be taken at the scale $\mu = 0$, since the final state photons are real [437]. In contrast, α_s is evaluated at $\mu = m_\Phi$ which, for the case of interest here, is $\mu = 750$ GeV. r_i^Φ are the so-called reduced couplings, the ratios of the couplings of the scalar Φ to the particle i normalised to SM values. These are calculated as

$$r_f^\Phi = \frac{v}{2M_f}(C^L_{\bar f f\Phi} + C^R_{\bar f f\Phi}),\tag{3.3}$$

$$r_s^\Phi = \frac{v}{2M_s^2} C_{ss^*\Phi},\tag{3.4}$$

$$r_v^\Phi = -\frac{v}{2M_v^2} C_{vv^*\Phi}.\tag{3.5}$$

Here, v is the electroweak VEV and C are the couplings between the scalar and the different fields with mass M_i ($i = f, s, v$). Furthermore,

$$\tau_x = \frac{m_\Phi^2}{4m_x^2}\tag{3.6}$$

holds and the loop functions are given by

$$A_f = 2(\tau + (\tau-1)f(\tau))/\tau^2,\tag{3.7}$$

$$A_s = -(\tau - f(\tau))/\tau^2,\tag{3.8}$$

$$A_v = -(2\tau^2 + 3\tau + 3(2\tau-1)f(\tau))\tau^2,\tag{3.9}$$

with

$$f(\tau) = \begin{cases} \arcsin^2\sqrt{\tau} & \text{for } \tau \le 1,\\ -\frac{1}{4}\left(\log\frac{1+\sqrt{1-\tau^{-1}}}{1-\sqrt{1-\tau^{-1}}} - i\pi\right)^2 & \text{for } \tau > 1. \end{cases}\tag{3.10}$$

For a pure pseudo-scalar state only fermions contribute, i.e. the LO widths read

$$\Gamma(A\to\gamma\gamma)_{\rm LO} = \frac{G_F\alpha^2 m_A^3}{32\sqrt{2}\pi^3}\left|\sum_f N_c^f Q_f^2 r_f^A A_f^A(\tau_f)\right|^2,\tag{3.11}$$

$$\Gamma(A\to gg)_{\rm LO} = \frac{G_F\alpha_s^2 m_A^3}{36\sqrt{2}\pi^3}\left|\sum_f 3 D_2^f r_f^A A_f^A(\tau_f)\right|^2,\tag{3.12}$$

where

$$A_f^A = f(\tau)/\tau,\tag{3.13}$$

and r_f^A takes the same form as r_f^Φ in Eq. (3.3), simply replacing $C^{L,R}_{\bar f f\Phi}$ by $C^{L,R}_{\bar f f A}$.

These formulae are used by `SPheno` and `FlexibleSUSY` to calculate the full LO contributions of any CP-even or odd scalar present in a model including all possible loop contributions at the scale $\mu = m_\Phi$. However, it is well known, that higher order corrections are important. Therefore, NLO, NNLO and even N^{3}LO corrections from the SM are adapted and used for any model under study. In case of heavy colour

fermionic triplets, the included corrections for the diphoton decay are

$$r_f^\Phi \to r_f \left(1 - \frac{\alpha_s}{\pi}\right), \tag{3.14}$$

$$r_s^\Phi \to r_s \left(1 + \frac{8\,\alpha_s}{3\pi}\right). \tag{3.15}$$

These expressions are obtained in the limit $\tau_f \to 0$ and thus applied only when $m_\Phi < m_f$. r_f^A does not receive any corrections in this limit. For the case $m_\Phi > 100 m_f$, we have included the NLO corrections in the light quark limit given by [419]

$$r_f^X \to r_f^X \left(1 + \frac{\alpha_s}{\pi}\left[-\frac{2}{3}\log 4\tau + \frac{1}{18}\left(\pi^2 - \log^2 4\tau\right) + 2\log\left(\frac{\mu_{\rm NLO}^2}{m_f^2}\right) + i\frac{\pi}{3}\left(\frac{1}{3}\log 4\tau + 2\right)\right]\right) \tag{3.16}$$

for $X = \Phi, A$. $\mu_{\rm NLO}$ is the renormalisation scale used for these NLO corrections, chosen to be $\mu_{\rm NLO} = m_\Phi/2$. In the intermediate range of $100 m_f > m_\Phi > 2m_f$, no closed expressions for the NLO correction exist. Our approach in this range was to extract the numerical values of the corrections from HDECAY [406] and to fit them. For the digluon decay rate, the corrections up to N^{3}LO are included and parametrised by

$$\Gamma(X \to gg) = \Gamma(X \to gg)_{\rm LO} \times \left(1 + C_X^{\rm NLO} + C_X^{\rm NNLO} + C_X^{\rm N^3LO}\right), \tag{3.17}$$

with [404,419,438–442]

$$C_\Phi^{\rm NLO} = \left(\frac{95}{4} - \frac{7}{6}N_F\right)\frac{\alpha_s}{\pi}, \tag{3.18}$$

$$C_\Phi^{\rm NNLO} = \left(370.196 + (-47.1864 + 0.90177 N_F)N_F + (2.375 + 0.666667 N_F)\log\frac{m_\Phi^2}{m_t^2}\right)\frac{\alpha_s^2}{\pi^2}, \tag{3.19}$$

$$C_\Phi^{\rm N^3LO} = \left(467.684 + 122.441\log\frac{m_\Phi^2}{m_t^2} + 10.941\left(\log\frac{m_\Phi^2}{m_t^2}\right)^2\right)\frac{\alpha_s^3}{\pi^3}, \tag{3.20}$$

and

$$C_A^{\rm NLO} = \left(\frac{97}{4} - \frac{7}{6}N_F\right)\frac{\alpha_s}{\pi}, \tag{3.21}$$

$$C_A^{\rm NNLO} = \left(171.544 + 5\log\frac{m_\Phi^2}{m_t^2}\right)\frac{\alpha_s^2}{\pi^2} \tag{3.22}$$

For pseudo-scalars we include only corrections up to NNLO as the N^3LO are not known for CP-odd scalars.

One has to keep in mind that the NLO up to N^{3}LO corrections are calculated in the SM under the assumption that only a (fermionic) colour triplet and the gluons play any role in the loops. Of course, in BSM models this must not necessarily be the case. For instance, in SUSY models gluinos would also contribute at NLO. The impact of these additional corrections is estimated in Sect. 3.7.2. Another possible effect is the presence of a scalar triplet, such as the SUSY top partners. However, it was found that the higher-order corrections for this case can be well approximated by the SM results, see Ref. [443]. Finally, other colour representations beyond triplets can induce an effective digluon coupling in BSM models. To our knowledge, NLO and higher order corrections for these cases have not yet been discussed in the literature. However, motivated by the observation of Ref. [443] that the K-factor for the higher-order corrections in the MSSM is nearly identical to the SM, because the largest contributions by-far come from final state gluons, we consider the SM corrections to also give the dominant effect at NLO and beyond for this case. However, we also provide a flag in SPheno that allows users to turn-off these corrections, if they think that such corrections are not appropriate for the case at hand. Similarly, in FlexibleSUSY these corrections may be turned off by means of a flag in the generated code.

In order to check the accuracy of our implementation, we compared the results obtained with SARAH–SPheno for the SM Higgs boson decays with the ones given in the CERN yellow pages [444]. In Fig. 7 we show the results for the Higgs branching ratios into two photons and two gluons with and without the inclusion of higher order corrections. One sees that good agreement is generally found when including higher order corrections. Figure 8 shows the relative difference of the partial widths $\Gamma(h \to \gamma\gamma)$ and $\Gamma(h \to gg)$ as calculated by SPheno and FlexibleSUSY compared to the benchmark values provided by the Higgs

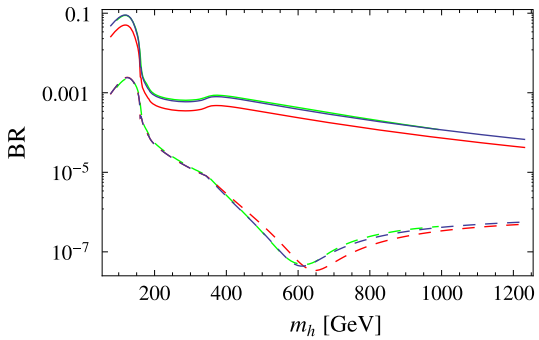

Fig. 7 Comparison of Br($h \to gg$) (*full lines*) and Br($h \to \gamma\gamma$) (*dashed lines*) as calculated by SPheno at LO (*red*) and including higher order corrections as described in the text (*blue*). The *green line* shows the values of the Higgs cross section working group

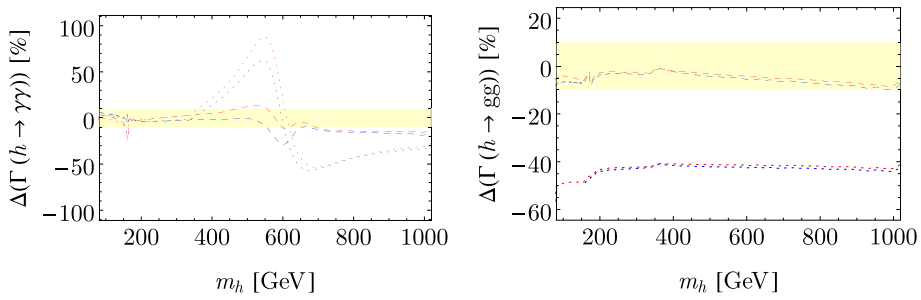

Fig. 8 *On the left* comparison of the relative difference in the partial width $\Gamma(h \to \gamma\gamma)$ as calculated by `SPheno` (in *red*) and `FlexibleSUSY` (in *blue*) to the benchmark values provided by the Higgs cross section working group. The LO results are shown by the *dotted lines*, while the NLO results are shown by the *dashed lines*. The *yellow rectangle* indicates ±10 % errors compared to the results from the Higgs cross section working group. *On the right* the same for the partial width $\Gamma(h \to gg)$

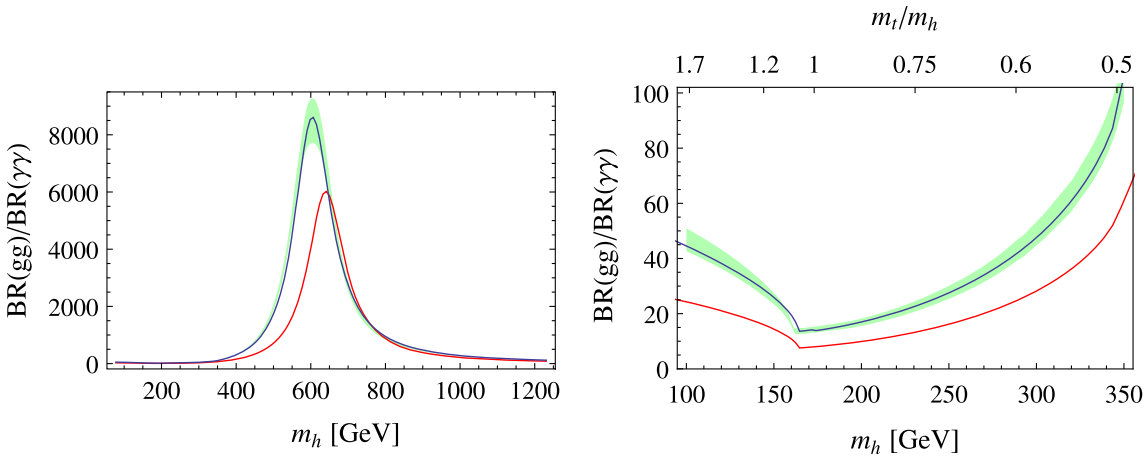

Fig. 9 $\mathrm{Br}(h \to gg)/\mathrm{Br}(h \to \gamma\gamma)$ as calculated by `SPheno` at LO (*red*) and including higher order corrections as described in the text. The *green band* shows the values of the Higgs cross section working group including a 10 % uncertainty. *On the right* we zoom into the range $m_h \in [0.5, 2]\, m_t$

cross section working group. While the results obtained from the two codes are not identical, there is good agreement between them for both partial widths. The differences between `SPheno` and `FlexibleSUSY` originate mainly from a different treatment of unknown higher-order corrections to the pole mass spectrum. In Fig. 9 we show the ratio $\mathrm{Br}(h \to gg)/\mathrm{Br}(h \to \gamma\gamma)$ and compare it again with the recommended numbers by the Higgs cross section working group [444]. Allowing for a 10 % uncertainty, we find that our calculation including higher order corrections agrees with the expectations, while the LO calculation predicts a ratio that is over a wide range much too small. The important range to look at is actually not the one with $m_h \sim 750$ GeV because this corresponds to a large ratio of the scalar mass compared to the top mass. Important for most diphoton models is the range where the scalar mass is smaller than twice the quark mass. In this mass range we find that the NLO corrections are crucial and can change the ratio of the diphoton and digluon rate up to a factor of 2. We also note that if we had used $\alpha(m_h)$ instead of $\alpha(0)$ in the LO calculation, the difference would have been even larger, with a diphoton rate overestimated by a factor $(\alpha(m_h)/\alpha(0))^2 \simeq (137/124)^2 \simeq 1.22$.

3.6 Monte-Carlo studies

3.6.1 *Interplay* `SARAH`*-spectrum-generator-MC-tool*

The tool chains `SARAH`–`SPheno`/`FlexibleSUSY`–MC-Tools have one very appealing feature: the implementation of a model in the spectrum generator (`SPheno` or `FlexibleSUSY`) as well as in a MC tool is based on just one single implementation of the model in `SARAH`. Thus, the user does not need to worry that the codes might use different conventions to define the model. In addition, `SPheno` also provides all widths for the particles so that this information can be used by the MC-Tool to save time.

3.6.2 *Effective diphoton and digluon vertices for neutral scalars*

The effective diphoton and digluon vertices calculated by `SPheno` or `FlexibleSUSY` are directly available in the UFO model files and the `CalcHep` model files: `SARAH` includes the effective vertices for all neutral scalars to two photons and two gluons, and the numerical values for these

vertices are read from the spectrum file generated with SPheno or FlexibleSUSY. For this purpose, a new block EFFHIGGSCOUPLINGS is included in these files, which contains the values for the effective couplings including all corrections outlined in Sect. 3.5.

It is important to mention that these effective couplings correspond to the decay of the scalar; if we use CalcHep or MadGraph to compute the decay $\Phi \to gg$ then the value matches (as closely as possible) the N^{3}LO value, which includes *real* emission processes such as $\Phi \to ggg$. Therefore, the corrections at NLO and beyond for $\Phi \to gg$ are not the same as $pp \to \Phi$ via gluon fusion [437]; the full N^{3}LO production cross-section includes all processes $gg \to \Phi$+jet and is therefore described by a different k-factor to the decay. This k-factor can for instance be obtained via

$$k = c_{\Phi gg} \cdot \frac{\sigma_{\rm SM}(pp \to H(M_\Phi) + \text{jet})}{\sigma_{\rm MC}(pp \to \Phi)} \tag{3.23}$$

where $c_{\Phi gg}$ is the ratio squared of the effective coupling between Φ and two gluons at LO in the considered model and the SM. These values can for instance be read off by the block HiggsBoundsInputHiggsCouplingsBosons in the SPheno spectrum file. $\sigma_{\rm SM}(pp \to H(M_\Phi))$ is the cross section for a SM-like Higgs with mass M_Φ. This value can be calculated for instance with Higlu [445] or Sushi [446] for the considered center-of-mass energy. SPheno also provides values for $c_{\Phi gg} \cdot \sigma_{\rm SM}(pp \to H(M_\Phi))$ for the most common energies in the blocks HiggsLHCX (X=7,8,13,14) and HiggsFCC.

On the other hand, this approach is not entirely appropriate for more refined collider analyses where the user would like to actually include, for example, a hard jet in the final state (without the full loop corrections to the effective vertex this is not an infra-red safe quantity). In this case, we note that around 750 GeV the effective vertex output by SARAH gives a fairly accurate result – to within 30 % – of the total production cross-section, at least in the Standard Model, when we compute $\sigma_{SM}(gg \to \Phi + \text{jet})$ using MadGraph and the standard cuts on momenta. This is illustrated in Fig. 10.

3.7 Accuracy of the diphoton calculation

Before concluding this section, we should draw the reader's attention to the question of how accurate the results are from SARAH in combination with SPheno and FlexibleSUSY. While every possible correction has been included, there are still some irreducible sources of uncertainty, as we shall discuss below.

3.7.1 Loop corrections to ZZ, WW, $Z\gamma$ production

So far in SARAH, loop-level decays are only computed for processes where the tree-level process is absent. This is to avoid the technical issues of infra-red divergences. If the particle that explains the 750 GeV excess is a scalar, then it must mix with the Higgs and acquire tree-level couplings to the Z and W bosons. The respective decays are fully taken into account at tree level. However, due to the existence of such terms, the loop corrections to the decays into Zs and Ws are more complicated and are therefore not yet available in SARAH. Even if hese technical issues do not apply for pseudo-scalar bosons, for which the decays into vector bosons are only possible at the loop level, these decays are also not yet available at the loop level. However, it should be mentioned that there are on-going efforts to close this gap in the near future and to provide the full one-loop corrections to any two-body decay of CP-even and -odd scalars.

That these loop induced decays are missing at the moment in SARAH can trigger two issues the user has to keep in mind. First, there are limits on the decays $S \to WW$ and $S \to ZZ$ which could be violated if the loop induced couplings between S and two massive vector bosons are too large. Therefore, one has to be careful when studying models with large additional $SU(2)$ representations. The second issue is that the prediction for the BR into two photons suffers from an additional uncertainty because of the missing contribution of the ZZ and WW decays to the total width.

To estimate the uncertainty incurred by their absence, let us assume that our 750 GeV resonance S couples to the $U(1)_Y$ and $SU(2)_L$ gauge bosons via the effective operators $SB_{\mu\nu}B^{\mu\nu}$ and $SW_{\mu\nu}W^{\mu\nu}$. If we can neglect the tree-level contributions to the decays and assume that the dominant contribution originates from a set of particles in the loops, which have the hypercharge Y and the Dynkin index $D_2(W)$ and dimension of the $SU(2)$ representation d_2, then the decay widths are approximately given by

$$\begin{aligned}
\frac{\Gamma(S \to ZZ)}{\Gamma(S \to \gamma\gamma)} &\simeq \frac{(\frac{D_2}{t_W^2} + t_W^2 d_2 Y^2)^2}{(d_2 Y^2 + D_2)^2}, \\
\frac{\Gamma(S \to Z\gamma)}{\Gamma(S \to \gamma\gamma)} &\simeq \frac{2}{t_W^2}\frac{(D_2 - t_W^2 d_2 Y^2)^2}{(d_2 Y^2 + D_2)^2}, \\
\frac{\Gamma(S \to WW)}{\Gamma(S \to \gamma\gamma)} &\simeq \frac{2D_2^2 \text{cosec}^4\theta_W}{(d_2 Y^2 + D_2)^2}.
\end{aligned} \tag{3.24}$$

where we abbreviated t_W for $\tan\theta_W$. Put together, the uncertainty that we find for the decay $S \to \gamma\gamma$ reads

$$\begin{aligned}
\frac{\delta\Gamma(S \to \text{anything})}{\Gamma(S \to \text{anything})} \simeq &\left[\frac{55D_2^2 - 2d_2 Y^2 D_2 + 0.69 d_2^2 Y^4}{(d_2 Y^2 + D_2)^2}\right] \\
&\times \text{Br}(S \to \gamma\gamma).
\end{aligned} \tag{3.25}$$

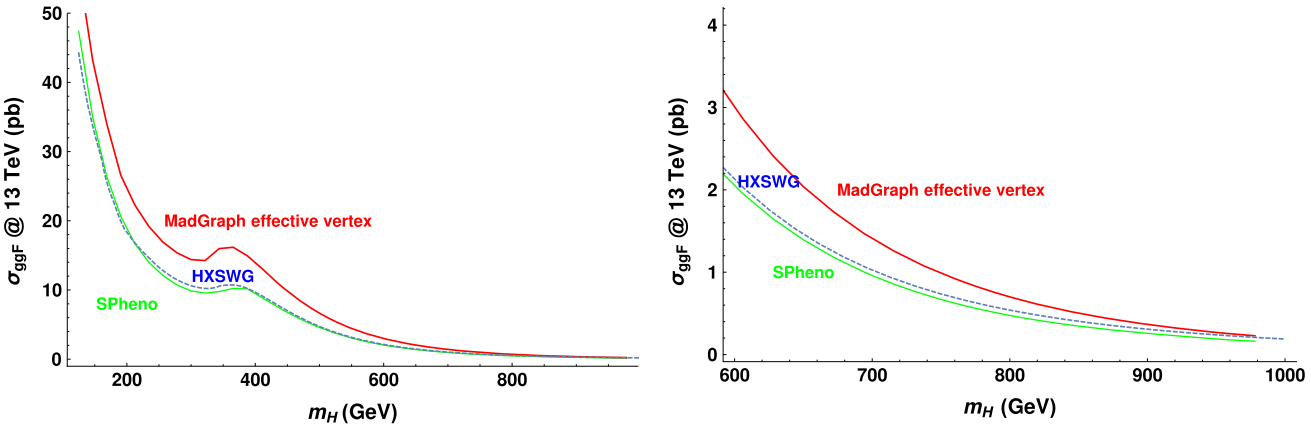

Fig. 10 Comparisons of the total Higgs production cross-section via gluon fusion in the Standard Model as a function of the Higgs mass, computed using the SPheno output from SARAH, the Higgs cross-section working group data, and in MadGraph using our effective vertex

The factor in square brackets is therefore largest for fields that only couple to $SU(2)_L$ gauge bosons, giving a factor of ~ 55, and for $SU(2)$ doublets with hypercharge $1/2$ it is 13, although the former case yields too many W bosons (the limit from run 1 searches is $\frac{\Gamma(S\to WW)}{\Gamma(S\to\gamma\gamma)} \lesssim 20$). Thus, provided that $\mathrm{Br}(S \to \gamma\gamma) \lesssim 10^{-3}$, the relative uncertainty is guaranteed to be less than 10 %. In such cases, the proportional error in the total width transfers directly into the proportional error in the total cross-section:

$$\frac{\delta\sigma(pp \to S \to \gamma\gamma)}{\sigma(pp \to S \to \gamma\gamma)} \simeq -\frac{\delta\Gamma(S \to \text{anything})}{\Gamma(S \to \text{anything})} \tag{3.26}$$

On the other hand, for models where the dominant decay channel of the singlet is into gluons, it is not possible to have $\mathrm{Br}(S \to \gamma\gamma) \lesssim 10^{-3}$ without violating constraints from dijet production, and the reader should be careful about the possible errors incurred. Fortunately, provided that the loop particles have a hypercharge the error is much smaller, for example in the case that $D_2 = 0$ the coefficient above is less than one, thus giving an error of $\sim 10^{-3}$ for $\mathrm{Br}(S \to \gamma\gamma) = 10^{-3}$.

3.7.2 BSM NLO corrections

As discussed above, SARAH includes the leading-order computation of the diphoton and digluon decay amplitudes including the effects of all Standard Model and Beyond-the-Standard-Model particles in the loops. Furthermore, it also includes the leading-log corrections to the digluon rate at NLO, NNLO and N^{3}LO order in α_s *in the Standard Model*, and some NLO corrections due to diagrams with an extra gluon to both the digluon and diphoton rates. However, the NLO corrections are absent for all other particles, which in the case of large Yukawa couplings or hierarchies could be sizeable. Two examples of such a diagrams are given in Fig. 11; in the context of supersymmetric theories, particularly important are diagrams involving the gluino, which (if it is a Majorana particle) would not couple to a singlet at leading order – naively their contribution is

$$\frac{\delta\Gamma(S \to gg/\gamma\gamma)}{\Gamma(S \to gg/\gamma\gamma)} \sim \frac{\alpha_s}{\pi} \log \frac{m_{\tilde{g}}^2}{\mu_{NLO}^2} \underset{m_{\tilde{g}}=2\ \text{TeV}}{\longrightarrow} \sim 10\,\%, \tag{3.27}$$

although as we shall discuss below this can be (potentially significantly) an underestimate.

3.7.3 Presence of light fermions

The higher order corrections to the Higgs production and decay via the effective digluon coupling is calculated in the SM using an effective-field-theory (EFT) approach. This is possible because the top mass is sufficiently heavy compared to the Higgs boson. Also the presence of vector-like quarks with masses below 750 GeV is already tightly constrained by direct searches at the LHC [447]. Therefore, for realistic scenarios the EFT approximation is also typically valid. Even so, one might wonder how large the additional uncertainty is due to the presence of light quarks. For a detailed discussion of this, we refer to Ref. [448]. The overall result is that the additional uncertainty is larger than the one stemming from the choice of the QCD scale. Nevertheless, it was found that the EFT computation still gives a good estimate for the overall K-factor.

3.7.4 Tree vs pole masses in loops

For consistency of the perturbative series and technical expediency, the masses inside loops (to calculate pole masses and loop decay amplitudes) are $\overline{\mathrm{MS}}$ or $\overline{\mathrm{DR}}'$ parameters, not the pole masses of observed particles. The difference

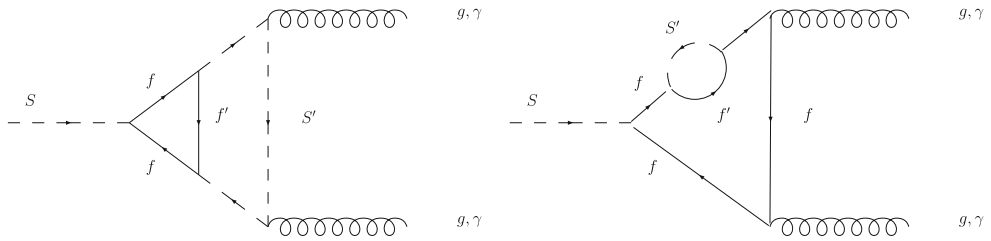

Fig. 11 Examples of potentially important NLO corrections

between calculations performed in this scheme and the on-shell scheme are at two-loop order, and so is generally small. However, in particular when there are large hierarchies or Yukawa couplings in a model, there can be a large difference between the Lagrangian parameters and the pole masses, and therefore a large discrepancy between the loop amplitudes calculated from these. In principle, this should be accounted for by including higher-order corrections such as the right-hand diagram in Fig. 11 – but applying such a correction to each propagator in the loop would actually correspond to a four-loop diagram. The effect of using the pole mass instead is to essentially resum part of these diagrams, which as is well known is relevant in the case of large hierarchies of masses – and so should give a more accurate result in that case.

If we define

$$\delta m^2 \equiv (m^2)^{\overline{\rm MS}/\overline{\rm DR}'} - (m^2)^{\text{on-shell}} \tag{3.28}$$

then for one dominant particle p in the loop, we can estimate the uncertainty as

$$\frac{\delta\Gamma(S \to gg/\gamma\gamma)}{\Gamma(S \to gg/\gamma\gamma)} \sim \begin{cases} -\frac{2\delta m^2}{m^2}\left(\frac{A'_p}{A_p}+1\right), & p = s, v, \\ -\frac{4\delta m}{m}\left(\frac{A'_p}{A_p}+\frac{1}{2}\right), & p = f, \end{cases} \tag{3.29}$$

where the factor of 1 or 1/2 assumes that the couplings $C_{\overline{p}p\Phi}$ do not depend upon the mass m_p (but the prefactor in r_p^Φ therefore does). For most values of m_p the loop functions are slowly changing (only peaking around $\tau_p = 1$) so we will have a proportional uncertainty in the result of $\frac{2\delta m_{s,v}^2}{m_{s,v}^2}$ or $\frac{2\delta m_f}{m_f}$. As an example, in supersymmetric theories the soft masses of coloured scalars $\tilde{S}'$ acquire a significant decrease from gluino loops:

$$\delta m^2_{\tilde{S}'} \simeq \frac{C_2(\tilde{S}')\alpha_s}{\pi} m^2_{\tilde{g}} \log \frac{m^2_{\tilde{g}}}{\mu^2_{NLO}}. \tag{3.30}$$

If the scalar is a colour triplet with a pole mass of 800 GeV, then for 2 TeV gluinos and the $\overline{\rm DR}'$ mass is ∼1100 GeV; but $\frac{\delta m^2_{\tilde{S}'}}{m^2_{\tilde{S}'}} \sim 1$! This corresponds to a shift of a factor of two in the amplitude, and, if the scalar dominates the total amplitude, a factor of four in $\Gamma(S \to gg/\gamma\gamma)$; in fact in this case SARAH would be potentially *underestimating* the diphoton rate. This is a relatively mild example regarding this excess: given that the vast majority of models proposed to explain the diphoton signature contain large Yukawa couplings and many new particles, there is a significant potential for large values of $\frac{\delta m^2}{m^2}$, about which the user should be careful. It is worth noting that this is an effect that would not be significant in the (N)MSSM, where the Higgs couplings to photons/gluons are dominated by the top quark (and, for photons, the W bosons) whose masses are protected by chiral symmetry from large shifts: this issue is a novelty for the 750 GeV excess.

For non-supersymmetric models, due to the fact that (almost) every parameter point is essentially fine-tuned, we have not calculated loop corrections to the masses by default, and this issue does not arise in the same way. The user is then free to regard the result as involving the pole masses of particles instead, if they so desire – the issue then becomes one of tuning the potentially large corrections to the other input parameters.

4 Models

A large variety of models have been proposed to explain the diphoton excess at 750 GeV. We have selected and implemented several possible models in SARAH. Our selection is not exhaustive, but we have tried to implement a sufficient cross-section which are representative of many of the ideas put forward in the context of renormalisable models. These are the ones that SARAH can handle. Their description is organised in the subsections that follow. Before we turn to this discussion we first want to mention other proposals which we do not deal with in this paper.

Many authors [16,35,50,59,67,72,99,144,150,190,192,207,249,251,265,298,301,319,331,341] have studied the excess with effective (non-renormalisable) models, which is sensible given that there are thus far no other striking hints of new physics at the LHC. As more data becomes available and the evidence for new physics becomes more substantial, one might want to UV complete these mod-

els, at which point the tools we are advertising become relevant and necessary. Other authors [42,52,60,73,114,122,131,233,235,273,293,297,308,315,320,323,346] considered strongly coupled models, in which the resonance is a composite state. This possibility would be favoured by a large width of the resonance, as first indications seem to suggest. Another possibility is to interpret the signal in the context of extra-dimensional models [5,9,29,30,48,84,125,141,203,225,312], with the resonance being a scalar, a graviton, a dilaton, or a radion, depending on the scenario. However, some of these interpretations are in tension with the non-observation of this resonance in other channels. In supersymmetry, the scalar partner of the goldstino could provide an explanation to the diphoton signal [97,147,167,335]. Other ideas, slightly more exotic, include: a model with a space-time varying electromagnetic coupling constant [135], Gluinonia [337], Squarkonium/Diquarkonium [299], flavons [244], axions in various incarnations [8,24,63,246,274,336], a natural Coleman–Weinberg theory [22,307], radiative neutrino mass models [264,325,327], and string-inspired models [19,132,188,240,254].

We turn now to the weakly coupled models, and list the ones which we have implemented in SARAH.

All model files are available for download at http://sarah.hepforge.org/Diphoton_Models.tar.gz and an overview of all implemented models is given in Tables 4 and 5, where we have divided the models into five different categories. The first three models can be regarded as toy models which simply extend the Standard Model by some basic ingredients for explaining the diphoton excess, namely a singlet scalar and a number of different vector-like fermions. The second category contains models which are also based on the SM gauge group but feature a more complicated structure than the toy models mentioned before. Table 5 contains a variety of non-supersymmetric models with an enlarged gauge group such as gauged $U(1)$ extensions or left-right-symmetric models, as well as some supersymmetric models, both with and without an enlarged gauge sector.

Some of the models which were implemented can be seen as a straightforward extension or a modification of known models like the Standard Model, the NMSSM, a two-Higgs-doublet model, or a $U(1)'$ model. They are derived from models already available in the SARAH model repository and will not be discussed here in detail. Note however, that some model classes, like left-right-symmetric models, are now for the first time publicly available for SARAH. For all the necessary information regarding the particle content, symmetries and the Lagrangian, we refer the interested reader to the documentation provided alongside the tarball containing the model files. As a selection, we discuss below in some detail the implementation of four rather involved models (one with scalar octets, two 3-3-1 models and one supersymmetric E_6-inspired model).

It is beyond the scope of this paper to discuss every model with its diphoton phenomenology in detail: many of the original papers for which we created the model files discussed their model in specific limits, e.g. decoupling complete parts of the sector without showing that the respective limit can even be consistently obtained. Therefore, a complete phenomenological study of each model would be necessary for checking all claims. Instead, we regard our model implementations as a starting point for the authors of these models or other researchers to perform a more thorough study themselves. Whenever benchmark points in terms of the model parameters were given in the respective literature, however, we have compared our results, and deviations are noted below.

In case of questions, comments or bug reports concerning these models, please, send an e-mail to `diphoton-tools@cern.ch` which includes all authors.

4.1 Validation

All SARAH model files which have been created, as well as the numerical codes derived thereof, have been validated by us using the following procedure:

1. First, the SARAH files themselves have been tested for consistency using basic SARAH commands, which are easy to use and we recommend these to readers. First of all, we have checked every model for anomalies as well as for the invariance under all gauge and discrete symmetries which is automatically done when the model is loaded within SARAH. Furthermore, the `CheckModel` command was executed which in addition checks the sanity of all field and parameter definitions as well as whether all possible particle admixtures have been correctly taken into account.
2. Whenever analytic formulas such as mass matrices were presented in the original studies which propose the model, we have reproduced and checked the respective expressions with SARAH.
3. For each model, we have produced and successfully compiled the tailor-made code for the spectrum generators SPheno and `FlexibleSUSY`.
4. Whenever the reference proposing the model has presented the necessary information to reproduce their results, we have done so. Differences are noted below.
5. The model files for `MadGraph` and `CalcHep` have been produced for all models and checked for consistency using the internal routines of the respective tools. Furthermore, we have computed representative processes like the production and/or decay of the candidate for the diphoton resonance and compared the obtained branching ratios between `MadGraph`, `CalcHep` and SPheno/`FlexibleSUSY`.

Table 4 Part I of the overview of proposed models to explain the diphoton excess which are now available in SARAH. Special characters are added in the last column if we found serious problems with the model during the implementation. The respective problem is described in the above text

Model	Name	Refs.	
Toy models with vector-like fermions			
CP-even singlet	SM+VL/CPevenS		
CP-odd singlet	SM+VL/CPoddS		
Complex singlet	SM+VL/complexS		
Models based on the SM gauge-group			
Portal dark matter	SM+VL/PortalDM	[108,228]	
Scalar octet	SM-S-Octet	[89,166]	♣
$SU(2)$ triplet quark model	SM+VL/TripletQuarks	[62]	
Single scalar leptoquark	LeptoQuarks/ScalarLeptoquarks	[53]	
Two scalar leptoquarks	LeptoQuarks/TwoScalarLeptoquarks	[106]	♠
Georgi-Machacek model	Georgi-Machacek	[116,184]	
THDM w. colour triplet	THDM+VL/min-3	[74]	
THDM w. colour octet	THDM+VL/min-8	[74]	
THDM-I w. exotic fermions	THDM+VL/Type-I-VL	[260,360]	
THDM-II w. exotic fermions	THDM+VL/Type-II-VL	[260,360]	
THDM-I w. SM-like fermions	THDM+VL/Type-I-SM-like-VL	[36]	
THDM-II w. SM-like fermions	THDM+VL/Type-II-SM-like-VL	[36]	
THDM w. scalar septuplet	THDM/ScalarSeptuplet	[227,317]	

6. For each model, we provide a set of input parameters which can be used to produce a valid spectrum which itself can then serve as an input for programs like MadGraph or CalcHep.

During the validation process, we noticed inconsistencies in the definition of some models when using the field content and symmetries as provided in the respective references. We therefore modified the respective model in order to restore consistency. For other models, we obtain results that are different to those quoted in the study proposing the model. We individually marked the affected models in the last column of the tables with a special character. The issues we found are the following:

- ♣ As explained in more detail in the following subsection, after the inclusion of higher-order corrections, the dijet constraints cut deeply into the allowed parameter space.
- ♠ We find disagreement with the diphoton rate as calculated in the original reference: we have reproduced the partial widths presented in Fig. 3 of Ref. [106] and find values which are roughly an order of magnitude smaller.
- †The $U(1)_D$ charge of the H' field as defined in Ref. [355] has been changed to -1 in order to make the Yukawa interaction terms gauge invariant.
- ‡The model cannot explain the diphoton excess with Yukawa couplings in the perturbative range, but the authors use values between 5 and 10. As stressed in Sect. 2.1.2.1, this renders the perturbative calculation, and hence the results, to be invalid.
- §We had to change the Yukawa interactions: in Ref. [138], they are defined as, e.g., $\overline{q_L} H_L^\dagger U_L$ which contracts to zero because of the implicit left/right projection operators. Moreover, in Refs. [138,149] the 'conjugate' assignments of the fields $H_{L/R}$ need to be exchanged in order to obtain a gauge-invariant Lagrangian. For more details see the actual model implementation or the notes provided with the model files.
- ¶We had to adapt the scalar potential as Eq. (6) and Eq. (7) in Ref. [90] are not gauge invariant. In the model implementation, we allow for every gauge-invariant term in the Lagrangian.
- △ Here, couplings of about 5 are needed to explain diphoton excess, rendering the perturbative calculation to be inconsistent.

4.2 Examples of model implementations

4.2.1 Scalar octet extension

- **Reference:** [89,166]
- **Model name:** SM-S-Octet

A charged scalar colour octet O coupled to a scalar singlet S was proposed in Refs. [89,166]. Here the singlet is the

Table 5 Part II of the overview of proposed models to explain the diphoton excess which are now available in SARAH. Special characters are added in the last column if we found serious problems with the model during the implementation. The respective problem is described in the above text

Model	Name	Refs.	
$U(1)$ extensions			
Dark $U(1)'$	`U1Extensions/darkU1`	[280]	
Hidden $U(1)$	`U1Extensions/hiddenU1`	[136]	
Simple $U(1)$	`U1Extensions/simpleU1`	[104]	
Scotogenic $U(1)$	`U1Extensions/scotoU1`	[355]	†
Unconventional $U(1)_{B-L}$	`U1Extensions/BL-VL`	[313]	
Sample of $U(1)'$	`U1Extensions/VLsample`	[107]	
Flavour-nonuniversal charges	`U1Extensions/nonUniversalU1`	[304]	
Leptophobic $U(1)$	`U1Extensions/U1Leptophobic`	[277]	‡
Z' mimicking a scalar resonance	`U1Extensions/trickingLY`	[102]	
Non-abelian gauge-group extensions of the SM			
LR without bidoublets	`LRmodels/LR-VL`	[138,149,153]	§
LR with $U(1)_L \times U(1)_R$	`LRmodels/LRLR`	[90]	¶
LR with triplets	`LRmodels/tripletLR`	[64]	
Dark LR	`LRmodels/darkLR`	[154]	
331 model without exotic charges	`331/v1`	[80]	
331 model with exotic charges	`331/v2`	[88]	
Gauged THDM	`GTHDM`	[250]	
Supersymmetric models			
NMSSM with vector-like top	`NMSSM+VL/VLtop`	[353]	△
NMSSM with **5**'s	`NMSSM+VL/5plets`	[180,220,350]	
NMSSM with **10**'s	`NMSSM+VL/10plets`	[180,220,350]	
NMSSM with **5**'s & **10**'s	`NMSSM+VL/10plets`	[220]	
NMSSM with **5**'s and RpV	`NMSSM+VL/5plets+RpV`	[180]	
Broken MRSSM	`brokenMRSSM`	[100]	
$U(1)'$-extended MSSM	`MSSM+U1prime-VL`	[258,449]	
E_6 with extra $U(1)$	`E6MSSMalt`	[110]	

Table 6 Extra scalar field content of the octet extended SM

Field	Gen.	$SU(3)_C$	$SU(2)_L$	$U(1)_Y$
S	1	**1**	**1**	0
O	1	**8**	**2**	$\frac{1}{2}$

750 GeV candidate, while the octet enters the loops that contribute to the generation of the couplings of the singlet to the gauge bosons. While Ref. [166] considers a toy model involving only the term $S|O|^2$, Ref. [89] takes the singlet extended Manohar-Wise model [450]. For the SARAH implementation we have used the full model. However, since the cubic and quartic terms in O do not play a significant role, they are turned off by default in the SARAH model file.

The extra particle content with respect to the SM is a real singlet S and a scalar colour octet O which is also charged under $SU(2)_L \times U(1)_Y$, see Table 6. The isospin components of O are

$$O^A = \begin{pmatrix} O^{+A} \\ O^{0A} \end{pmatrix}, \tag{4.1}$$

where $A = 1, \ldots, 8$ is the adjoint colour index. The full scalar

$$\begin{aligned} V = {} & \frac{1}{2} m_S^2 S^2 + \lambda_S S^4 - \mu^2 |H|^2 + \lambda_H |H|^4 + \kappa_1 S^2 |H|^2 \\ & + 2m_O^2 \mathrm{Tr}(O^\dagger O) + \kappa_2 S^2 \mathrm{Tr}(O^\dagger O) \\ & + \lambda_1 |H|^2 \mathrm{Tr}(O^\dagger O) + \lambda_2 H_i^\dagger H_j \mathrm{Tr}(O_j^\dagger O_i) \\ & + \lambda_6 \mathrm{Tr}(O^\dagger O O^\dagger O) + \lambda_7 \mathrm{Tr}(O_i^\dagger O_j O_j^\dagger O_i) \\ & + \lambda_8 \mathrm{Tr}(O^\dagger O)^2 + \lambda_9 \mathrm{Tr}(O_i^\dagger O_j) \mathrm{Tr}(O_j^\dagger O_i) \\ & + \lambda_{10} \mathrm{Tr}(O_i O_j) \mathrm{Tr}(O_i^\dagger O_j^\dagger) + \lambda_{11} (O_i O_j O_j^\dagger O_i^\dagger) \\ & + \Big(\lambda_3 H_i^\dagger H_j^\dagger \mathrm{Tr}(O_i O_j) + \lambda_4 H_i^\dagger \mathrm{Tr}(O_j^\dagger O_j O_i) \\ & + \lambda_5 H_i^\dagger \mathrm{Tr}(O_j^\dagger O_i O_j) + \text{h.c.} \Big) . \end{aligned} \tag{4.2}$$

Electroweak symmetry-breaking (EWSB) is driven by the VEV of the neutral component of the SM Higgs doublet, which can be decomposed as

$$H^0 = \frac{1}{\sqrt{2}}\left(v + \phi_H + i\,\sigma_H\right). \tag{4.3}$$

Here $\phi_H \equiv h$ is the Higgs boson, to be identified with the 125 GeV state discovered at the LHC. Similarly, the singlet S receives a VEV, and the neutral component of the octet is split into its CP-even and CP-odd eigenstates:

$$S = v_S + \phi_S, \quad O^0 \to \frac{1}{\sqrt{2}}\left(O^R + i\,O^I\right). \tag{4.4}$$

We will now briefly discuss the parameter space of the model in order to justify our choice of input parameters. First, we consider the tadpole equations, which can be automatically derived by SARAH. Their solution for μ^2 and κ_1 is

$$\begin{aligned}\mu^2 &= -\frac{1}{v^2}(\lambda_H v^4 - m_S^2 v_S^2 - 4\lambda_S v_S^4),\\ \kappa_1 &= -\frac{1}{v^2}(m_S^2 + 4\lambda_S v_S^2).\end{aligned} \tag{4.5}$$

The tree-level mass matrix for the CP-even neutral scalars in the (ϕ_H, ϕ_S) basis is given by

$$\begin{aligned}\mathcal{M}^2 &= \begin{pmatrix} \mu^2 + 3\lambda_H v^2 + \kappa_1 v_S^2 & 2\kappa_1 v v_S \\ 2\kappa_1 v v_S & m_S^2 + \kappa_1 v^2 + 12\lambda_S v_S^2 \end{pmatrix}\\ &= \begin{pmatrix} 2\lambda_H v^2 & -\frac{2v_S}{v}(m_S^2 + 4\lambda_S v_S^2) \\ -\frac{2v_S}{v}(m_S^2 + 4\lambda_S v_S^2) & 8\lambda_S v_S^2 \end{pmatrix}.\end{aligned} \tag{4.6}$$

We note that, in general, there is singlet-doublet mixing. There are two reasons to consider a small singlet-doublet mixing angle, θ. First, the stringent constraints derived from Higgs physics measurements, and second, the required suppressed decay widths into Higgses, Ws and Zs in order to fit the diphoton signal – indeed in [89] values of $\sim 10^{-2}$ were found to be required. If we have a small mixing angle, then we can write

$$\mathcal{M}^2 \sim \begin{pmatrix} m_h^2 & s_\theta c_\theta (m_h^2 - m_{750}^2) \\ s_\theta c_\theta (m_h^2 - m_{750}^2) & m_{750}^2 \end{pmatrix}. \tag{4.7}$$

This implies $\lambda_S > 0$, but also

$$\mu^2 \simeq -\frac{1}{2}m_h^2 + \frac{v_S^2}{v^2}(m_S^2 + \frac{1}{2}m_{750}^2). \tag{4.8}$$

However, we also have $v_S^2 \sim m_{750}^2/8\lambda_S$, and so

$$\mu^2 \simeq -\frac{1}{2}m_h^2 + \frac{1.2}{\lambda_S}(m_S^2 + \frac{1}{2}m_{750}^2). \tag{4.9}$$

We thus require a tachyonic m_S^2 for the SM Higgs mass condition:

$$m_S^2 \simeq -\frac{1}{2}m_{750}^2 + \frac{\lambda_S}{1.2}(\mu^2 + \frac{1}{2}m_h^2) \lesssim -(500\,\text{GeV})^2 \tag{4.10}$$

where in the last step we have taken $\lambda_S = 1.2$, a rather large value. If we want $\kappa_1 \sim -1$ then we require $m_S^2 \sim -(600\,\text{GeV})^2$. On the other hand, from the second tadpole equation we have

$$m_S^2 = -\kappa_1 v^2 - \frac{1}{2}m_{750}^2, \tag{4.11}$$

which, if we require $|\kappa_1| < 2$, gives

$$-(630\,\text{GeV})^2 \le m_S^2 \le -(400\,\text{GeV})^2, \tag{4.12}$$

so putting these together we find the narrow window

$$-(630\,\text{GeV})^2 \le m_S^2 \le -(500\,\text{GeV})^2. \tag{4.13}$$

Alternative implementation in SARAH

The above discussion suggests to use a different choice for the input parameters of the model in our SARAH implementation: ideally we would like the particle masses, the mixing and only dimensionless couplings to be the inputs. We shall take the input parameters to be

$$m_h, m_{750}, s_\theta, \lambda_S. \tag{4.14}$$

In terms of these the other parameters are determined to be

$$\begin{aligned}\lambda_H &= \frac{c_\theta^2 m_h^2 + s_\theta^2 m_{750}^2}{2v^2}, \qquad v_S^2 = \frac{c_\theta^2 m_{750}^2 + s_\theta^2 m_h^2}{8\lambda_S},\\ m_S^2 &= -\kappa_1 v^2 - \frac{1}{2}m_{750}^2, \qquad \kappa_1 v v_S = s_\theta c_\theta (m_h^2 - m_{750}^2),\\ \to \kappa_1 &= \frac{\sqrt{2\lambda_S}\, s_\theta c_\theta (m_h^2 - m_{750}^2)}{v\sqrt{(c_\theta^2 m_{750}^2 + s_\theta^2 m_h^2)}} \simeq -4.3 \times s_\theta \sqrt{\lambda_S}.\end{aligned} \tag{4.15}$$

The exact version of these equations is implemented in SARAH and can be selected using the InputFile →"SPheno_diphoton.m" option in MakeAll or MakeSPheno.

Octet masses

One further input is taken in [89]: the physical mass of the octet scalars. These are given in terms of the Lagrangian parameters as:

$$\begin{aligned}m_{O_r^0}^2 &= m_O^2 + \kappa_2 v_S^2 + \frac{v^2}{2}(\lambda_1 + \lambda_2 + 2\,\text{Re}\lambda_3),\\ m_{O_i^0}^2 &= m_O^2 + \kappa_2 v_S^2 + \frac{v^2}{2}(\lambda_1 + \lambda_2 - 2\,\text{Re}\lambda_3),\end{aligned}$$

$$m^2_{O^+} = m^2_O + \kappa_2 v_S^2 + \frac{1}{2}\lambda_1 v^2. \tag{4.16}$$

The values of λ_i are taken to be small and equal in order for the octets to have similar masses, but since this is not the general case, we do not impose this choice in SARAH. The choice in that paper does however hide the possibility of tachyonic m^2_O (and hence possible charge/colour breaking minima) – indeed, if we insist that $m^2_O > 0$ we have a lower bound on the masses of

$$m^2_{O^{0,+}} > \frac{\kappa_2}{8\lambda_S} m^2_{750}. \tag{4.17}$$

Clearly this is violated for $m_{O^{0,+}} = 600$ GeV when $\kappa_2 \sim 1, \lambda_S \ll 1$. On the other hand, this does not guarantee a problem.

The desired vacuum has energy

$$\begin{aligned} V_0 &= \frac{m_S^2 v_S^2}{2} - \frac{\lambda_H}{4} v^4 + \lambda_S v_S^4 \\ &\simeq -\frac{1}{8} v^2 m_h^2 - v_S^2 \left(\frac{1}{2}\kappa_1 v^2 + \frac{1}{4} m^2_{750} - \frac{m^2_{750}}{8} \right) \\ &\simeq -\frac{1}{8} v^2 m_h^2 - \frac{m^2_{750}}{8\lambda_S} \left(-2 s_\theta \sqrt{\lambda_S} + \frac{m^2_{750}}{8} \right). \end{aligned} \tag{4.18}$$

If we instead concentrate on the potential terms containing the octets, where only one component develops a VEV, we find

$$\begin{aligned} V(O^R) &= \frac{1}{2}(O^R)^2 \left[m_O^2 + \frac{1}{8}(\lambda_9 + \lambda_{10} + \frac{1}{9}\lambda_6 + \frac{1}{9}\lambda_7 + \frac{1}{9}\lambda_{11})(O^R)^2 \right], \\ V(O^I) &= \frac{1}{2}(O^I)^2 \left[m_O^2 + \frac{1}{8}(\lambda_9 + \lambda_{10} + \frac{1}{9}\lambda_6 + \frac{1}{9}\lambda_7 + \frac{1}{9}\lambda_{11})(O^I)^2 \right], \\ V(O^+) &= |O^+|^2 \left[m_O^2 + \frac{1}{4}(\lambda_9 + \lambda_{10} + \frac{1}{9}\lambda_6 + \frac{1}{9}\lambda_7 + \frac{1}{9}\lambda_{11})|O^+|^2 \right]. \end{aligned} \tag{4.19}$$

Arranging for the additional minimum of the potential to be higher than the colour-breaking one then places a *lower* bound on the octet self-couplings, but for the phenomenology of the diphoton excess – when we neglect loop corrections to the mass of the octet – they play no other role.

Comments on fitting the excess

In [89] the authors find that the diphoton excess can be easily fit with octets at 600 or 1000 GeV and $\kappa_2 \sim 1.5$ or 4.5, respectively. The scenario involves merely the simplifying assumption $\lambda_1 = \lambda_2 = \lambda_3$ so that the octets are of approximately equal mass. The ratio between the digluon and diphoton decay rates is then

$$\frac{\Gamma(S \to gg)}{\Gamma(S \to \gamma\gamma)} \simeq \frac{9}{2}\frac{\alpha_s^2}{\alpha^2}. \tag{4.20}$$

In [89] this is quoted as $\simeq$715. In SARAH, before any NLO corrections are applied, the running of the Standard Model gauge couplings yields $\alpha_s(750\,\text{GeV}) = 0.091$ and we use $\alpha(0) \simeq 137^{-1}$, giving a ratio of 700, in good agreement. However, when we include corrections up to N^{3}LO, this ratio rises to 1150, putting the model near the boundary of exclusion due to dijet production at 8 TeV. These differences are illustrated in plots produced from SARAH/SPheno in Fig. 12. To produce these plots, all branching ratios/widths are calculated in SPheno, as is the production cross-section of the resonance at 8 TeV. To calculate 13 TeV cross-sections the 8 TeV cross-section was rescaled by the parton luminosity factor for gluons of 4.693.

4.2.2 3-3-1 models

Models based on the $\mathrm{SU(3)_c \times SU(3)_L \times U(1)_{\mathcal{X}}}$ gauge symmetry [451–457], 331 for short, constitute an extension of the SM that could explain the number of generations of matter fields. This is possible as anomaly cancellation forces the number of generations to be equal to the number of quark colours.

Regarding the diphoton excess, 331 models automatically include all the required ingredients to explain the hint. First, the usual $SU(2)_L$ Higgs doublet must be promoted to a $SU(2)_L$ triplet, the new component being a singlet under the standard $\mathrm{SU(3)_c \times SU(2)_L \times U(1)_Y}$ symmetry. Similarly, the group structure requires the introduction of new coloured fermions to complete the $SU(3)_L$ quark multiplets, these exotic quarks being $\mathrm{SU(3)_c \times SU(2)_L \times U(1)_Y}$ vector-like singlets after the breaking of $\mathrm{SU(3)_c \times SU(3)_L \times U(1)_{\mathcal{X}}}$. Therefore, $\mathrm{SU(3)_c \times SU(3)_L \times U(1)_{\mathcal{X}}}$ models naturally embed the simple *singlet + vector-like fermions* framework proposed to explain the diphoton excess.

There are several variants of $\mathrm{SU(3)_c \times SU(3)_L \times U(1)_{\mathcal{X}}}$ models. These are characterized by their β parameter,[9] which defines the electric charge operator as[10]

$$Q = T_3 + \beta\, T_8 + \mathcal{X}. \tag{4.21}$$

First, in Sect. 4.2.2.1 we consider the model in Ref. [80]. This 331 variant has $\beta = 1/\sqrt{3}$, which fixes the electric charges of all the states contained in the $SU(2)_L$ triplets and anti-triplets to the usual $0, \pm 1$ values. In Sect. 4.2.2.2 we consider a 331 model with $\beta = -\sqrt{3}$, a value leading to exotic electric charges. This 331 variant has been discussed in the context of the diphoton excess in [88,243,459]. Although the mechanism to explain the diphoton excess is exactly the

[9] See [458] for a complete discussion of 331 models with generic β.

[10] Equation (4.21) assumes that the $SU(3)$ generators are $T_a = \frac{\lambda_a}{2}$, with λ_a ($a = 1, \ldots, 8$) the Gell-Mann matrices. However, this is not the convention used in SARAH, see below.

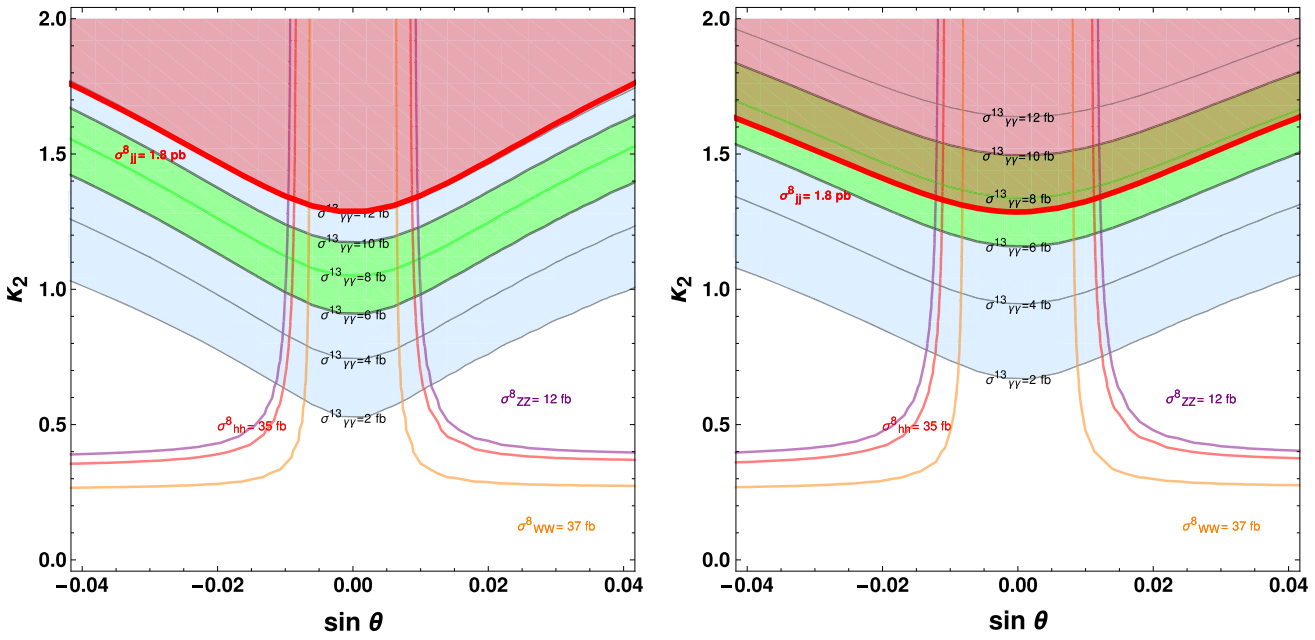

Fig. 12 Scan over sine of Higgs-singlet mixing angle θ and κ_2 for octet masses of 600 GeV, $\lambda_S = 0.07$ corresponding to $v_S \simeq 1000$ GeV. The *contours* show the 750 GeV resonance production cross-sections σ^X_{YY} at energy X TeV decaying into channel YY. *On the left plot*, only leading order contributions to the decays are used; *on the right*, all corrections up to N^{3}LO available in SARAH are included

same as in [80], the presence of the exotic states leads to slightly different numerical results.

On the SU(3) generators in SARAH The most common choice for the $SU(3)$ generators is $T_a = \frac{\lambda_a}{2}$, with λ_a ($a = 1, \ldots, 8$) the Gell-Mann matrices. However, this is just one of the possible representations. In fact, SARAH uses a different set of matrices, $T_a^{\text{SARAH}} = \frac{\Lambda_a}{2}$, following the conventions of Susyno [460]. The relation between the non-diagonal matrices in the two bases is

$$\lambda_1 = \Lambda_1, \tag{4.22a}$$
$$\lambda_2 = \Lambda_4, \tag{4.22b}$$
$$\lambda_4 = -\Lambda_6, \tag{4.22c}$$
$$\lambda_5 = -\Lambda_3, \tag{4.22d}$$
$$\lambda_6 = \Lambda_2, \tag{4.22e}$$
$$\lambda_7 = \Lambda_5. \tag{4.22f}$$

Concerning the diagonal matrices, the usual $\lambda_{3,8}$ Gell-Mann matrices,

$$\lambda_3 = \begin{pmatrix} 1 & 0 & 0 \\ 0 & -1 & 0 \\ 0 & 0 & 0 \end{pmatrix}, \quad \lambda_8 = \frac{1}{\sqrt{3}} \begin{pmatrix} 1 & 0 & 0 \\ 0 & 1 & 0 \\ 0 & 0 & -2 \end{pmatrix}, \tag{4.23}$$

are replaced by $\Lambda_{7,8}$,

$$\Lambda_7 = \frac{1}{\sqrt{3}} \begin{pmatrix} 2 & 0 & 0 \\ 0 & -1 & 0 \\ 0 & 0 & -1 \end{pmatrix}, \quad \Lambda_8 = \begin{pmatrix} 0 & 0 & 0 \\ 0 & 1 & 0 \\ 0 & 0 & -1 \end{pmatrix}. \tag{4.24}$$

The electric charge operator can be written, using the conventions in SARAH, as

$$Q^{\text{SARAH}} = -T_8 - \beta\, T_7 + \mathcal{X}. \tag{4.25}$$

This in turn implies that the charge assignments in the $SU(3)$ multiplets must be adapted as well. For example, one can easily check that the electric charges of the first and third components of a $SU(3)$ triplet t are exchanged when going from the usual Gell-Mann representation to the basis choice employed in SARAH,

$$t = \begin{pmatrix} t_1 \\ t_2 \\ t_3 \end{pmatrix} \quad \longrightarrow \quad t^{\text{SARAH}} = \begin{pmatrix} t_3 \\ t_2 \\ t_1 \end{pmatrix}. \tag{4.26}$$

In the following we will use the standard conventions based on the Gell-Mann matrices in order to keep the discussion as close to the original works as possible. However, we emphasize that the implementation of the 331 models in SARAH requires this dictionary between the bases. It should also be noted that in the current implementation in SARAH of the 331 models described below, vertices involving four vector bosons in the generated model files for CalcHep cannot yet be handled correctly. In order to generate model files that will work with CalcHep, one must therefore exclude these vertices from being written out by SARAH by specifying `Exclude -> {VVVV}` in the options of SARAH's MakeCHep.

Table 7 Fermionic and scalar particle content of the `331-v1` model. The scalar and fermion fields are shown in the top and bottom of the table respectively

Field	Gen.	$SU(3)_C$	$SU(2)_L$	$U(1)_{\mathcal{X}}$	$U(1)_{\mathcal{L}}$	$\mathbb{Z}_2$
Φ_1	1	**1**	$\bar{\mathbf{3}}$	$\frac{2}{3}$	$\frac{2}{3}$	+
Φ_2	1	**1**	$\bar{\mathbf{3}}$	$-\frac{1}{3}$	$-\frac{4}{3}$	+
Φ_3	1	**1**	$\bar{\mathbf{3}}$	$-\frac{1}{3}$	$\frac{2}{3}$	−
Φ_X	1	**1**	$\bar{\mathbf{3}}$	$-\frac{1}{3}$	$-\frac{4}{3}$	+
ψ_L	3	**1**	$\bar{\mathbf{3}}$	$-\frac{1}{3}$	$-\frac{1}{3}$	+
e_R	3	**1**	**1**	-1	-1	+
s	3	**1**	**1**	0	1	+
$Q_L^{1,2}$	2	**3**	**3**	0	$-\frac{2}{3}$	+
Q_L^3	1	**3**	$\bar{\mathbf{3}}$	$\frac{1}{3}$	$\frac{2}{3}$	−
u_R	3	**3**	**1**	$\frac{2}{3}$	0	+
T_R	1	**3**	**1**	$\frac{2}{3}$	0	−
d_R	3	**3**	**1**	$-\frac{1}{3}$	0	−
D_R, S_R	2	**3**	**1**	$-\frac{1}{3}$	0	+

4.2.2.1 331 model without exotic charges

- **Reference:** [80]
- **Model name:** `331/v1`

The model is based on the $\mathrm{SU(3)_c} \times \mathrm{SU(3)_L} \times \mathrm{U(1)}_{\mathcal{X}}$ gauge symmetry, extended with a global $U(1)_{\mathcal{L}}$ and an auxiliary $\mathbb{Z}_2$ symmetry to forbid some undesired couplings. The fermionic and scalar particle content of the model is summarized in Table 7. In addition, due to the extended group structure, the model contains 17 gauge bosons: the usual 8 gluons; 8 W_i bosons associated to $SU(3)_L$ and the B boson associated to $U(1)_{\mathcal{X}}$.

The fermionic $SU(3)_L$ triplets of the model can be decomposed as

$$\psi_L = \begin{pmatrix} \ell^- \\ -\nu \\ N^c \end{pmatrix}_L^{e,\mu,\tau}, \; Q_L^1 = \begin{pmatrix} u \\ d \\ D \end{pmatrix}_L, \; Q_L^2 = \begin{pmatrix} c \\ s \\ S \end{pmatrix}_L, \; Q_L^3 = \begin{pmatrix} b \\ -t \\ T \end{pmatrix}_L. \tag{4.27}$$

The notation used for the extra quarks that constitute the third components of the $SU(3)_L$ triplets $Q_L^{1,2,3}$ is motivated by the fact that their electric charges are $-1/3$ and $2/3$ for D/S and T, respectively. The scalar multiplets can be written as

$$\Phi_1 = \begin{pmatrix} \phi_1 \\ -\phi_1^- \\ S_1^- \end{pmatrix}, \quad \Phi_2 = \begin{pmatrix} \phi_2^+ \\ -\phi_2 \\ S_2 \end{pmatrix}, \quad \Phi_3 = \begin{pmatrix} \phi_3^+ \\ -\phi_3 \\ S_3 \end{pmatrix}, \quad \Phi_X = \begin{pmatrix} \phi_X^+ \\ -\phi_X \\ X \end{pmatrix}. \tag{4.28}$$

While ϕ_1^-, $\phi_{2,3}^+$ and S_1^- are electrically charged scalars, the components $\phi_{1,2,3,X}$, $S_{2,3}$ and X are neutral.

The Yukawa Lagrangian of the model can be split as

$$\mathcal{L}_Y = \mathcal{L}_Y^q + \mathcal{L}_Y^\ell, \tag{4.29}$$

where

$$\begin{aligned} \mathcal{L}_Y^q = {} & \bar{Q}_L^{1,2}\, y^u u_R \Phi_1^* + \bar{Q}_L^3\, \tilde{y}^d d_R \Phi_1 \\ & + \bar{Q}_L^{1,2}\, \bar{y}^d \hat{d}_R \Phi_2^* + \bar{Q}_L^3\, \bar{y}^u T_R \Phi_2 \\ & + \bar{Q}_L^3\, \tilde{y}^u u_R \Phi_3 + \bar{Q}_L^{1,2}\, y^d d_R \Phi_3^* \\ & + \bar{Q}_L^{1,2}\, \bar{y}_X^d \hat{d}_R \Phi_X + \bar{Q}_L^3\, \bar{y}_X^u T_R \Phi_X + \text{h.c.}, \end{aligned} \tag{4.30}$$

and

$$\mathcal{L}_Y^\ell = y^\ell \bar{\psi}_L e_R \Phi_1 + y^a \overline{\psi_L^c} \psi_L \Phi_1 + y^s \bar{\psi}_L\, s\, \Phi_2 + \frac{m_s}{2} \overline{s^c}\, s + \text{h.c.} \tag{4.31}$$

We defined $\hat{d}_R \equiv (D_R, S_R)$. We note that Eq. (4.31) leads to an inverse seesaw mechanism for neutrino masses [461,462]. Here, y^a is anti-symmetric while m_s is symmetric, whereas the rest of Yukawa couplings are generic matrices, including those in Eq. (4.30). An additional term $y_X^s \bar{\psi}_L s \Phi_X$ could be added to Eq. (4.31), but given that $\langle \Phi_X \rangle = 0$, it does not contribute to neutrino masses and we will drop it for simplicity. Finally, the scalar potential is given by

$$\begin{aligned} V = {} & \sum_i \mu_i^2 |\Phi_i|^2 + \lambda_i |\Phi_i|^4 + \sum_{i \neq j} \lambda_{ij} |\Phi_i|^2 |\Phi_j|^2 \\ & + f\,(\Phi_1 \Phi_2 \Phi_3 + \text{h.c.}) + \frac{\kappa}{2} \left[(\Phi_2^\dagger \Phi_X)^2 + \text{h.c.} \right], \end{aligned} \tag{4.32}$$

where $i = 1, 2, 3, X$. The $\mathbb{Z}_2$-soft-breaking term, $f \Phi_1 \Phi_2 \Phi_3$, is required to break unwanted accidental symmetries in the scalar potential.

We will assume the following symmetry breaking pattern

$$\langle \Phi_1 \rangle = \frac{1}{\sqrt{2}} \begin{pmatrix} k_1 \\ 0 \\ 0 \end{pmatrix}, \quad \langle \Phi_2 \rangle = \frac{1}{\sqrt{2}} \begin{pmatrix} 0 \\ 0 \\ n \end{pmatrix}, \quad \langle \Phi_3 \rangle = \frac{1}{\sqrt{2}} \begin{pmatrix} 0 \\ k_3 \\ 0 \end{pmatrix}, \quad \langle \Phi_X \rangle = \begin{pmatrix} 0 \\ 0 \\ 0 \end{pmatrix}. \tag{4.33}$$

4.2.2.2 331 model with exotic charges

- **Reference:** [88] (see also [243,459] for similar constructions)
- **Model name:** `331/v2`

Now, we will consider a 331 variant with $\beta = -\sqrt{3}$, as discussed in the context of the diphoton excess in [88]. The fermionic and scalar particle content of the model is summarized in Table 8. In addition, the model contains 17

Table 8 Fermionic and scalar particle content of the 331-v2 model. The scalar and fermion fields are shown in the top and bottom of the table respectively

Field	Gen.	$SU(3)_C$	$SU(2)_L$	$U(1)_{\mathcal{X}}$
ρ	1	**1**	**3**	1
η	1	**1**	**3**	0
χ	1	**1**	**3**	-1
ψ_L	3	**1**	$\bar{\mathbf{3}}$	-1
e_R	3	**1**	**1**	-1
E_R	3	**3**	**3**	-2
$Q_L^{1,2}$	2	**3**	**3**	$\frac{2}{3}$
Q_L^3	1	**3**	$\bar{\mathbf{3}}$	$-\frac{1}{3}$
u_R	3	**3**	**1**	$\frac{2}{3}$
T_R	1	**3**	**1**	$-\frac{4}{3}$
d_R	3	**3**	**1**	$-\frac{1}{3}$
D_R, S_R	2	**3**	**1**	$\frac{5}{3}$

gauge bosons: the usual 8 gluons; 8 W_i bosons associated to $SU(3)_L$ and the B boson associated to $U(1)_{\mathcal{X}}$.

The fermionic $SU(3)_L$ triplet representations of the model can be decomposed as

$$\psi_L = \begin{pmatrix} \ell^- \\ -\nu \\ E^{--} \end{pmatrix}_L^{e,\mu,\tau}, \; Q_L^1 = \begin{pmatrix} u \\ d \\ D \end{pmatrix}_L, \; Q_L^2 = \begin{pmatrix} c \\ s \\ S \end{pmatrix}_L, \; Q_L^3 = \begin{pmatrix} b \\ -t \\ T \end{pmatrix}_L. \tag{4.34}$$

Due to the choice $\beta = -\sqrt{3}$, the electric charges for the extra quarks that constitute the third components of the $SU(3)_L$ triplets $Q_L^{1,2,3}$ are $5/3, 5/3$ and $-4/3$, respectively. The scalar triplets can be written as

$$\rho = \begin{pmatrix} \rho^+ \\ \rho^0 \\ \rho^{++} \end{pmatrix}, \quad \eta = \begin{pmatrix} \eta^0 \\ \eta_1^- \\ \eta_2^+ \end{pmatrix}, \quad \chi = \begin{pmatrix} \chi^- \\ \chi^{--} \\ \chi^0 \end{pmatrix}. \tag{4.35}$$

Therefore, the particle spectrum of the model contains the exotic quarks in Eq. (4.34), as well as the doubly-charged fermion E^{--} and the scalars ρ^{++} and χ^{--}.

The Yukawa Lagrangian of the model can be split as

$$\mathcal{L}_Y = \mathcal{L}_Y^q + \mathcal{L}_Y^\ell, \tag{4.36}$$

where

$$\begin{aligned} \mathcal{L}_Y^q = {} & y^d \, \overline{Q_L^{1,2}} \, \rho \, d_R + \tilde{y}^d \, \overline{Q_L^3} \, \eta^* \, d_R \\ & + y^u \, \overline{Q_L^{1,2}} \, \eta \, u_R + \tilde{y}^u \, \overline{Q_L^3} \, \rho^* \, u_R \\ & + y^J \, \overline{Q_L^{1,2}} \, \chi \, \hat{d}_R + \tilde{y}^J \, \overline{Q_L^3} \, \chi^* \, T_R + \text{h.c.}, \end{aligned} \tag{4.37}$$

where we have defined $\hat{d}_R \equiv (D_R, S_R)$, and

$$\mathcal{L}_Y^\ell = y^\ell \, \overline{\psi_L} \, \eta^* \, e_R + y^E \, \overline{\psi_L} \, \chi^* \, E_R + \text{h.c.} \tag{4.38}$$

We note that the exotic fermions E, D, S and T only couple to the χ scalar triplet, and thus only via its vacuum expectation value (VEV) they will acquire masses. Finally, the scalar potential is given by

$$\begin{aligned} V = {} & \mu_1^2 |\rho|^2 + \lambda_1 |\rho|^4 + \mu_2^2 |\eta|^2 + \lambda_2 |\eta|^4 + \mu_3^2 |\chi|^2 \\ & + \lambda_3 |\chi|^4 + \lambda_{12} |\rho|^2 |\eta|^2 + \lambda_{13} |\eta|^2 |\chi|^2 \\ & + \lambda_{23} |\eta|^2 |\chi|^2 + + \tilde{\lambda}_{12} (\rho^\dagger \eta)(\eta^\dagger \rho) + \tilde{\lambda}_{13} (\rho^\dagger \chi)(\chi^\dagger \rho) \\ & + \tilde{\lambda}_{23} (\eta^\dagger \chi)(\chi^\dagger \eta) \\ & + \sqrt{2} \, f \left(\epsilon_{ijk} \, \rho^i \eta^j \chi^k + \text{h.c.} \right). \end{aligned} \tag{4.39}$$

We will assume the following symmetry breaking pattern

$$\langle \rho \rangle = \frac{1}{\sqrt{2}} \begin{pmatrix} 0 \\ v_1 \\ 0 \end{pmatrix}, \quad \langle \eta \rangle = \frac{1}{\sqrt{2}} \begin{pmatrix} v_2 \\ 0 \\ 0 \end{pmatrix}, \quad \langle \chi \rangle = \frac{1}{\sqrt{2}} \begin{pmatrix} 0 \\ 0 \\ v_3 \end{pmatrix}. \tag{4.40}$$

In this case, the non-zero VEV of χ is responsible for the breaking $SU(3)_L \times U(1)_X \to SU(2)_L \times U(1)_Y$. The requirement that this occurs at a scale much above the EW scale then imposes a hierarchy amongst the VEVs, namely that $v_3 \gg v_1, v_2$. Consequently, one of the CP-even scalar states is predominantly from the χ triplet and decouples from the SM. This scalar is then identified as the candidate for the 750 GeV resonance in this model. The decays of this state into two photons proceed via loops involving the heavy fermions, as well as those involving the charged scalars and additional charged vector bosons.

4.2.3 E_6-inspired SUSY model with extra $U(1)$

- **Reference:** [110]
- **Model name:** `SUSYmodels/E6SSMalt`

E_6-inspired SUSY models predict extra SM-gauge singlets and extra exotic fermions, so they immediately have the ingredients that many authors have tried to use to fit the diphoton excess. These models are often motivated as a solution to the μ-problem of the MSSM, because the extra $U(1)$ gauge symmetry forbids the μ-term, while when one of the singlet fields develops a VEV at the TeV scale this breaks the extra $U(1)$ giving rise to a massive Z' vector boson and at the same time generates an effective μ term through the singlet interaction with the up- and down-type Higgs fields, $\lambda \hat{S} \hat{H}_u \hat{H}_d$. The matter content of the model at low energies

fills three generations of complete **27**-plet representations of E_6, which ensures that anomalies automatically cancel.

A number of models of this nature have been proposed as explanations of the diphoton excess [110,275,463]. The example we implement here [110] is a variant of the E$_6$SSM [464,465]. In this version two singlet states develop VEVs and the idea is that the 750 GeV excess is explained by one of these singlet states with a loop-induced decay through the exotic states.

In E_6 models the extra $U(1)$ which extends the SM gauge group is given as a linear combination of $U(1)_\psi$ and $U(1)_\chi$ which appear from the breakdown of the E_6 symmetry as $E_6 \to SO(10) \times U(1)_\psi$ followed by $SO(10)$ into $SU(5)$, $SO(10) \to SU(5) \times U(1)_\chi$. In the E$_6$SSM and the variant implemented here the specific combination is,

$$U(1)_N = \frac{1}{4}U(1)_\chi + \frac{\sqrt{15}}{4}U(1)_\psi. \tag{4.41}$$

To allow one-step gauge coupling unification some incomplete multiplets must be included in the low energy matter content. So in addition to the matter filling complete **27** representations of E_6 there are also two $SU(2)$ multiplets $\hat{H}'$ and $\hat{\overline{H}}'$, which are the only components from additional **27′** and $\overline{\mathbf{27}}'$ representations that survive to low energies. All gauge anomalies cancel between these two states, so they do not introduce any gauge anomalies. Furthermore, the low energy matter content of the model beyond the MSSM includes three generations of exotic diquarks,[11] $\hat{D}_i$, $\hat{\overline{D}}_i$, three generations of SM singlet superfields $\hat{S}_i$ and extra Higgs-like states $H^u_{1,2}$ and $H^d_{1,2}$ that do not get VEVs.

The full set of superfields are given in Table 9 along with their representations under $SU(3)$ and $SU(2)$ and their charges under the two U(1) gauge groups and the discrete symmetries, which we will now discuss.

The $\mathbb{Z}_2^L$ symmetry plays a role similar to R-parity in the MSSM, being imposed to avoid rapid proton decay in the model. However with this imposed there are still terms in the superpotential that can lead to dangerous flavour changing neutral currents (FCNCs). To forbid these, an approximate $\mathbb{Z}_2^H$ symmetry is imposed. In the original E$_6$SSM model only $\hat{S}_3$, $\hat{H}_d$ and $\hat{H}_u$ were even under the $\mathbb{Z}_2^H$ symmetry, however in this variant S_2 is also even under this approximate symmetry.

The full superpotential before imposing any discrete symmetries is given by

$$W_{E6} = W_0 + W_1 + W_2, \tag{4.42}$$

Table 9 The representations of the chiral superfields under the $SU(3)_C$ and $SU(2)_L$ gauge groups, and their $U(1)_Y$ and $U(1)_N$ charges without the E_6 normalisation. The GUT normalisations are $\sqrt{\frac{5}{3}}$ for $U(1)_Y$ and $\sqrt{40}$ for $U(1)_N$. The transformation properties under the discrete symmetries $\mathbb{Z}_2^H$, $\mathbb{Z}_2^L$ are also shown, where '+' indicates the superfield is even under the symmetry and '−' indicates that it is odd under the symmetry

Field	Gen	$SU(3)_C$	$SU(2)_L$	$U(1)_Y$	$U(1)_N$	$\mathbb{Z}_2^H$	$\mathbb{Z}_2^L$
$\hat{Q}_i$	3	**3**	**2**	$\frac{1}{6}$	1	−	+
$\hat{u}^c_i$	3	$\overline{\mathbf{3}}$	**1**	$-\frac{2}{3}$	1	−	+
$\hat{d}^c_i$	3	$\overline{\mathbf{3}}$	**1**	$\frac{1}{3}$	2	−	+
$\hat{L}_i$	3	**1**	**2**	$-\frac{1}{2}$	2	−	−
$\hat{e}^c_i$	3	**1**	**1**	1	1	−	−
$\hat{N}^c_i$	3	**1**	**1**	0	0	−	−
$\hat{S}_i$	2	**1**	**1**	0	5	+	+
$\hat{S}_1$	1	**1**	**1**	0	5	−	+
$\hat{H}_u$	1	**1**	**2**	$\frac{1}{2}$	−2	+	+
$\hat{H}_d$	1	**1**	**2**	$-\frac{1}{2}$	−3	+	+
$\hat{H}^u_\alpha$	2	**1**	**2**	$\frac{1}{2}$	−2	−	+
$\hat{H}^d_\alpha$	2	**1**	**2**	$-\frac{1}{2}$	−3	−	+
$\hat{D}_i$	3	**3**	**1**	$-\frac{1}{3}$	−2	−	+
$\hat{\overline{D}}$	3	$\overline{\mathbf{3}}$	**1**	$\frac{1}{3}$	−3	−	+
$\hat{L}_4$	1	**1**	**2**	$-\frac{1}{2}$	2	−	+
$\hat{\overline{L}}_4$	1	**1**	$\overline{\mathbf{2}}$	$\frac{1}{2}$	−2	−	+

where

$$W_0 = \lambda_{ijk}\hat{S}_i\hat{H}^d_j\hat{H}^u_k + \kappa_{ijk}\hat{S}_i\hat{D}_j\hat{\overline{D}}_k + h^N_{ijk}\hat{N}^c_i\hat{H}^u_j\hat{L}_k + h^U_{ijk}\hat{u}^c_i\hat{H}^u_j\hat{Q}_k + h^D_{ijk}\hat{d}^c_i\hat{H}^d_j\hat{Q}_k + h^E_{ijk}\hat{e}^c_i\hat{H}^d_j\hat{L}_k, \tag{4.43}$$

$$W_1 = g^Q_{ijk}\hat{D}_i\hat{Q}_j\hat{Q}_k + g^q_{ijk}\hat{\overline{D}}_i\hat{d}^c_j\hat{u}^c_k, \tag{4.44}$$

$$W_2 = g^N_{ijk}\hat{N}^c_i\hat{D}_j\hat{d}^c_k + g^E_{ijk}\hat{e}^c_i\hat{D}_j\hat{u}^c_k + g^D_{ijk}\hat{Q}_i\hat{L}_j\hat{\overline{D}}_k. \tag{4.45}$$

However, with the discrete symmetries imposed and integrating out the heavy right-handed neutrinos, the superpotential in this specific variant reduces to,[12]

$$\begin{aligned} W_{E_6SSM\text{ variant}} &= W^{(\mu=0)}_{MSSM} \\ &+ \sum_{\alpha=2}^{3}\sum_{i=1}^{3}\hat{S}^\alpha(\lambda_{\alpha i}\hat{H}^i_u\hat{H}^i_d + \kappa_{\alpha i}\hat{D}^i\hat{\overline{D}}^i) \\ &+ \mu'\hat{H}'\hat{\overline{H}}' + h^E_{4j}(\hat{H}_d\hat{H}')\hat{e}^c_j \end{aligned} \tag{4.46}$$

[11] In the original E$_6$SSM these states could be either diquark or leptoquark in nature, depending on the choice of a discrete symmetry, but in the model considered here the allowed superpotential terms for the decay of these exotic quarks imply they are diquark.

[12] In the paper proposing this variant to explain the excess [110], the terms involving the surviving Higgs states on the second line are omitted from the superpotential.

One should remember that the $\mathbb{Z}_2^H$ can only be an approximate symmetry as otherwise the exotic quarks could not decay. In this variant the exotic quarks decay through the $\mathbb{Z}_2^H$ violating interactions of W_1.

In the paper it is assumed that the singlet mixing can be negligible and the numerical calculation was performed under this assumption, neglecting any mixing between the singlet state which decays to $\gamma\gamma$ via the exotic states and the other CP-even Higgs states from the standard $SU(2)$ doublets. However it is clear that there must be some mixing from the D-terms, and therefore if that is included one important check would be to test whether other decays are sufficiently suppressed. Moreover, the parameters needed to simultaneously get a 125 GeV SM-like Higgs state and a 750 GeV singlet-dominated state are not given. In this respect we note that the singlet VEVs appear both in the diagonal entries of the mass matrix and in the off-diagonal entries that mix the singlet states with the doublet states.

We finally note that other similar E_6 models have also been proposed in the context of the diphoton excess. These include a model by two authors from the original paper [275], a model with a different $U(1)$ group at low energies [466], and a model that is still E_6-inspired, but where no extra $U(1)$ survives down to low energies [269].

5 Study of a natural SUSY explanation for the diphoton excess

We show in this section how one can use the described setup to perform easily a detailed study of a new model that aims at explaining the diphoton anomaly. This model was not proposed before in the literature to explain the diphoton excess and offers a very rich phenomenology. We will not only discuss the main phenomenological features of the model, but we will also show the necessary steps to obtain this information with the discussed tools. However, we emphasise once again that we are not aiming at a thorough exploration of the entire phenomenology of the model, something that would be clearly beyond the purpose of this example.

5.1 The model

We are now going to study a SUSY model which enhances the tree-level Higgs mass due to non-decoupling D-terms. The model is based on that proposed in Ref. [467] as a natural SUSY model which allows for light stops compatible with the measured Higgs boson mass, extended by three generations of pairs of vector-like quarks and leptons. We want to achieve a tree-level enhancement of the SM-like Higgs mass and an explanation of the diphoton excess via the loop-induced decay of a CP-odd scalar. In addition, we will also check whether one can get a broad diphoton resonance in this model.

Table 10 Scalars and fermions in the $U(1)_X$-extended MSSM

SF	Spin 0	Spin $\frac{1}{2}$	Generations	$U(1)_Y$	$SU(2)_L$	$SU(3)_C$	$U(1)_X$
$\hat{q}$	$\tilde{q}$	q	3	$\frac{1}{6}$	**2**	**3**	0
$\hat{l}$	$\tilde{l}$	l	3	$-\frac{1}{2}$	**2**	**1**	0
$\hat{d}$	$\tilde{d}_R^*$	d_R^*	3	$\frac{1}{3}$	**1**	$\overline{\mathbf{3}}$	$\frac{1}{2}$
$\hat{u}$	$\tilde{u}_R^*$	u_R^*	3	$-\frac{2}{3}$	**1**	$\overline{\mathbf{3}}$	$-\frac{1}{2}$
$\hat{e}$	$\tilde{e}_R^*$	e_R^*	3	1	**1**	**1**	$\frac{1}{2}$
$\hat{\nu}$	$\tilde{\nu}_R^*$	ν_R^*	3	0	**1**	**1**	$-\frac{1}{2}$
$\hat{U}$	$\tilde{U}^*$	U^*	3	$-\frac{2}{3}$	**1**	$\overline{\mathbf{3}}$	$-\frac{1}{2}$
$\hat{\bar{U}}$	$\tilde{\bar{U}}$	$\bar{U}$	3	$\frac{2}{3}$	**1**	**3**	$\frac{1}{2}$
$\hat{E}$	$\tilde{E}^*$	E^*	3	1	**1**	**1**	$\frac{1}{2}$
$\hat{\bar{E}}$	$\tilde{\bar{E}}$	$\bar{E}$	3	-1	**1**	**1**	$-\frac{1}{2}$
$\hat{H}_d$	H_d	$\tilde{H}_d$	1	$-\frac{1}{2}$	**2**	**1**	$-\frac{1}{2}$
$\hat{H}_u$	H_u	$\tilde{H}_u$	1	$\frac{1}{2}$	**2**	**1**	$\frac{1}{2}$
$\hat{\eta}$	η	$\tilde{\eta}$	1	0	**1**	**1**	-1
$\hat{\bar{\eta}}$	$\bar{\eta}$	$\tilde{\bar{\eta}}$	1	0	**1**	**1**	1
$\hat{S}$	S	$\tilde{S}$	1	0	**1**	**1**	0

The matter field content is shown in Table 10 and the considered superpotential reads:

$$\begin{aligned} W = & -Y_d\,\hat{d}\,\hat{q}\,\hat{H}_d - Y_e\,\hat{e}\,\hat{l}\,\hat{H}_d + Y_u\,\hat{u}\,\hat{q}\,\hat{H}_u \\ & + Y_\nu\,\hat{\nu}\,\hat{l}\,\hat{H}_u + Y_x\,\hat{\nu}\,\hat{\bar{\eta}}\,\hat{\nu} + (\mu + \lambda\hat{S})\,\hat{H}_u\,\hat{H}_d \\ & + \hat{S}(\xi + \lambda_X\,\hat{\eta}\,\hat{\bar{\eta}}) + M_S\,\hat{S}\,\hat{S} \\ & + \frac{1}{3}\kappa\,\hat{S}\,\hat{S}\,\hat{S} + \tilde{M}_E\hat{e}\hat{\bar{E}} + \tilde{M}_U\hat{u}\hat{\bar{U}} \\ & + \hat{S}(\lambda_e\,\hat{E}\,\hat{\bar{E}} + \lambda_u\,\hat{U}\,\hat{\bar{U}}) + M_e\,\hat{E}\,\hat{\bar{E}} + M_u\,\hat{U}\,\hat{\bar{U}} \\ & + Y'_e\,\hat{E}\,\hat{l}\,\hat{H}_d + Y'_u\,\hat{U}\,\hat{q}\,\hat{H}_u. \end{aligned} \tag{5.1}$$

We will not make the simplifying assumption that mixings between the MSSM states and the new vector-like fields can be neglected. Of course, such mixing could have been forbidden by choosing different $U(1)_X$ charges for the new particles. However, in such case there would be a conserved $\mathbb{Z}_2$ symmetry associated to the vector-like states (under which all vector-like superfields are odd and the rest are even) that would make the lightest of them absolutely stable. This would be a problem unless that state is neutral and colourless, and thus this scenario can only be viable if we also consider additional singlet vector-like states, such as vector-like partners for the right-handed neutrinos, and make them lighter than the other vector-like states. Thus, this setup would predict two stable particles to make the dark matter. Such a scenario could also be studied with the tools presented here. However, we decided not to consider this option in the following.

The other main ingredients of the model are the general soft-SUSY breaking terms, which read

$$\begin{aligned}
-\mathcal{L} = &\big[T_d \tilde{d}\tilde{q} H_d + (T_e \tilde{e} + T'_e \tilde{E})\tilde{l} H_d + (T_u \tilde{u} + T'_u \tilde{U})\tilde{q} H_u \\
&+ T_\nu \tilde{\nu}\tilde{l} H_u + T_x \tilde{\nu}\bar{\eta}\tilde{\nu} + (B_\mu + T_\lambda S) H_u H_d \\
&+ S(t_\xi + T_X \eta\bar{\eta}) + B_S SS \\
&+ \frac{1}{3} T_\kappa SSS + S(T_E \tilde{E}\tilde{\bar{E}} + T_U \tilde{U}\tilde{\bar{U}}) \\
&+ B_E \tilde{E}\tilde{\bar{E}} + B_U \tilde{U}\tilde{\bar{U}} + \tilde{B}_E \tilde{e}\tilde{\bar{E}} + \tilde{B}_U \tilde{u}\tilde{\bar{U}} + \text{h.c.}\big] \\
&+ \tilde{q}^\dagger m_q^2 \tilde{q} + \tilde{u}^\dagger m_u^2 \tilde{u} \\
&+ \tilde{d}^\dagger m_d^2 \tilde{d} + \tilde{e}^\dagger m_e^2 \tilde{e} + \tilde{l}^\dagger m_l^2 \tilde{l} + \tilde{U}^\dagger m_U^2 \tilde{U} \\
&+ \tilde{\bar{U}}^\dagger m_{\bar{U}}^2 \tilde{\bar{U}} + \tilde{E}^\dagger m_E^2 \tilde{E} + \tilde{\bar{E}}^\dagger m_{\bar{E}}^2 \tilde{\bar{E}} \\
&+ (\tilde{U}^\dagger m_{Uu}^2 \tilde{u} + \tilde{E}^\dagger m_{Ee}^2 \tilde{E} + \text{h.c.}) + m_{H_d}^2 |H_d|^2 \\
&+ m_{H_u}^2 |H_u|^2 + m_{H_s}^2 |S|^2 + m_\eta^2 |\eta|^2 + m_{\bar{\eta}}^2 |\bar{\eta}|^2 \\
&+ (M_1 \lambda_B \lambda_B + M_2 \lambda_W \lambda_W \\
&+ M_3 \lambda_g \lambda_g + M_X \lambda_X \lambda_X + M_{1X} \lambda_B \lambda_X + \text{h.c.})
\end{aligned} \tag{5.2}$$

Note that we have included the gaugino mass term M_{1X} arising from gauge kinetic mixing. All the terms shown in Eq. (5.2) are automatically added by SARAH based on the information provided by the user about the particle content and the superpotential. Several scalar fields acquire VEVs. We decompose them as

$$H_d^0 = \frac{1}{\sqrt{2}}(\phi_d + v_d + i\sigma_d), \quad H_u^0 = \frac{1}{\sqrt{2}}(\phi_u + v_u + i\sigma_u), \tag{5.3}$$

$$\eta = \frac{1}{\sqrt{2}}\left(\phi_\eta + v_\eta + i\sigma_\eta\right), \quad \bar{\eta} = \frac{1}{\sqrt{2}}\left(\phi_{\bar{\eta}} + v_{\bar{\eta}} + i\sigma_{\bar{\eta}}\right), \tag{5.4}$$

$$S = \frac{1}{\sqrt{2}}(\phi_s + v_S + i\sigma_s). \tag{5.5}$$

We define $\tan\beta = \frac{v_u}{v_d}$, $v = \sqrt{v_d^2 + v_u^2}$ as well as $\tan\beta_x = \frac{v_\eta}{v_{\bar{\eta}}}$, $x = \sqrt{v_\eta^2 + v_{\bar{\eta}}^2}$. In addition, the sneutrinos are decomposed with respect to their CP eigenstates,

$$\tilde{\nu}_{L,i} \to \frac{1}{\sqrt{2}}\left(\phi_{L,i} + i\sigma_{L,i}\right), \quad \tilde{\nu}_{R,i} \to \frac{1}{\sqrt{2}}\left(\phi_{R,i} + i\sigma_{R,i}\right), \tag{5.6}$$

which in general have different masses due to the Majorana mass-term $Y_X\langle\bar{\eta}\rangle$ in the superpotential. Since H_d^0 and H_u^0 carry charges under both $U(1)$ gauge groups, there will be non-zero Z–Z' mixing even in the limit of vanishing gauge kinetic mixing. The list of particle mixings, which go beyond the usual MSSM mixings reads

$$(B, W_3, B') \longrightarrow (\gamma, Z, Z'), \tag{5.7}$$

$$(\phi_d, \phi_u, \phi_\eta, \phi_{\bar{\eta}}, \phi_s) \longrightarrow h_i, \quad i = 1\ldots5, \tag{5.8}$$

$$(\sigma_d, \sigma_u, \sigma_\eta, \sigma_{\bar{\eta}}, \sigma_s) \longrightarrow A_i^0, \quad i = 1\ldots5, \tag{5.9}$$

$$(\phi_{L,i}, \phi_{R,i}) \longrightarrow \tilde{\nu}_j^R, \quad i = 1\ldots3,\ j = 1\ldots6, \tag{5.10}$$

$$(\sigma_{L,i}, \sigma_{R,i}) \longrightarrow \tilde{\nu}_j^I, \quad i = 1\ldots3,\ j = 1\ldots6, \tag{5.11}$$

$$(\tilde{B}, \tilde{W}_3, \tilde{H}_d^0, \tilde{H}_u^0, \tilde{X}, \tilde{\eta}, \tilde{\bar{\eta}}, \tilde{S}) \longrightarrow \tilde{\chi}_i^0, \quad i = 1\ldots8, \tag{5.12}$$

$$(e_{L,i}, \bar{E}_i^*)/(e_{R,i}, E_i) \longrightarrow e_j, \quad i = 1\ldots3,\ j = 1\ldots6, \tag{5.13}$$

$$(u_{L,i}, \bar{U}_i^*)/(u_{R,i}, U_i) \longrightarrow u_i, \quad i = 1\ldots3,\ j = 1\ldots6, \tag{5.14}$$

$$(\tilde{e}_{L,i}, \tilde{e}_{R,i}, \tilde{E}_i, \tilde{\bar{E}}_i) \longrightarrow \tilde{e}_j, \quad i = 1\ldots3,\ j = 1\ldots12, \tag{5.15}$$

$$(\tilde{u}_{L,i}, \tilde{u}_{R,i}, \tilde{U}_i, \tilde{\bar{U}}_i) \longrightarrow \tilde{u}_j, \quad i = 1\ldots3,\ j = 1\ldots12, \tag{5.16}$$

The model files which implement this model in SARAH are available in the SARAH model repository as U1xMSSM3G. A FlexibleSUSY model file for the model is also available in the current release of FlexibleSUSY. Finally, we provide all files to reproduce the computations that follow at http://sarah.hepforge.org/U1xMSSM_example.tar.gz.

5.2 Analytical results with Mathematica

Before we perform a numerically precise study of the model, we show how already with just SARAH and Mathematica one can gain a lot of information about a new model.

5.2.1 Consistency checks

The model is initialised after loading it in SARAH via

```
<<SARAH.m;
Start["U1xMSSM"];
```

SARAH automatically performs some basic consistency checks for the model. For instance, it checks whether the model is free from gauge anomalies:

Table 11 Fermions in the considered model. We show here the names used by SARAH during the Mathematica session as well as the names in the output files for Monte-Carlo tools. Here, g denotes a generation index and c a colour index

LaTeX	SARAH	Output
$\tilde{\chi}_i^- = \begin{pmatrix} \lambda_i^- \\ \lambda_i^{+,*} \end{pmatrix}$	Cha[{g}] = (Lm[{g}] / conj[Lp[{g}]])	C
$\tilde{\chi}_i^0 = \begin{pmatrix} \lambda_i^0 \\ \lambda_i^{0,*} \end{pmatrix}$	Chi[{g}] = (L0[{g}] / conj[L0[{g}]])	N
$d_{i\alpha} = \begin{pmatrix} D_{L,i\alpha} \\ D_{R,i\alpha}^* \end{pmatrix}$	Fd[{g, c}] = (FDL[{g, c}] / conj[FDR[{g, c}]])	d
$e_i = \begin{pmatrix} E_{L,i} \\ E_{R,i}^* \end{pmatrix}$	Fe[{g}] = (FEL[{g}] / conj[FER[{g}]])	e
$u_{i\alpha} = \begin{pmatrix} U_{L,i\alpha} \\ U_{R,i\alpha}^* \end{pmatrix}$	Fu[{g, c}] = (FUL[{g, c}] / conj[FUR[{g, c}]])	u
$\nu_i = \begin{pmatrix} \lambda_{\nu,i} \\ \lambda_{\nu,i}^* \end{pmatrix}$	Fv[{g}] = (Fvm[{g}] / conj[Fvm[{g}]])	nu
$\tilde{g}_\alpha = \begin{pmatrix} \lambda_{\tilde{g},\alpha} \\ \lambda_{\tilde{g},\alpha}^* \end{pmatrix}$	Glu[{c}] = (fG[{c}] / conj[fG[{c}]])	go

```
Checking for anomalies:
 {(hypercharge)^3, (left)^3,  (color)^3, (extra)^3,
  (hypercharge)x(gravity)^2,
  (extra)x(gravity)^2,
  (left)^2 x hypercharge,
  (color)^2 x hypercharge,
  (extra)^2 x hypercharge,
  (hypercharge)^2 x extra,
  (left)^2 x extra,
  (color)^2 x extra,
   Witten Anomalyleft}
```

One can see that SARAH tests all different combinations of gauge anomalies and, given that no warning is printed on the screen, confirms that all of them cancel. Similarly, it also checks that all terms in the superpotential are in agreement with all global and local symmetries. More detailed checks can be carried out by running CheckModel[] when the initialisation is finished.

After a few seconds, a message is printed telling that the model is loaded.

```
All Done. U1xMSSM is ready!
```

5.2.2 Particles and parameters

An overview of all particles and parameters present in this model is given in Tables 11, 12 and 13. The user has also access to this information by calling

```
Particles[EWSB]
```

to get all particles present after EWSB and by calling

```
parameters
```

to see all existing parameters. Moreover, it is possible to get similar tables as the ones shown here in LaTeX-format for each model via the commands

```
ModelOutput[EWSB];
MakeTeX[WriteSARAH->True];
```

5.2.3 Gauge sector

Before we discuss the matter sector or the scalar potential, we have a brief look at the gauge bosons. We make use of the mass matrices calculated by SARAH during the initialisation of the model. We find a handy expression for the mass matrix of the neutral gauge bosons in the limit of vanishing gauge kinetic mixing ($g_{X1} = g_{1X} = 0$) via

```
matV = Simplify[MassMatrix[VZp] /. {gX1 -> 0, g1X -> 0}]
  //. {vd^2 + vu^2 -> v^2,  x1^2 + x2^2 -> x^2}
```

Table 12 Scalars, vector bosons and ghosts in the considered model. We show here the names used by SARAH during the Mathematica session as well as the names in the output files for Monte-Carlo tools. Here, t denotes a generation index and c a colour index

LaTeX	SARAH	Output	LaTeX	SARAH	Output
$\tilde{d}_{i\alpha}$	Sd[{g, c}]	sd	$\tilde{u}_{i\alpha}$	Su[{g, c}]	su
$\tilde{e}_i$	Se[{g}]	se	ν_i^j	SvIm[{g}]	nI
ν_i^R	SvRe[{g}]	nR	h_i	hh[{g}]	h
A_i^0	Ah[{g}]	Ah	H_i^-	Hpm[{g}]	{Hm, Hp}
$g_{\alpha\rho}$	VG[{c, lorentz}]	g	γ_ρ	VP[{lorentz}]	A
Z_ρ	VZ[{lorentz}]	Z	Z'_ρ	VZp[{lorentz}]	Zp
W_ρ^-	VWm[{lorentz}]	{Wm, Wp}			
η_α^G	gG[{c}]	gG	η^γ	gP	gA
η^Z	gZ	gZ	$\eta^{Z'}$	gZp	gZp
η^-	gWm	gWm	η^+	gWmC	gWpC

which reads

$$\begin{pmatrix} \frac{g_1^2 v^2}{4} & -\frac{1}{4} g_1 g_2 v^2 & \frac{1}{4} g_1 g_X v^2 \\ -\frac{1}{4} g_1 g_2 v^2 & \frac{g_2^2 v^2}{4} & -\frac{1}{4} g_2 g_X v^2 \\ \frac{1}{4} g_1 g_X v^2 & -\frac{1}{4} g_2 g_X v^2 & \frac{1}{4} g_X^2 \left(v^2 + 4x^2\right) \end{pmatrix}. \tag{5.17}$$

Note, that MassMatrix[VP] and MassMatrix[VZ] would have given the same result. We can check the eigenvalues of this matrix to first order in $\frac{v^2}{x^2}$ using the Series command of Mathematica

```
Simplify[Normal[Series[Eigenvalues[matV]
  /. v -> r x, {r, 0, 2}]] /. r -> v/x, {x > 0, gX > 0}]
```

and find

$$\left\{0, \quad \frac{1}{4}(g_1^2 + g_2^2)v^2, \quad \frac{1}{4} g_X^2 (4x^2 + v^2)\right\} \tag{5.18}$$

As expected, the first two eigenvalues are just the ones of the SM gauge bosons, while the mass of the new gauge boson is given by

$$M_{Z'} = \frac{1}{2} g_X \sqrt{4x^2 + v^2}. \tag{5.19}$$

We will use this relation in the following to replace x by $M_{Z'}$ in all equations.

5.2.4 Scalar sector

Solving the tadpole equations We turn now to the scalar sector of the model. First, we make a list with a few simplifying assumptions which we are going to use in the following

```
assumptions = {
 conj[x_] -> x, RXi[__] -> 0,
 gX1 -> 0, g1X -> 0,
 x1 -> X/Sqrt[2], x2 -> X/Sqrt[2],
       X -> Sqrt[4 MZp^2 - gX^2 v^2]/(2 gX),
 vd -> v Cos[ArcTan[TB]], vu -> v Sin[ArcTan[TB]],
 T[kappa] -> 0 , kappa -> 0,
       T[lambdaH] -> 0, lambdaH -> 0, L[lw] -> 0};
```

Here we assume all parameters to be real, remove any complex conjugation (conj) and use the Landau gauge (RXi[_]->0), then we turn off again gauge kinetic mixing and take the VEVs of η and $\bar{\eta}$ to be equal. In the fourth line, we parametrise v_d and v_u as usual in terms of v and $\tan\beta$. Finally, we set the parameters κ, T_κ, λ, T_λ and L_ξ to zero. We can now solve the tadpole equations, stored by SARAH in TadpoleEquations[Eigenstates], with respect to the parameters $m^2_{H_d}, m^2_{H_u}, m^2_\eta, m^2_S$ and ξ using the aforementioned assumptions:

Table 13 Names of parameters in the considered model used by SARAH within Mathematica and in the output for other codes

LaTeX	SARAH	Output	LaTeX	SARAH	Output	LaTeX	SARAH	Output
g_1	g1	g1	g_2	g2	g2	g_3	g3	g3
g_X	gX	gX	g_{YX}	g1X	gYX	g_{XY}	gX1	gXY
lw	lw	lw	L_{lw}	L[lw]	Llw	$\tilde{M}_E$	MtE	MtE
$\tilde{B}_E$	B[MtE]	BtE	M_E	MVE	mve	B_E	B[MVE]	Bmve
μ	\[Mu]	Mu	B_μ	B[\[Mu]]	Bmu	M_S	MS	ms
B_S	B[MS]	Bms	$\tilde{M}_U$	MtU	MtU	$\tilde{B}_U$	B[MtU]	BtU
M_U	MVU	mvu	B_U	B[MVU]	Bmvu	Y_d	Yd	Yd
T_d	T[Yd]	Td	Y_e	Ye	Ye	T_e	T[Ye]	Te
Y'_e	Yep	yep	T'_e	T[Yep]	Tyep	λ_C	lambdaC	lamc
T_{λ_C}	T[lambdaC]	Tlc	λ_E	lambdaE	lame	T_{λ_E}	T[lambdaE]	Tle
λ_H	lambdaH	lamh	T_{λ_H}	T[lambdaH]	Tlh	κ	kappa	kap
T_κ	T[kappa]	Tkap	λ_U	lambdaU	lamu	T_{λ_U}	T[lambdaU]	Tlu
Y_u	Yu	Yu	T_u	T[Yu]	Tu	Y'_u	Yup	yup
T'_u	T[Yup]	Tyup	Y_x	Yn	Yx	T_x	T[Yn]	Tx
Y_ν	Yv	Yv	T_ν	T[Yv]	Tv	m_q^2	mq2	mq2
m_l^2	ml2	ml2	$m_{H_d}^2$	mHd2	mHd2	$m_{H_u}^2$	mHu2	mHu2
m_d^2	md2	md2	m_u^2	mu2	mu2	m_{uUX}^2	muUX2	muux2
m_e^2	me2	me2	m_{eEX}^2	meEX2	meex2	m_ν^2	mvR2	mv2
m_η^2	mC12	mC12	$m_{\bar{\eta}}^2$	mC22	mC22	m_S^2	mS2	ms2
m_{UX}^2	mUX2	mux2	m_{UXp}^2	mUXp2	muxp2	m_{EX}^2	mEX2	mex2
m_{EXp}^2	mEXp2	mexp2	M_1	MassB	M1	M_2	MassWB	M2
M_3	MassG	M3	M_{BL}	MassBX	MBp	$M_{BB'}$	MassBBX	MBBp
v_d	vd	vd	v_u	vu	vu	v_η	x1	x1
$v_{\bar{\eta}}$	x2	x2	xS	xS	xS	$Z^{\gamma ZZ'}$	ZZ	ZZ
Z^W	ZW	ZW	$Z^{\tilde{W}}$	ZfW	ZfW	$\phi_{\tilde{g}}$	PhaseGlu	pG
Z^D	ZD	ZD	Z^U	ZU	ZU	Z^E	ZE	ZE
Z^i	ZVI	ZVI	Z^R	ZVR	ZVR	Z^H	ZH	ZH
Z^A	ZA	ZA	Z^+	ZP	ZP	N	ZN	ZN
U	UM	UM	V	UP	UP	U^V	UV	UV
U_L^e	ZEL	ZEL	U_R^e	ZER	ZER	U_L^d	ZDL	ZDL
U_R^d	ZDR	ZDR	U_L^u	ZUL	ZUL	U_R^u	ZUR	ZUR
e	e	el	Θ_W	ThetaW	TW	β	\[Beta]	betaH
Θ'_W	ThetaWp	TWp	α^{-1}	v	v	v		

```
sol = Simplify[
 Solve[(TadpoleEquations[EWSB] //. assumptions) == 0,
   {mHd2, mHu2, mC12, lw, mS2}][[1]]
                ];
```

We have saved the solution in the variable sol for further usage.

Obtaining a 750 GeV pseudo-scalar We use the solution and our assumptions to get simpler expressions for the mass matrix of the CP-even (called hh) and CP-odd (called Ah) scalars:

```
mH = FullSimplify[MassMatrix[hh] /. sol //. assumptions]
mA = FullSimplify[MassMatrix[Ah] /. sol //. assumptions]
```

These matrices can be expressed as

$$m_H^2 \simeq \begin{pmatrix} m_H^{2,\mathrm{MSSM}} & m_H^{2,\mathrm{mix}} \\ (m_H^{2,\mathrm{mix}})^T & m_H^{2,X} \end{pmatrix}, \quad m_A^2 \simeq \begin{pmatrix} m_A^{2,\mathrm{MSSM}} & 0 \\ 0 & m_A^{2,X} \end{pmatrix} \tag{5.20}$$

with

$$m_H^{2,\mathrm{MSSM}} \simeq \begin{pmatrix} t_\beta B(\mu) + \frac{v^2(g_1^2+g_2^2+g_X^2)}{4\left(t_\beta^2+1\right)} & -B(\mu) - \frac{t_\beta v^2(g_1^2+g_2^2+g_X^2)}{4\left(t_\beta^2+1\right)} \\ -B(\mu) - \frac{t_\beta v^2(g_1^2+g_2^2+g_X^2)}{4\left(t_\beta^2+1\right)} & \frac{B(\mu)}{t_\beta} + \frac{t_\beta^2 v^2(g_1^2+g_2^2+g_X^2)}{4\left(t_\beta^2+1\right)} \end{pmatrix}, \tag{5.21}$$

$$m_H^{2,\mathrm{mix}} \simeq \begin{pmatrix} \frac{1}{4} g_X v \sqrt{\frac{4M_{Z'}^2 - g_X^2 v^2}{2t_\beta^2+2}} & -\frac{1}{4} g_X v \sqrt{\frac{4M_{Z'}^2 - g_X^2 v^2}{2t_\beta^2+2}} & 0 \\ -\frac{1}{4} g_X t_\beta v \sqrt{\frac{4M_{Z'}^2 - g_X^2 v^2}{2t_\beta^2+2}} & \frac{1}{4} g_X t_\beta v \sqrt{\frac{4M_{Z'}^2 - g_X^2 v^2}{2t_\beta^2+2}} & 0 \end{pmatrix}, \tag{5.22}$$

$$m_A^{2,\mathrm{MSSM}} \simeq \begin{pmatrix} t_\beta B(\mu) & B(\mu) \\ B(\mu) & \frac{B(\mu)}{t_\beta} \end{pmatrix}. \tag{5.23}$$

We omit here the analytical expressions for $m_A^{2,X}$ and $m_H^{2,X}$ because of their length and since they are not needed for the following brief discussion. The mass matrix for the CP-odd states is block-diagonal since the MSSM part is unchanged, while we have mixing in the CP-even sector among all five components.[13] The additional D-Terms can be found in the MSSM block, $m_H^{2,\mathrm{MSSM}}$. This also explains our choice of a pseudo-scalar as the resonance behind the diphoton excess: the tree-level mixing between the scalar singlet and the doublets would cause tree-level decays of a 750 GeV scalar into all kinds of SM particles. In particular, those into WW and ZZ are constrained and could easily spoil our setup as an explanation of the excess in this model. Of course, we have to check whether it is possible to obtain a pseudo-scalar of the correct mass, and get the corresponding scalar sufficiently heavy so as to escape detection. For that purpose, we calculate the eigenvalues of the lower 3×3 block of the pseudo-scalar mass matrix, and fix B_S by demanding to have a pseudo-scalar of the correct mass:

```
Eigenvalues[Take[mA, {3, 5}, {3,5}]];
sol750 = Solve[%[[2]] == M750^2, B[MS]][[1]];
```

We now make an arbitrary choice for the numerical values of the remaining parameters, except $m_{\tilde{\eta}}^2$ and $M_{Z'}$,

```
num =  {g1 -> 0.36, g2 -> 0.65, v -> 246,
  B[\[Mu]] -> 10^6, \[Mu] -> 1000,
  TB -> 20, gX -> 0.5, MS -> -100, xS -> 500,
  T[lambdaC] -> -200, lambdaC -> -0.2, M750 -> 750}
```

and calculate all CP-even and CP-odd mass eigenvalues for specific values of $m_{\tilde{\eta}}^2$ and $M_{Z'}$:

```
Sqrt /@ Eigenvalues[
  MassMatrix[Ah] //. assumptions //. sol /. sol750  ↪
      //. assumptions /.
     num /. mC22 -> 10^6 /. MZp -> 3000 ]
Sqrt /@ Eigenvalues[
  MassMatrix[hh] //. assumptions //. sol /. sol750 //. ↪
      assumptions /.
     num /. mC22 -> 10^6 /. MZp -> 3000 ]
```

The results are

```
{4477.72, 1792.7, 750., 6.60725*10^-6, 0.}
{4477.74, 3319.15, 2797.53, 822.054, 94.6205}
```

[13] The mixing between the MSSM scalars and S is vanishing here only because of our simplifying assumption $\lambda = 0$ but is non-zero in general.

Thus, as expected, we have two massless (up to numerical errors) states in the CP-odd sector, which are the neutral Goldstone bosons to be eaten by the Z and Z' gauge bosons, accompanied by a particle with a mass of 750 GeV. In the scalar sector we find the lightest state with a mass very close to M_Z and another scalar below 1 TeV. However, checking the composition of the 750 and 825 GeV particles via

```
Eigensystem[MassMatrix[hh] //. assumptions //. sol /. ↪
    sol750 //. assumptions /.
     num /. mC22 -> 10^6 /. MZp -> 3000 ][[2, -2]]
 {0., 0., -0.704932, -0.704932, -0.0783774}
Eigensystem[MassMatrix[Ah] //. assumptions //. sol /. ↪
    sol750 //. assumptions /.
     num /. mC22 -> 10^6 /. MZp -> 3000 ][[2, -3]]
 {0., 0., -0.299786, -0.299786, 0.90568}
```

we see that the CP-odd state is, as expected, mainly a singlet while the CP-even one is mainly a X-Higgs (composed by ϕ_η and $\phi_{\bar{\eta}}$). That looks already very promising.

and create a contour plot using this function. The result is depicted in Fig. 13, where one sees that for $m_{\bar{\eta}} \gg M_{Z'}$ it is indeed possible to find a tree-level mass well above 100 GeV, while for $m_{\bar{\eta}} \ll M_{Z'}$ the tree-level mass approaches M_Z.

Is there a second light scalar? One can now start to play also with the values we have chosen for `num` to see how the eigenvalues of both matrices change. One finds, for instance, that it is also possible to get a second, relatively light scalar in the model. With the values

```
num = {..., lambdaC -> -0.3, MS -> -100, xS -> 3500,
  TL -> -225,  MZp ->2500, mC22->100}
```

we find a tree-level mass of 38 GeV for the lightest CP-even scalar, which is mainly a mixture of η and $\bar{\eta}$. It will be interesting to see if this scenario is still in agreement with all experimental constraints and how important the loop corrections are.

Higgs mass enhancement via non-decoupling D-terms Now, we want to confirm that one gets non-decoupling D-terms in this model which cause an enhancement of the tree-level mass of the SM-like scalar. For this purpose, we define a simple function which calculates the lightest CP-even mass for input values of $m_{\bar{\eta}}$ and $M_{Z'}$,

```
TreeMH[msoft_, mzp_] :=
  Sqrt[Eigenvalues[mH /. sol750 /. num
    /. mC22 -> msoft^2 /. MZp -> mzp ][[-1]]];
```

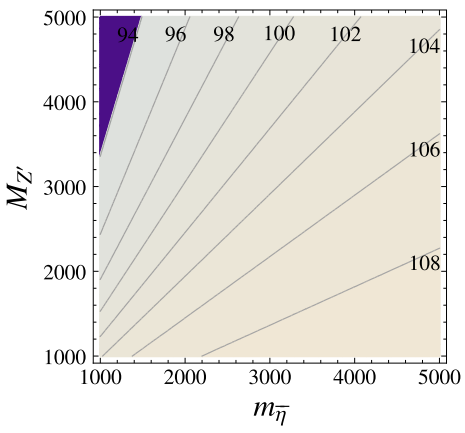

Fig. 13 Contours of the mass of the lightest CP-even scalar in the model as a function of $M_{Z'}$ and $m_{\bar{\eta}}$

How to obtain a broad width? So far, we have not considered the total decay width of the 750 GeV scalar. The experimental data shows a slight preference for a rather large width of about 40 GeV, which is not easy to accommodate in weakly coupled models, typically requiring a large branching ratio into invisible states. Therefore, it would be interesting to see if this can be realised in this model. There are three possibilities for invisible decays: (i) neutralinos, (ii) (heavy) neutrinos, (iii) sneutrinos. We are going to consider the third option here. For this purpose, we have to check two ingredients: can the mass of the sneutrinos be sufficiently light and how can the coupling to the 750 GeV scalar be maximised? To get a feeling for that, we first consider the mass matrix of the CP-even and CP-odd sneutrinos. We assume that flavour and left-right mixing effects are negligible. In that case, it is sufficient to take a look only at the (4,4) entry of the mass matrices:

```
MassMatrix[SvIm][[4, 4]]
MassMatrix[SvRe][[4, 4]]
```

After some simplifications, we get the following expressions from SARAH:

$$M^2_{\tilde{\nu}^I,\tilde{\nu}^R} = \frac{1}{8}\frac{g_X^2 v^2}{(1+t_\beta^2)} - \frac{1}{8}\frac{g_X^2 t_\beta^2 v^2}{(1+t_\beta^2)} + m^2_{\nu,11} + \frac{Y^2_{x,11}}{4g_X^2}(4M^2_{Z'} - g_X^2 v^2) \pm \left(\frac{v_S Y_{x,11}}{2\sqrt{2}g_X}\lambda_C\sqrt{4M^2_{Z'} - g_X^2 v^2} + \frac{1}{2g_X}\sqrt{4M^2_{Z'} - g_X^2 v^2}T_{x,11}\right). \quad (5.24)$$

We see that the terms in the second line, $\propto T_x M_{Z'}$ and $\propto v_S \lambda_C Y_x$, induce a mass splitting between the CP-even and CP-odd states. Thus, in order to have the decay $A \to \tilde{\nu}^I \tilde{\nu}^R$ kinematically allowed, these terms must be individually small or cancel each other. In addition, one has to compensate the large terms $\sim M_{Z'}$ in order to get sufficiently light sneutrinos. This could be done by assuming a negative $m^2_\nu = -\frac{1}{4g_X^2}(4M^2_{Z'} - g_X^2 v^2)Y^2_{x,11}$. Of course, we must check whether this leads to spontaneous R-parity breaking via sneutrino VEVs, and for this purpose one can use `Vevacious`, see below.

We can now check the vertex $A\tilde{\nu}^I\tilde{\nu}^R$ using the same assumptions:

```
Vertex[{Ah, SvIm, SvRe}][[2, 1]]
```

and we obtain after some simplification[14]

$$\frac{1}{2}\frac{1}{\sqrt{2}g_X}\lambda_C\sqrt{4M^2_{Z'} - g_X^2 v^2}Y_{x,11}Z^A_{35} + \lambda_C v_S Y_{x,11}Z^A_{33} - \sqrt{2}Z^A_{34}T_{x,11}. \quad (5.25)$$

If the pseudo-scalar is a pure singlet, only the term $\propto Z^A_{35}$ contributes. This term is independent of v_S and T_x, i.e. we can reduce the mass splitting between the CP-even and CP-odd sneutrinos by adjusting these parameters without having a negative impact on the coupling strength to the 750 GeV scalar.

5.2.5 Vector-like sector

Before we finish the analytical discussion of the masses, we briefly discuss the extended matter sector. The mass matrices responsible for the mixing between the SM fermions and the vector-like fermions can be obtained from SARAH by calling

```
MassMatrix[Fe]
MassMatrix[Fu]
```

which return

$$m_e = \begin{pmatrix} \frac{v_d Y_e}{\sqrt{2}} & -\frac{v_d Y'_e}{\sqrt{2}} \\ 0 & \frac{\lambda_e v_S}{\sqrt{2}} + M_e \end{pmatrix}, \quad m_u = \begin{pmatrix} \frac{v_u Y_u}{\sqrt{2}} & \frac{v_u Y'_u}{\sqrt{2}} \\ 0 & \frac{\lambda_u v_S}{\sqrt{2}} + M_u \end{pmatrix}. \quad (5.26)$$

Thus, for large λ_i ($i = u, e$) and v_S, there are two important sources for the mass of the vector-like states. The full sfermion matrices containing the new scalars are too lengthy to be shown here. We only check the new mass matrix for one generation of the vector-like selectrons which are the 7th and 10th gauge eigenstates. We can pick the values via

```
({{M[[7, 7]], M[[7, 10]]}, {M[[7, 10]], M[[10, 10]]}} /.
      M -> (MassMatrix[Se]))
```

and obtain by setting all parameters to be diagonal

$$\begin{pmatrix} \frac{\tilde{D}+4\left(t_\beta^2+1\right)\left(\lambda_e^2 v_S^2+2\sqrt{2}\lambda_e M_e v_S+2m_E^2+2M_e^2\right)}{8\left(t_\beta^2+1\right)} & B_E + \lambda_e\left(\frac{\lambda_X M^2_{Z'}}{4g_X^2} - \frac{\lambda_X v^2}{16} + \xi + \sqrt{2}M_S v_S\right) \\ B_E + \lambda_e\left(\frac{\lambda_X M^2_{Z'}}{4g_X^2} - \frac{\lambda_X v^2}{16} + \xi + \sqrt{2}M_S v_S\right) & \frac{4\left(t_\beta^2+1\right)\left(\lambda_e^2 v_S^2+2\sqrt{2}\lambda_e M_e v_S+2m_E^2+2M_e^2\right)-\tilde{D}}{8\left(t_\beta^2+1\right)} \end{pmatrix} \quad (5.27)$$

where we have defined $\tilde{D} = (t_\beta^2 - 1)v^2(2g_1^2 + g_X^2)$. There is a potentially dangerous term $\lambda_e \xi$ which rapidly increases for increasing λ_e. To keep all scalar masses positive, it is necessary to choose a rather large B_E as well. Therefore, we are going to choose always

$$B_E = -\lambda_e(\xi + \sqrt{2}M_S v_S), \quad B_U = -\lambda_u(\xi + \sqrt{2}M_S v_S) \quad (5.28)$$

in our numerical study to circumvent tachyonic scalars.

[14] We give for simplicity the results in LaTeXformat. The SARAH internal conventions for the vertices are the following: the results for each vertex are returned as arrays in the format `{Particles,{Coeff1,Lor1},{Coeff2,Lor2}}`: first, the involved particles with the names for their generation and colour indices are shown and then the coefficients for the different Lorentz structures are given. For the example of a triple scalar vertex, {Coeff2,Lor2} is absent, and `Lor1` is just `1`. For vertices involving fermions, `PL` and `PR` are used for the polarisation operators.

5.2.6 RGEs and gauge kinetic mixing

We have so far made the simplifying assumption that gauge kinetic mixing vanishes. However, if the two Abelian gauge groups are not orthogonal, kinetic mixing would be generated via RGE running even if it vanishes at some energy scale. Thus, one of the first checks on the RGEs of the model we can make is whether the two $U(1)$ gauge groups are orthogonal. For this purpose, we first calculate the one-loop RGEs with `SARAH` via

```
CalcRGEs[TwoLoop->False];
```

We have chosen one-loop RGEs only to save time. Without the `TwoLoop->False` flag, the full two-loop RGEs would have been calculated automatically. Other options for `CalcRGEs are`:

- `ReadLists`: If the RGEs have already be calculated, the results are saved in the output directory. The RGEs can be read from these files instead of doing the complete calculation again.
- `VariableGenerations`: Some theories contain heavy superfields which should be integrated out above the SUSY scale. Therefore, it is possible to calculate the RGEs assuming the number of generations of specific superfields as free variable to make the dependence on these fields obvious. The new variable is named `NumberGenerations[X]`, where `X` is the name of the superfield.
- `NoMatrixMultiplication`: Normally, the β-functions are simplified by writing the sums over generation indices as matrix multiplication. This can be switched off using this option.
- `IgnoreAt2Loop`: The calculation of 2-loop RGEs for models with many new interactions can be very time-consuming. However, often one is only interested in the dominant effects of the new contributions at the 1-loop level. Therefore, `IgnoreAt2Loop -> $LIST` can be used to neglect parameters at the two-loop level The entries of $LIST can be superpotential or soft SUSY-breaking parameters as well as gauge couplings.
- `WriteFunctionsToRun`: Defines if a file should be written to evaluate the RGEs numerically in `Mathematica`

We can now check the entries in `BetaGauge` and find

$$\begin{aligned}16\pi^2\beta_{g_Y} &= 15g_Y^3 + 15g_Y\, g_{YX}^2 \\ &\quad + 16\sqrt{\frac{3}{5}}g_Y\, g_{YX}\, g_X + 32\sqrt{\frac{3}{5}}g_Y^2\, g_{XY} \\ &\quad + 16\sqrt{\frac{3}{5}}g_{YX}^2\, g_{XY} + 15g_{YX}\, g_X\, g_{XY} \\ &\quad + 15g_Y\, g_{XY}^2, \end{aligned} \tag{5.29}$$

$$\begin{aligned}16\pi^2\beta_{g_X} &= 15g_{YX}^2\, g_X + 15g_X^3 + 16\sqrt{\frac{3}{5}}g_Y\, g_X\, g_{XY} \\ &\quad + 15g_X\, g_{XY}^2 \\ &\quad + g_{YX}\left(32\sqrt{\frac{3}{5}}g_X^2 + 15g_Y\, g_{XY} + 16\sqrt{\frac{3}{5}}g_{XY}^2\right), \end{aligned} \tag{5.30}$$

$$\begin{aligned}16\pi^2\beta_{g_{XY}} &= 15g_{YX}^3 + 32\sqrt{\frac{3}{5}}g_{YX}^2\, g_X + 15g_{YX}\, g_X^2 \\ &\quad + g_Y^2\left(15g_{YX} + 16\sqrt{\frac{3}{5}}g_X\right) \\ &\quad + g_Y\left(16\sqrt{\frac{3}{5}}g_{YX}\, g_{XY} + 15g_X\, g_{XY}\right), \end{aligned} \tag{5.31}$$

$$\begin{aligned}16\pi^2\beta_{g_{YX}} &= 15g_{YX}^3 + 32\sqrt{\frac{3}{5}}g_{YX}^2\, g_X + 15g_{YX}\, g_X^2 \\ &\quad + g_Y^2\left(15g_{YX} + 16\sqrt{\frac{3}{5}}g_X\right) \\ &\quad + g_Y\left(16\sqrt{\frac{3}{5}}g_{YX}\, g_{XY} + 15g_X\, g_{XY}\right). \end{aligned} \tag{5.32}$$

The standard normalisation factor $\sqrt{5/3}$ for the hypercharge has been included. One can see that the β-functions for g_{YX} and g_{XY} are non-zero even in the limit $g_{XY}, g_{YX} \to 0$, i.e. these couplings will be induced radiatively. Thus, in general one has not only two couplings g_1 and g_X in this model, but a gauge coupling matrix G defined as

$$G = \begin{pmatrix} g_{YY} & g_{XY} \\ g_{YX} & g_{XX} \end{pmatrix}. \tag{5.33}$$

In the limit of vanishing kinetic mixing, $g_{YX} = g_{XY} = 0$, the relations $g_{YY} = g_1$ and $g_{XX} = g_X$ hold. Even if gauge kinetic mixing is present, one has the freedom to perform a change in basis to bring G into a particular form. The most commonly considered cases are the symmetric basis with $g_{XY} = g_{YX}$ and the triangle basis with $g_{YX} = 0$. The triangle basis has the advantage that the new scalars do not contribute to the electroweak VEV, and the entire impact of gauge kinetic mixing is encoded in one new coupling $\tilde{g}$. The relations between g_{ij} $(i, j = X, Y)$ and $g_1, g_X, \tilde{g}$ are [468]

$$g_1 = \frac{g_{YY}g_{XX} - g_{XY}g_{YX}}{\sqrt{g_{XX}^2 + g_{XY}^2}}, \tag{5.34}$$

$$g_X = \sqrt{g_{XX}^2 + g_{XY}^2}, \tag{5.35}$$

$$\tilde{g} = \frac{g_{YX}g_{XX} + g_{YY}g_{XY}}{\sqrt{g_{XX}^2 + g_{XY}^2}}. \tag{5.36}$$

It is interesting to see how large $\tilde{g}$ is naturally. With 'naturally' we mean under the assumption that the off-diagonal g_{YX} and g_{XY} couplings vanish at some high scale Λ and are generated by RGE running down to the SUSY scale. Thus, in this setup, the size of gauge kinetic mixing is a function of Λ and g_X at this scale. We can write a simple `Mathematica` function to get a feeling for the off-diagonal gauge couplings:

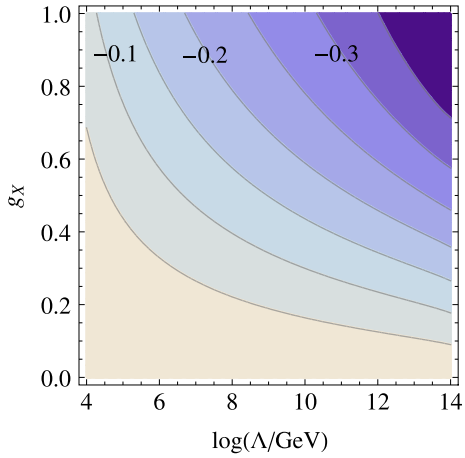

Fig. 14 Gauge kinetic mixing $\tilde{g}$ at the SUSY scale as a function of the high energy scale Λ, where it is assumed to vanish, and of the coupling $g_X(\Lambda)$

```
<< "Output/U1yMSSM/RGEs/RunRGEs.m";
RunningGKM[scale_, gXIN_] := Block[{},
   logS = scale;
   runUp = RunRGEs[{g1 -> 0.45}, 3, logS, TwoLoop -> ↪
       False][[1]];
   runDown = RunRGEs[{g1 -> (g1[logS] /. runUp), gX -> ↪
       gXIN}, logS, 3, TwoLoop -> False][[1]];
   g1run = Sqrt[3/5] g1[3] /. runDown;
   gXrun = gX[3] /. runDown;
   g1Xrun = Sqrt[3/5] g1X[3] /. runDown;
   gX1run = gX1[3] /. runDown;
   g1out = (g1run*gXrun - g1Xrun gX1run)/Sqrt[gXrun^2 ↪
       + gX1run^2];
   gXout = Sqrt[gXrun^2 + gX1run^2];
   g1Xout = (g1Xrun gXrun + g1run gX1run)/Sqrt[gXrun^2 ↪
       + gX1run^2];
   Return[{g1out, gXout, g1Xout}];
   ];
```

In the first line, we load the file written by `SARAH` which provides the RGEs in a form which `Mathematica` can solve. This file also contains the function `RunRGEs` that can be used to solve the RGEs numerically. As boundary condition, we used $g_1 = 0.45$ at the scale 1 TeV. After the running we rotate the couplings to the basis where g_{XY} vanishes. We can make a contour plot via

```
ContourPlot[RunningGKM[lambda, gx][[3]],
    {lambda, 4, 17}, {gx, 0, 1},  ContourLabels -> True]
```

and get the result shown in Fig. 14. Thus, we find that at the SUSY scale the gauge mixing coupling $\tilde{g}$ is negative and not much smaller than an ordinary gauge coupling unless Λ is assumed to be very small.

5.2.7 *Boundary conditions and free parameters*

For the subsequent numerical analysis we are going to assume some simplified boundary conditions applied at the SUSY scale:

$$m_q^2 = m_d^2 = m_u^2 = m_l^2 = m_e^2 = m_E^2 = m_{\tilde{E}}^2 = m_U^2 = m_{\tilde{U}}^2 \equiv \mathbf{1} m_{SUSY}^2, \tag{5.37}$$

$$\lambda_e = \mathbf{1}\lambda_E, \quad \lambda_u \equiv \mathbf{1}\lambda_U, \tag{5.38}$$

$$M_e = \mathbf{1}M_E, \quad M_u \equiv \mathbf{1}M_U, \tag{5.39}$$

$$T_i = A_0 Y_i \ (i = \{u, e, d\}), \quad T_i' = A_0 Y_i' \ (i = \{u, e\}),$$

$$T_i = A_0 \lambda_i \ (i = \{U, E\}), \tag{5.40}$$

$$T_\lambda = A_\lambda \lambda, \quad T_X = A_X \lambda_X, \tag{5.41}$$

$$M_1 = M_2 = \frac{1}{2} M_3 = M_X \equiv M_\lambda. \tag{5.42}$$

In addition, we can set $Y_\nu = 0$ since this parameter is highly constrained to be small by the small neutrino masses. In addition, we set the mixing parameters $m_{eE}^2, m_{uU}^2, \tilde{M}_E, \tilde{M}_U, \tilde{B}_E, \tilde{B}_U, M_{1X}$ to zero and also assume vanishing λ, κ, and T_κ. However, we stress that this is just done to keep the following discussion short and simple. All effects of these parameters can be included without any additional efforts. Thus, the free parameters mainly considered in the following are

$$\begin{aligned} &m_{SUSY}, M_\lambda, \mu, B_\mu, A_0, \tan\beta, \\ &g_X, g_{1X}, M_{Z'}, m_{\tilde{\eta}}, \tan\beta_X, \lambda_X, A_X, Y_x, \\ &M_S, B_S, v_s, A_\lambda, \\ &\lambda_E, \lambda_U, M_E, M_U, Y_u', Y_e'. \end{aligned}$$

The tadpole equations are solved for $m_{H_d}^2, m_{H_u}^2, m_{\tilde{\eta}}^2, m_S^2$ and ξ, while B_E and B_U are fixed via Eq. (5.28).

5.3 Analysis of the important loop corrections to the Higgs mass

We now turn to the numerical analysis of this model. In the first step, we have written a `SPheno.m` file for the boundary conditions, see Sect. 5.2.7, and generated the `SPheno` code with the `SARAH` command

```
MakeSPheno[];
```

We copy the generated Fortran code to a new sub-directory of `SPheno-3.3.8` and compile it via

```
$ cd $PATH/SPheno-3.3.8
$ mkdir U1xMSSM
$ cp $PATH/SARAH/Output/U1xMSSM/EWSB/SPheno/* U1xMSSM/
$ make Model=U1xMSSM
```

We now have an executable `SPhenoU1xMSSM` which expects the input parameters from a file called `LesHouches.in.U1xMSSM`. The `SPheno` code provides many important calculations which would be very time-consuming to be performed 'by hand' for this model, but could be expected to be relevant. A central point is the calculation of the pole mass spectrum at the full one-loop (and partially two-loop) level. In particular, the loop corrections from the vector-like states are known to be very important. However, the focus in the literature has usually been only on the impact on the SM-like Higgs. We can automatically go beyond that and consider the corrections to the 750 GeV state as well. Moreover, `SPheno` calculates all additional two-loop corrections in the gaugeless limit including all new matter interactions. Thus, we can check the impact of the vector-like states even at two-loop level. These effects have not been studied in any of the SUSY models proposed so far to explain the diphoton excess. Of course, `SPheno` also makes a very precise prediction for the diphoton and digluon decay rate of all neutral scalars as described in Sect. 3.5, and it checks for any potential decay mode. Thus, it is impossible to miss any important decay as sometimes has happened in the literature when discussing the diphoton excess. Finally, there are also other important constraints for this model like those from flavour observables or Higgs coupling measurements. As will be shown in the next sections, all of this can be checked automatically with `SPheno` and tools interacting with it.

If not mentioned otherwise, we make the following choice for the input parameters

$$\begin{aligned} m_{SUSY} &= 1.5 \text{ TeV}, M_\lambda = 1 \text{ TeV}, \\ \tan\beta &= 20, \quad \tan\beta_x = 1, \quad g_X = 0.5, \quad M_{Z'} = 3 \text{ TeV}, \\ m_{\tilde{\eta}} &= 2 \text{ TeV}, \\ \mu &= 1 \text{ TeV}, \quad B_\mu = (1 \text{ TeV})^2, \quad v_S = 0.5 \text{ TeV}, \\ M_S &= -0.1 \text{ TeV}, \quad B_S = 3.895 \text{ TeV}^2, \\ \lambda_X &= -0.2, \quad A_X = 1 \text{ TeV}, \quad \lambda_E = \lambda_U = 1, \\ M_E &= 0.4 \text{ TeV}, \quad M_U = 1 \text{ TeV}. \end{aligned}$$

5.3.1 New loop corrections to the SM-like Higgs

In this model we have two new important loop corrections to the SM-like Higgs: (i) the corrections from vector-like states, proportional to Y_u' and Y_e', and (ii) the new corrections from the extended gauge sector. The corrections from vector-like (s)tops up to two-loop have been discussed in detail in Ref. [426] using the `SARAH`/`SPheno` framework. There are several important effects which are often neglected in studies of vector-like states which only make use of the one-loop effective potential: the momentum effects at one-loop, the two-loop corrections, and the shift of the top-Yukawa coupling. In general, the user does not need to worry about these

details because SARAH/SPheno take care of them automatically. However, it might be interesting to have an intuitive feeling about the size of the different effects. Since it demands some 'hacking' of the code to disentangle the calculation in that way, we are not making this analysis here, but we briefly summarise the main results of Ref. [426] in Fig. 15. We see that all these effects can alter the Higgs mass by several GeV. Thus, an estimated uncertainty of about 2–3 GeV when using only the one-loop effective potential approximation is usually over optimistic.

Furthermore, in models with non-decoupling D-terms the new loop corrections are usually neglected in the literature. Therefore, we are going to check whether this is a good approximation or not. For this purpose we show the SM-like Higgs pole mass at tree and one-loop level as a function of g_X for two different values of $M_{Z'}$. Since SPheno performs the two-loop corrections in the gaugeless limit, additional corrections from the extended gauge sector are not included at two-loop, and we concentrate on the one-loop effects here. For this purpose, we use the different flags in the Les Houches input file from SPheno to turn the corrections at the different loop levels on or off:

```
Block SPhenoInput    # SPheno specific input
 ...
  7   A              # Skip 2-loop Higgs corrections
 55   B              # Calculate loop corrected masses
```

Here, A and B are either 1 or 0. With flag 55 the entire loop-corrections to all masses can be turned on (1) or off (0), while flag 7 only skips (1) or includes (0) the two-loop corrections in the Higgs sector. The results are shown in Fig. 16. All scans have been performed using the Mathematica package SSP [469] for which SARAH already writes a template input when generating the SPheno code (SSP_Template.m.U1xMSSM) for a given model. We see that the tree-level mass rises quickly with increasing g_X. However, for both $M_{Z'}$ values this shift is compensated to some extent when one-loop corrections are included. Thus, the inclusion of non-decoupling D-terms only at tree-level would overestimate the positive effect on the SM-like Higgs mass by 20–30 %. In addition, we also see that off-diagonal gauge couplings of a realistic size arising from gauge kinetic mixing reduce the positive effect from the non-decoupled D-terms on the Higgs mass by a few GeV.

5.3.2 Loop corrections to the 750 GeV scalar

There are also important loop corrections to all other scalars in the model if large Yukawa-like couplings are present. We discuss this briefly for the 750 GeV pseudo-scalar: in Fig. 17, the mass at tree, one- and two-loop level for varying $\lambda_V \equiv \lambda_e = \lambda_u$ for two different values of m_{SUSY}, 1.5 and 2.5 TeV, is given. For $m_{SUSY} = 1.5$ TeV there is only a moderate difference between tree-level, one- and two-loop for $\lambda_V \to 0$, but for λ_V of $O(1)$ the one-loop corrections cause a shift by 100 GeV and more, which is compensated to some extent by the two-loop corrections. For larger m_{SUSY} we see already a large positive shift for small λ_V, which quickly increases and reaches 300–400 GeV for $\lambda_V \sim 0.8$. For even larger values of λ_V, the difference between tree-level and the loop corrected mass becomes smaller. Still, the overall shift is more than 100 GeV, and this would be highly overestimated by only including one-loop corrections. As we will see in the next section, one needs $\lambda_V \sim O(1)$ to explain the diphoton signal. For this value, a naive tree-level analysis gives a mass for the lightest CP-odd state which is far off the correct value. Thus, one has to be much more careful with the choice for B_S.

5.4 Diphoton and digluon rate

We now discuss the diphoton and digluon decay rate of the pseudo-scalar, and its dependence on the new Yukawa-like couplings. As we have just seen, large couplings induce a non-negligible mass shift. Therefore, it is necessary to adjust B_S carefully to get the correct mass, 750 GeV, after including all loop corrections. This can be done by SSP, which can adjust B_S for each point to obtain the correct mass within 5 GeV uncertainty. The results for the calculated diphoton and digluon rate at LO and with the higher order corrections discussed in Sect. 3.5 are shown in Fig. 18. In order to see the size of the higher order corrections, one can use the flag 521 in SPheno to turn them on and off

```
Block SPhenoInput    # SPheno specific input
 ...
 521   1             # Diphoton/Digluon widths including higher order
```

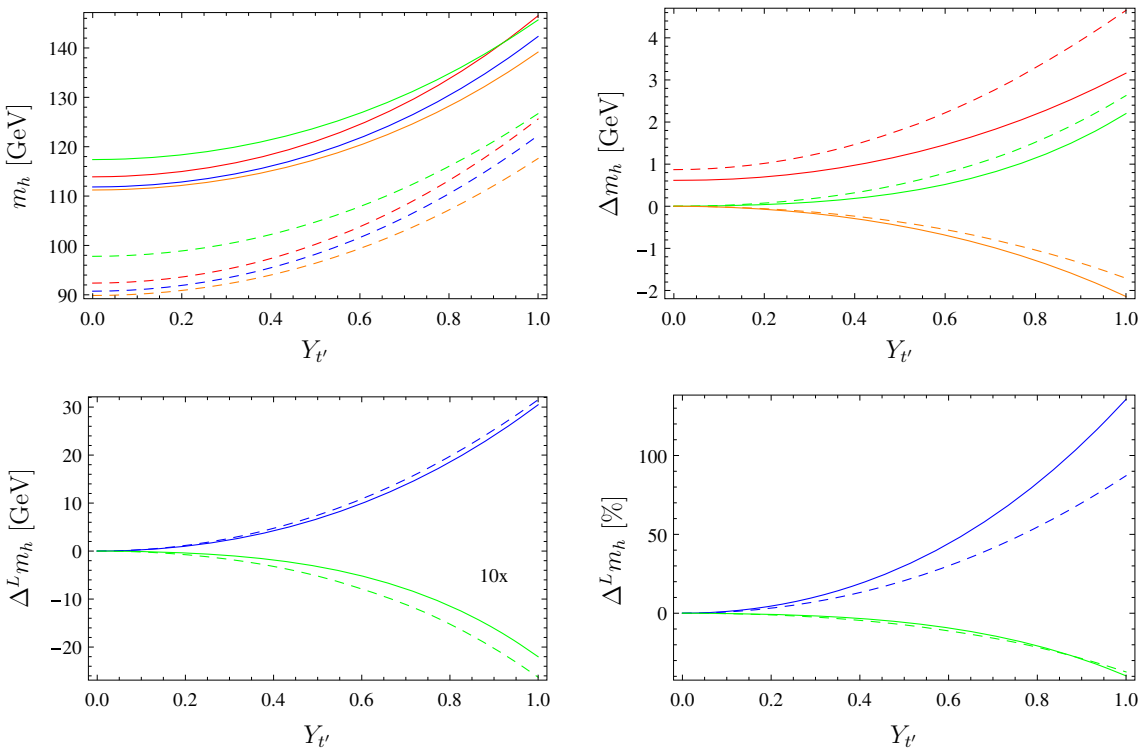

Fig. 15 *Top left* light Higgs mass as a function of $Y_{t'}$ (which corresponds to $Y'_{u,33}$ in this model) with all other entries of Y'_u vanishing. The *red line* corresponds to the effective potential calculation at one-loop, *orange* is the one-loop corrections with external momenta but neglecting the new threshold correction stemming from vector-like states, *blue* is the full one-loop calculation including the momentum dependence and all thresholds, and *green* includes the dominant two-loop corrections together with the full one-loop correction. *Top right* impact of the threshold corrections (*red*), the momentum dependence at one-loop (*orange*) and the two-loop corrections (*green*), given as the difference $\Delta m_h = m_h - m_h(1\text{L}, p^2 \neq 0, \text{all thresholds})$. *Bottom left* absolute size of the one- (*blue*) and two-loop (*green*) corrections stemming from the vector-like states. For better readability we re-scaled the two-loop corrections by a factor of 10. *Bottom right* relative importance of the one- (*blue*) and two-loop (*green*) corrections normalised to the size of the purely MSSM-like corrections. The *solid lines* are for $\tan\beta = 10$ and the *dashed* ones are for $\tan\beta = 2$. Here, a mass of 1 TeV for the vector-like quarks was assumed. These plots are taken from Ref. [426]

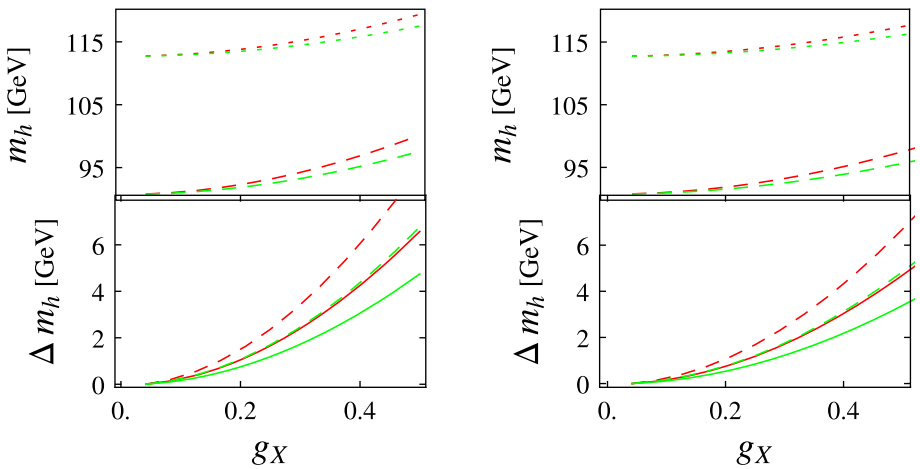

Fig. 16 Mass of the SM-like Higgs as a function of g_X at tree-level (*dashed*) and one-loop (*full line*). The *red lines* are without gauge-kinetic mixing, for the *green* ones we set $g_{1X} = \frac{1}{5} g_X$. $M_{Z'}$ *on the left* is 3 and 4 TeV *on the right*. *On the bottom* we show the difference $\Delta m_h \equiv m_h(g_X) - m_h(g_X = 0)$ at tree-level (*dashed*) and including loop corrections (*full*) for the case with gauge kinetic mixing (*green*) and without (*red*)

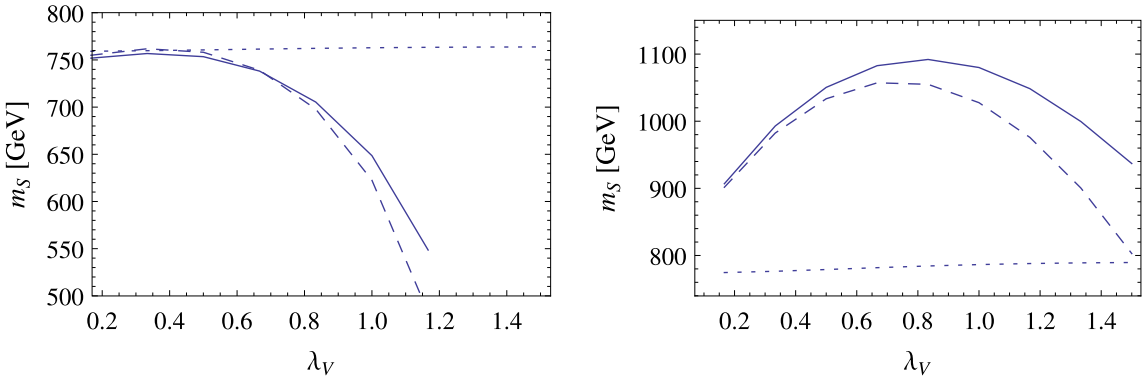

Fig. 17 Mass of the CP-odd scalar with a tree-level mass of 750 GeV (*dotted*), at one-loop (*dashed*) and two-loop (*full*) for a variation of $\lambda_V \equiv \lambda_e = \lambda_u$. *On the left* we set $m_{SUSY} = 1.5$ TeV, *on the right* $m_{SUSY} = 2.5$ TeV

This can also be achieved in `FlexibleSUSY` by setting a flag in the generated C++ code as desired. Note that, as discussed in Sect. 3.5, there is close agreement for the diphoton and digluon effective vertices computed using `SPheno` and `FlexibleSUSY`. Therefore we present here only the results obtained using `SPheno`. Nevertheless, it might be often helpful to compare the results between both codes since they use a slightly different matching and renormalisation procedure which results in some differences in the mass spectrum and consequently also in the calculated decays and branching ratios. Therefore, these differences can be used as a rough estimate of the theoretical uncertainty of the different calculations.

One finds the expected behaviour: the partial widths rise quadratically with the coupling. For about $\lambda_V \simeq 1.0$ one has $\Gamma(S \to \gamma\gamma)/M_S \sim 10^{-6}$, which is necessary to explain the observed excess. In Fig. 18 we also show a comparison between a purely LO calculation and the one including the higher order QCD corrections described in Sect. 3.5. There is no change for the decay into two photons, because its NLO corrections for a pseudo-scalar are non vanishing only for $m_A > 2M_F$. Instead, the digluon width is enhanced by a factor of 2 when including NLO and NNLO QCD corrections. This also changes the ratio of the digluon-to-diphoton width from about 10 (LO only) to 20 (including higher orders).

5.5 Constraints on choice of parameters

5.5.1 Singlet-doublet mixing

So far, we made some strong assumptions about some parameters in this model. In particular, we set the coupling between the singlet and the two Higgs doublets $\lambda = 0$. This raises the question how sensitive the results are to this choice. For this purpose, we can test what happens if we slightly deviate from it. The branching ratios of the CP-odd scalar of 750 GeV mass, which is nearly a pure singlet, as a function of λ are shown in Fig. 19. For comparison we also show the branching ratios for the CP-even scalar with a mass around 800 GeV. This particle is mainly a mixture of η and $\bar{\eta}$ with a small singlet component. For both particles we depict the branching ratios when calculating only tree-level masses and when including loop-corrections. At the tree level we find that the impact of λ on the branching ratios of A is very small. This does not change much when including the loop corrections to the pseudo-scalar rotation matrix. On the other hand, for vanishing λ we already have a large branching ratio of the CP-even scalar into hh even at tree level. Moreover, the decay modes into two massive vector bosons or $t\bar{t}$ at tree level increase very quickly with λ and for $\lambda > 0.01$ they already dominate. At one-loop level, the large dependence on λ is no longer visible, because for very small λ the branching ratios into massive SM vector bosons and fermions are already large. This can be seen in Fig. 20 where we compare the doublet fraction of the two states at tree level and one loop. In general, the behaviour shows that a CP-odd scalar might be a much less fine-tuned candidate for the observed excess.

5.5.2 Constraints from Higgs coupling measurements

We have seen in the `Mathematica` session that it is possible to obtain two light scalars at tree-level. One question is: is this also possible when including all loop contributions? In order to address this question we change some input parameters to

$$
\begin{aligned}
&m_{SUSY} = 1.75 \text{ TeV}, \quad \tan\beta = 20, \quad m_{\bar{\eta}} = 1 \text{ TeV},\\
&M_{Z'} = 2.5 \text{ TeV}, \quad v_S = 3.5 \text{ TeV},\\
&B_S = 45000 \text{ GeV}^2, \quad \lambda_X = -0.3,\\
&A_X = 750 \text{ GeV}.
\end{aligned}
$$

The pole masses and the doublet fraction of two lightest CP-even states as a function of $\tan\beta_X$ is shown in Fig. 21. We find the very strong dependence on $\tan\beta_X$, known in many $U(1)$ extensions [468,470,471]. One difference here is that, due

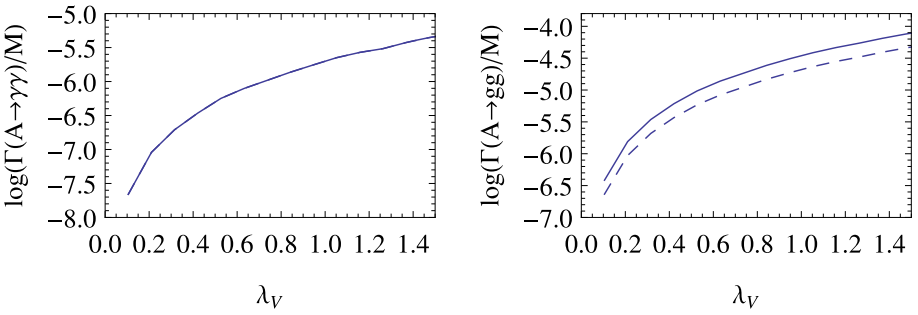

Fig. 18 Partial widths into two photons (*left*) and two gluons (*right*) of the lightest pseudo-scalar, normalised to the mass M_S. B_S was adjusted to keep the mass constant within (750 ± 5) GeV. The *solid lines* were drawn including higher order QCD corrections to loop induced decays, the *dashed* ones at leading order only

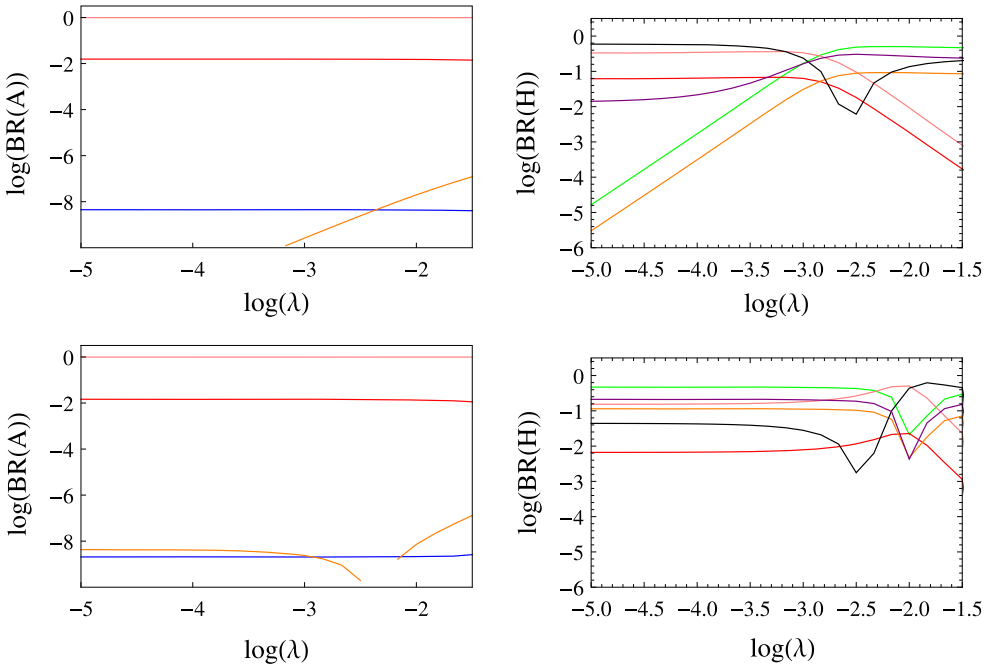

Fig. 19 Branching ratios of the 750 GeV CP-odd particle (*left*), and a CP-even scalar (*right*) close in mass as function of λ. In the *first row* the tree-level rotation matrices are used, while in the *second row* the rotation matrices including loop corrections are used. Here, we set $A_\lambda = 1$ TeV. The *colour code* is as follows: $\gamma\gamma$ (*pink*), gg (*red*), hZ (*blue*), $t\bar{t}$ (*orange*), hh (black), ZZ (*purple*), W^+W^- (*green*)

to the mixing with the singlet, the light state in the extended sector does not become massless for $\tan\beta_X = 1$, but for small deviations from it. We see in Fig. 21 that the SM-like Higgs gets a positive mass shift after the level crossing, while the mass of the lightest state drops very quickly. Of course, it is important to know if such light Higgs-like particles are compatible with all limits from Higgs searches at LEP, Tevatron and the LHC. For this purpose, we can make use of `HiggsBounds`, which checks whether the decay rates of a scalar into SM states are compatible with the observations at all experiments performed so far. If any of these rates is above 1 (normalised to the SM expectation), such a parameter point would be ruled out. Similarly, we can use `HiggsSignals` to obtain a χ^2 estimator for each parameter point, based on how well the measured Higgs properties are reproduced. In order to use `HiggsBounds` and `HiggsSignals`, we set the flag

```
1 Block SPhenoInput    # SPheno specific input
2 ...
3 76 1                 # Write HiggsBounds file
```

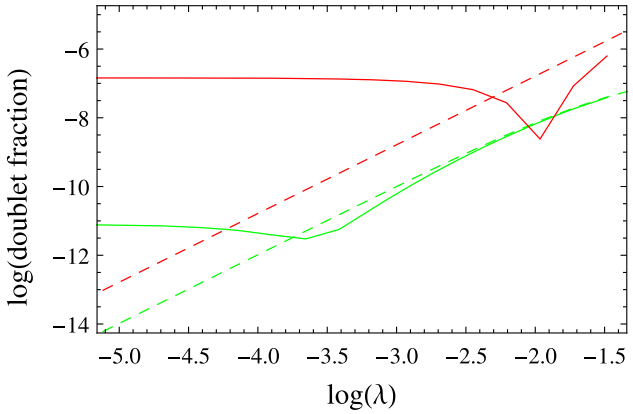

Fig. 20 Doublet fraction of the 750 GeV pseudo-scalar (*green*) and the 800 GeV scalar (*red*) at tree-level (*dashed lines*) and including loop corrections (*full lines*), as function of λ

in the input file for SPheno. In this way, SPheno writes out all files which are necessary to run HiggsBounds and HiggsSignals via the effective couplings input mode (effC). However, there is one caveat: SPheno does not automatically write the file MHall_uncertainties which gives an estimate for the theoretical uncertainty in the mass prediction of all scalars. The reason is that SPheno cannot do such an estimate automatically. However, if this file is missing, HiggsBounds and HiggsSignals would assume that the uncertainty is zero. Therefore, we add this file by hand and assume a 3 GeV uncertainty for all masses. We can now use this setup to make a scan in the (tan β_X,λ) plane, for instance by using the SSP option to automatically call HiggsBounds and HiggsSignals during a parameter scan. The results are shown in Fig. 22. One can see that both, the discovery potential and the χ^2 value, are very sensitive on small changes in these two parameters. The reason is mainly the large dependence of the masses of the two lightest scalars and their mixing. One sees that the best χ^2 value is found close to the tan β_X range where the SM-like particle is the second lightest CP-even state, and the lightest one is about 80 GeV. In addition, for a very small stripe close to $\lambda = 0$ also points with very light scalars with masses below 40 GeV pass all constraints, but for slightly larger values of λ the mixing already becomes too large and the points are excluded by $e^+e^- \to (h_1)Z \to (b\bar{b})Z$ from LEP searches.

5.5.3 *Large decay width and constraints from vacuum stability*

We have already considered the possibility to enhance the total decay width of the CP-odd scalar via decays in pairs of right-sneutrinos. In our tree-level analysis with SARAH we found that one can reduce the mass splitting between the two mass eigenstates by demanding

$$T_x = -\frac{1}{\sqrt{2}}\lambda_X v_S Y_x. \tag{5.43}$$

In addition, as already discussed above, one has to use a negative soft-mass for the sneutrinos,

$$m_\nu^2 = -\frac{Y_x^2}{4g_X^2}\left(4M_{Z'}^2 - g_X^2 v^2\right), \tag{5.44}$$

to get the states light enough. This immediately raises two questions: (i) how large can the total width be for large values of Y_x? (ii) Is the electroweak vacuum stable or not? First of all, we notice that a negative m_ν^2 does not necessarily imply spontaneous R-parity violation, as shown in Ref. [472], in contrast to some claims in this direction in the previous literature. However, the danger of disastrous vacuum decays increases, of course, with decreasing m_ν^2. Therefore, we use Vevacious to check the stability of the potential. For this purpose, we have written a second SARAH model file where we include the possibility of VEVs for the right sneutrinos. We also added in this new implementation those mixings among states which were forbidden by R-parity conservation. This is actually necessary because Vevacious calculates the one-loop corrections to the effective potential and the full mass matrices are required. The Vevacious model file is generated via

```
MakeVevacious[];
```

We can now run a point with SPheno. If we turn on

```
Block SPhenoInput    # SPheno specific input
 ...
530 1                # Write Blocks for Vevacious
```

we can pass the SPheno spectrum file in a second step to Vevacious, which finds all minima of the potential with the additional VEV. If the global minimum is not the local one found by SPheno with correct EWSB, Vevacious uses CosmoTransitions [473] to get the life-time of 'our' vacuum. If our survival probability is found to be below 10 %, we label the points as short-lived. Metastable points with a longer life-time are called long-lived. We choose the

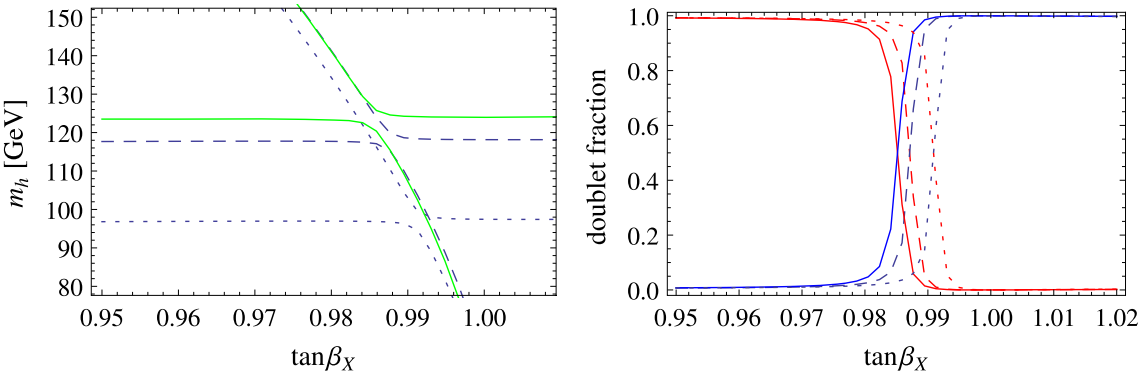

Fig. 21 *Left* the masses of the two lightest CP-even eigenstates as a function of tan β_X at tree-level (*dotted*), one-loop (*dashed*) and two-loop (*full green line*). *Right* the corresponding doublet fraction of the lightest (*blue*) and second lightest (*red*) scalar at tree-level (*dotted*), one-loop (*dashed*) and two-loop (*full*) levels

following set of input parameters[15]

$$m_{SUSY} = 2.5\ \text{TeV}, \quad \tan\beta = 10, \quad \tan\beta_x = 1, \quad g_X = 0.5,$$
$$M_{Z'} = 2.5\ \text{TeV}, \quad m_{\tilde{\eta}} = 1\ \text{TeV}, \quad v_S = 0.5\ \text{TeV},$$
$$B_S = 755000\ \text{GeV}^2, \quad \lambda_X = -0.4, \quad A_X = 0.4\ \text{TeV}.$$

The final result is summarised in Fig. 23.[16] To maximise the effect on the total width, we take all sneutrinos to be degenerate and with the same coupling to the 750 GeV scalar.

We see that we can get a large total width of the pseudo-scalar for large diagonal entries in Y_x. Up to values of Y_x of 0.25, which corresponds to a total width of 15 GeV, the vacuum is absolutely stable. One can even reach $Y_x \sim 0.36$ ($\Gamma \sim 30$ GeV) before the life-time of the correct vacuum becomes too short. The dependence of the tunnelling time on the value of m_v^2 is shown in the middle of Fig. 23. One might wonder how dangerous this vacuum decay is, since spontaneous R-parity violation is not a problem per se. However, we show also in the right plot in Fig. 23 that the electroweak VEV v changes dramatically in the global minimum. Therefore, these points are clearly ruled out.

Even if we cannot reach a width of 45 GeV with the chosen point, we see that the principle idea to enhance the width is working very well. Thus, with a bit more tuning of the parameters, one might even be able to accommodate this value. Furthermore, as the diphoton rate decreases with increasing total width, the relevant couplings or masses would need to be adjusted in order to maintain the explanation of the $\gamma\gamma$ excess. However, this is beyond the scope of this example. We emphasise that, since the large coupling responsible for the large width is a dimensionful parameter, it will not generate a Landau pole. Thus, the large width hypothesis does not necessarily point to a strongly coupled sector close to the observed resonance.

5.5.4 Dark matter relic density

We have seen in the last section that light sneutrinos are a good possibility in this model to enhance the width of the 750 GeV particle. Of course, it would be interesting to see if they can also be a dark matter candidate. For this purpose, we can implement the model in `MicrOmegas` to calculate the relic density and to check current limits from direct and indirect detection experiments. In order to implement the model in `MicrOmegas`, it is sufficient to generate the model files for `CalcHep` with `SARAH` via

```
MakeCHep[]
```

and copy the generated files into the `work/models` directory of a new `MicrOmegas` project. `SARAH` also writes main files which can be used to run `MicrOmegas`. For instance, the file `CalcOmega.cpp` calculates the dark matter relic density and writes the result as well as all important annihilation channels to an external file. This information can then be stored when running a parameter scan. The parameters are easily exchanged between `MicrOmegas` and a `SARAH`-based spectrum generator by copying the spectrum file into the main directory of the current `MicrOmegas` project directory.[17] However, it is important to remember that `MicrOmegas` cannot handle complex parameters. Therefore, one has to make sure, even in the case without CP violation, that all rotation matrices of Majorana fermions are real. This can be done by using the following flag for `SPheno`:

[15] This choice might be a bit unlucky but shows the dangers of the two-loop effective potential calculation: in the gauge-less limit, one of the pseudo-scalars has a tree-level mass close to 0. This causes divergences ('Goldstone catastrophe') [474,475] and makes it necessary to turn off the 2L corrections in `SPheno` via the flag `7` set to `1`.

[16] For this example we had to turn off the thermal corrections to the tunnelling by inserting `vcs.ShouldTunnelThermally = False` in `Vevacious.py` because `CosmoTransitions` failed otherwise to calculate the tunnelling time in the six-dimensional potential.

[17] If the spectrum file is not called `SPheno.spc.$MODEL`, one can change the file-name by editing the fourth line in `func1.mdl` written by `SARAH`.

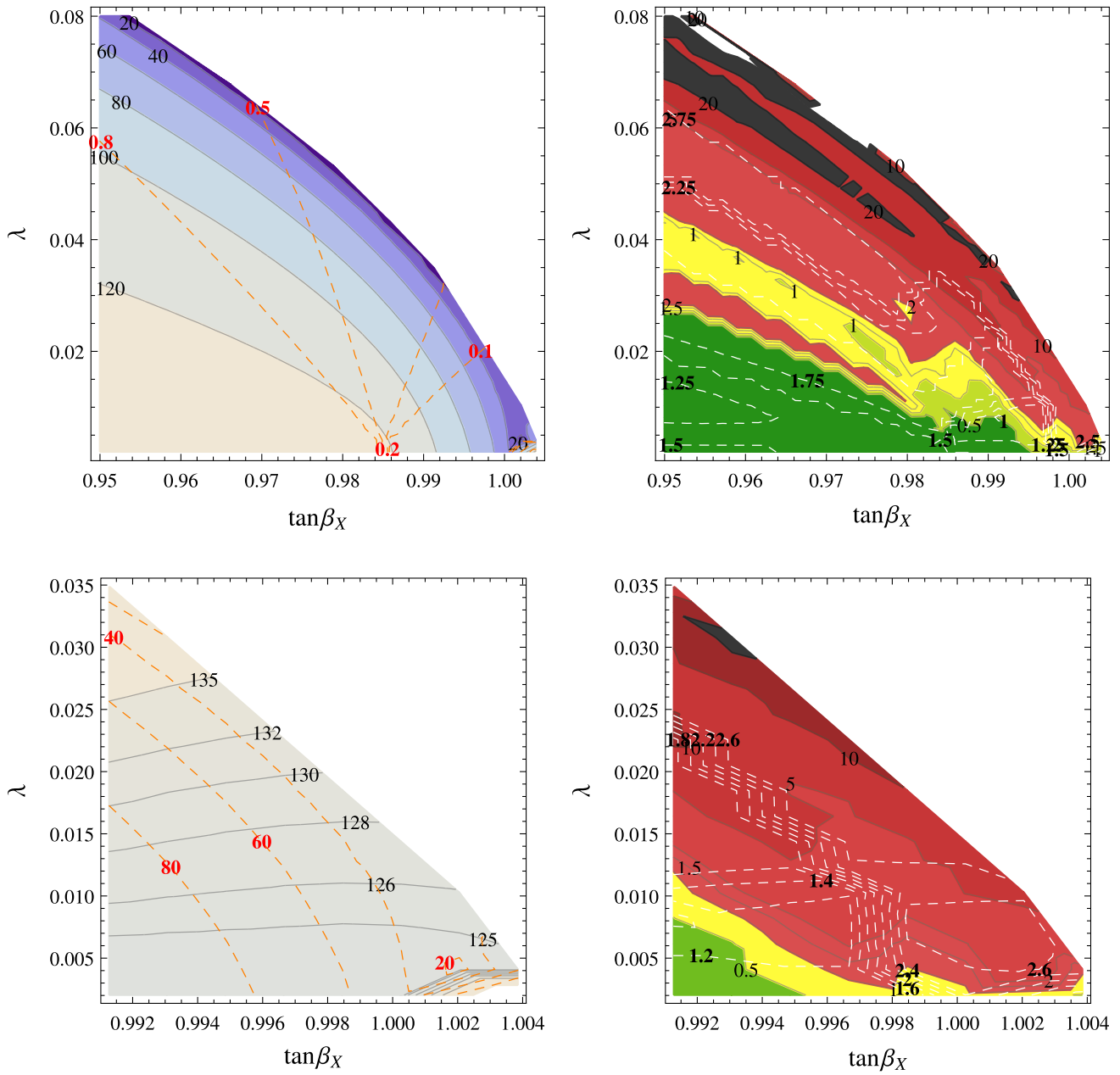

Fig. 22 *First row on the left*, we show the mass of the lightest CP-even scalar in the $(\tan\beta_X, \lambda)$ plane. *On top* of this, we give the *contour lines* for constant values of the doublet fraction of the lightest scalar (*orange lines* with *red labels*). *On the right* we show the results from `HiggsBounds` and `HiggsSignals` (*white contour lines* with *bold labels* for constant χ^2 divided by the number of considered Higgs observables: 81) in the same plane. The *red shaded* regions are excluded by Higgs searches. *Second row* zoom into the region with $\tan\beta_X$ close to 1. *On the left* the mass of the two lightest CP-even scalars are shown. The plot on the right provides the same information as the one in the first row

```
Block SPhenoInput    # SPheno specific input
  ...
50 0                 # Majorana phases: use only positive masses
```

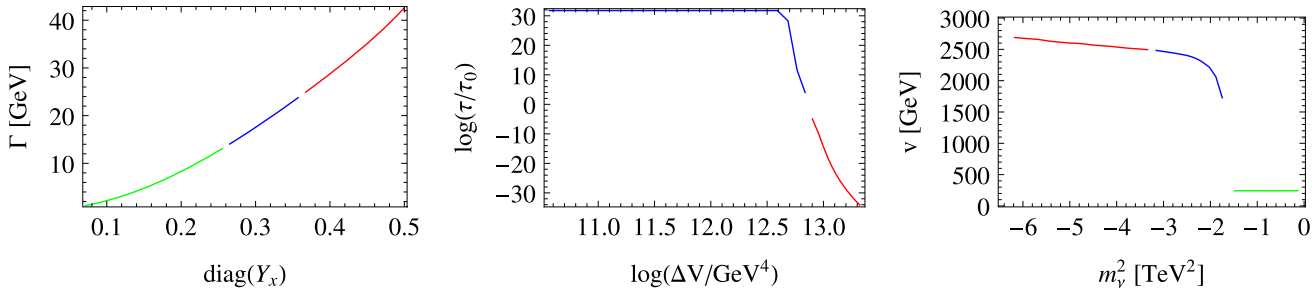

Fig. 23 *Left* total width of the 750 GeV particle as function of the diagonal entries in Y_x. The stability of the vacuum has been checked with `Vevacious`: the *green* region is absolutely stable, in the *blue* region the vacuum is unstable but long-lived, while in the *red* region the EW vacuum would decay too fast. *Middle* the life-time τ in ages of the universe, τ_0, as a function of the potential difference between the electroweak minimum and the global one. Note that the largest value `Vevacious` returns is 10^{30}. *Right* the value of the electroweak VEV v at the global minimum of the potential as function of the diagonal entries of m_ν^2

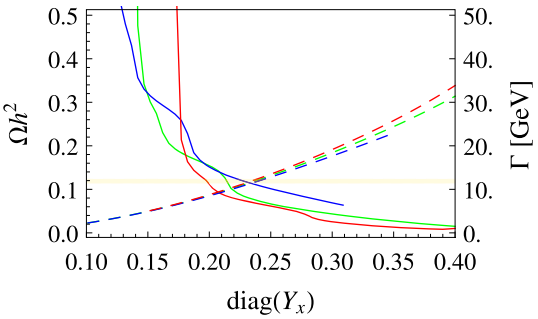

Fig. 24 Dark matter relic density Ωh^2 (*solid lines*) of the lightest sneutrino and total width of the 750 GeV scalar (*dashed lines*) as function of Y_x. For the *green line* the relation Eq. (5.44) was used, while the *red* and *blue lines* deviate from this relation by $\pm 0.4\,\%$. The *yellow shaded* region is the 3σ band of Planck + WP + hihgL + BAO [476]

The results from a small scan[18] are shown in Fig. 24. Here, we have used again the condition of Eq. (5.44) as well as very small deviations from it. One can see that the impact of this small variation on the total width is marginal, but the relic density is clearly affected. Thus, with some tuning of the parameters one can expect that it is possible to explain the dark matter relic density and the total width by light right-handed sneutrinos. However, also finding such a point is again beyond the scope of the example here.

Moreover, there are plenty of other dark matter candidates which mainly correspond to the gauge eigenstates $\tilde{S}$, $\tilde{X}$, $\tilde{\eta}$, $\tilde{\tilde{\eta}}$ beyond the ones from the MSSM. The properties of all of them could be checked with `MicrOmegas` as well. A detailed discussion of neutralino and sneutrino dark matter in $U(1)$ extensions of the MSSM and different mechanism to obtain the correct abundance was given for instance in Ref. [477].

[18] The relic density calculation for this model can be very time-consuming, especially for the sneutrinos where a large number of co-annihilation channels have to be calculated: the first parameter point might take several hours, all following points should take no longer than seconds, if no new channels are needed.

5.5.5 Flavour constraints

As mentioned above, we decided to include in this model mixing terms between the extra vector-like fermions and the MSSM particles in order to let the new states decay. In this way, we have a safe solution to circumvent any potential cosmological problem. If one assumes the new coupling matrices to have a generic form, i.e. large entries of $O(1)$, including off-diagonal ones as well, they can trigger flavour violation effects. For instance, let us assume that Y_e' has the following form

$$Y_e' = \begin{pmatrix} X & \alpha & \gamma \\ \alpha & X & \beta \\ \gamma & \beta & X \end{pmatrix}, \tag{5.45}$$

with degenerate diagonal entries X, and flavour violating entries α, β, γ. We can now check how strong the constraints on α, β, γ would be for given X. For this purpose, we use the results from `SPheno` for $\mathrm{Br}(\mu \to 3e)$, $\mathrm{Br}(\tau \to 3\mu)$, $\mathrm{Br}(\tau \to 3e)$, and μ–e conversion in Ti and Au, and compare the results with the current experimental limits, see Fig. 25. We find, for instance for $X = 0.1$, that α must be smaller than $\sim 10^{-9}$, while the limits on β, γ, obtained from τ decays, can still be as large as $O(10^{-6})$.

If other vector-like states mixing with the left-handed quarks or the right-handed down-like quarks are present – as would be the case for instance when assuming 5 or 10-plets of $SU(5)$ – there would also be stringent constraints on their couplings: they would cause tree-level contributions to ΔM_{B_s}. Since these observables are also calculated by `SPheno`, one can easily check the limits on models featuring those states.

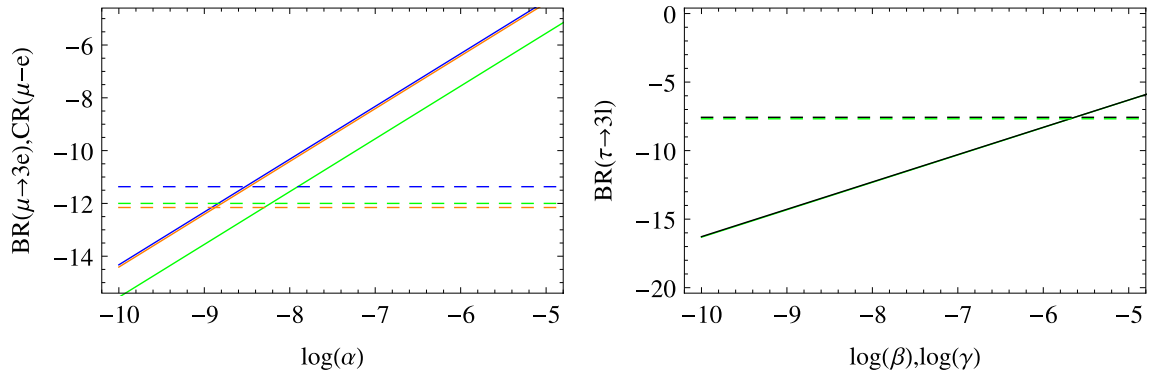

Fig. 25 *Left* Br($\mu \to 3e$) (*green*), and μ–e conversion in Ti (*blue*) or Au (*orange*). *Right* Br($\tau \to 3\mu$) (*green*), Br($\tau \to 3e$) (*black*). The *dashed lines* are the current experimental limits [478–481]. Here, we used $X = 0.1$

5.6 Z' mass limits

So far, we have picked a Z' mass of at least 2.5 TeV. Of course, we have to check that this is consistent with current exclusion limits. Recent exclusion limits for $pp \to Z' \to e^+e^-$ have been released by ATLAS using 13 TeV data and 3.2 fb^{-1} [482]. To compare the prediction for our model with these numbers, we can use the `UFO` model files generated by `SARAH` via

```
MakeUFO[];
```

and add them to `MadGraph`. For this purpose, we copy the `SARAH` generated files to a subdirectory `models/U1xMSSM` of the `MadGraph` installation. Afterwards, we generate all necessary files to calculate the cross section for the process under consideration by running in `MadGraph`

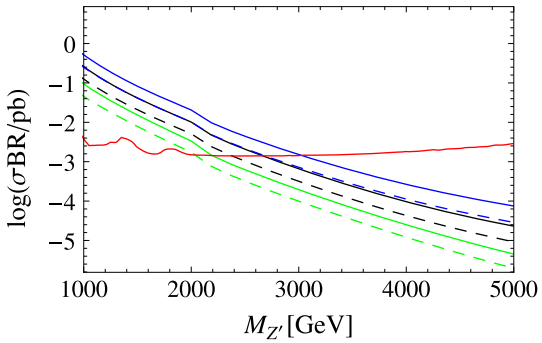

Fig. 26 Limit on $M_{Z'}$ for three different values of g_X: 0.3 (*green*), 0.5 (*black*), 0.7 (*blue*). For the *dashed line*, we assumed in addition $g_{1X} = -\frac{1}{5}g_X$, while for the *full lines* gauge kinetic mixing has been neglected. The *red line* shows the exclusion limit from ATLAS [482]

```
import model U1xMSSM -modelname
generate  p p > Zp > e1 e1bar
output pp_Zp_ee
```

Note the option `-modelname` when loading the model. This ensures that `MadGraph` is using the names for the particles as defined in our model implementation. Using the default names of `MadGraph` causes naming conflicts because of the extended Higgs sector. One can give the spectrum files written by `SPheno` as input (`param_card.dat`) for `MadGraph`. One just has to make sure that the blocks written for `HiggsBounds` and `HiggsSignals` are turned off because the `SLHA` parser of `MadGraph` is not able to handle them. This can be done by setting the following flag in the Les Houches input file:

```
Block SPhenoInput    # SPheno specific input
 ...
520 0               # Write effective Higgs couplings
                    # (HiggsBounds blocks)
```

In principle, one could also change the mass directly in the `param_card` without re-running `SPheno` for each point. However, the advantage of `SPheno` is that it calculates the width of the Z' gauge boson including SUSY and non-SUSY states. This usually has some impact on the obtained limits [471,483,484]. We can now scan over $M_{Z'}$ for fixed values of g_X and compare the predicted cross section with the exclusion limits. In addition, we can also check the impact of gauge-kinetic mixing: as we have seen, these couplings are negative and can be sizeable. Therefore, we compare

the results without gauge kinetic mixing and when setting $g_{1X} = -\frac{1}{5} g_X$ at the SUSY scale. The results are summarised in Fig. 26. We see that for $g_X = 0.5$ the limit is about 2.8 TeV without gauge-kinetic mixing. Including kinetic mixing, it gets reduced by about 200 GeV. Thus, one sees that kinetic mixing is not necessarily a small effect. This contradicts some claims that sometimes appear in the literature, where it is often argued that kinetic mixing can be ignored. In particular, we emphasise that this is very relevant when discussing a GUT theory with RGE running over many orders of magnitude in energy scale.

6 Summary

We have given an overview on weakly-coupled renormalisable models proposed to explain the excess observed by ATLAS and CMS around 750 GeV in the diphoton channel. We have pointed out that many of the papers quickly written after the announcement of the excess are based on assumptions and simplifications which are often unjustified and can lead to wrong conclusions. A very common mistake is the lack of inclusion of higher order corrections to the digluon and diphoton decay rates, which results in underestimating the ratio typically by a factor of 2. Several authors assume that the new 750 GeV scalar does not mix with the SM Higgs, which is often not justified. Including such a mixing can give large constraints. These and other problems can be easily avoided by using SARAH and related tools which were created with the purpose of facilitating precision studies of high energy physics models. In particular, the link between SARAH and the spectrum generators FlexibleSUSY and SPheno is a powerful approach to obtain the mass spectrum and all the rotation matrices for any given model *without neglecting flavour mixing, complex phases or 1st and 2nd generation Yukawa couplings*. Optionally, one can also include all the important radiative corrections up to two loops. In addition, we have improved the functionality of FlexibleSUSY and SPheno to calculate the diphoton and digluon decay widths of neutral scalars, including the higher order QCD corrections up to N^{3}LO. One can now pass on this information directly to Monte-Carlo tools, like CalcHep and MadGraph, by using the appropriate model files generated with SARAH.

In order to study as many models in as much detail as possible, we have created a database of SARAH model files for many of the ideas proposed so far in the literature. The database is also meant to provide many examples in the context of the diphoton excess with which the novel user can try out to familiarise with SARAH, in order to build up the level of expertise needed to implement their own models in the future.

Finally, we have introduced an attractive SUSY model which combines the idea of non-decoupling D-terms with the explanation of the diphoton excess. We have used this as a new example to show how to use SARAH to first understand the model analytically at leading order. As a second step, we have performed a numerical analysis of the important loop corrections to the different masses, checked limits from Higgs searches, neutral gauge bosons searches, and from lepton flavour violation. We have demonstrated that this model could explain a large width of the 750 GeV scalar, but in this context limits from spontaneous R-parity violation become important. These limits can be checked by using the interface to Vevacious.

Acknowledgments We thank Martin Winkler for beta-testing and valuable impact, and Michael Spira for helpful discussions. Mark Goodsell acknowledges support from Agence Nationale de Recherche Grant ANR-15-CE31-0002 "HiggsAutomator," and would like to thank Pietro Slavich and Luc Darmé for interesting discussions. Avelino Vicente acknowledges financial support from the "Juan de la Cierva" program (27-13-463B-731) funded by the Spanish MINECO as well as from the Spanish Grants FPA2014-58183-P, Multidark CSD2009-00064 and SEV-2014-0398 (MINECO), FPA2011-22975 and PROMETEOII/2014/084 (Generalitat Valenciana), and is grateful to Wei-Chih Huang for discussions about the GTHDM model. Manuel E. Krauss is supported by the BMBF Grant 00160287 and thanks Cesar Bonilla for useful discussions on left-right models. Lorenzo Basso acknowledges support by the OCEVU Labex (ANR-11-LABX- 0060) and the A*MIDEX project (ANR-11-IDEX-0001-02), funded by the "Investissements d'Avenir" French government program managed by the ANR. The work by Peter Athron is in part supported by the ARC Centre of Excellence for Particle Physics at the Tera-scale. Dylan Harries is supported by the University of Adelaide and the ARC Centre of Excellence for Particle Physics at the Tera-scale. Florian Staub thanks Alfredo Urbano for discussions about the Georgi-Machacek model and for testing the model file.

Funded by SCOAP^3.

References

1. ATLAS Collaboration, M. Aaboud et al., Search for resonances in diphoton events at $\sqrt{s}$ = 13 TeV with the ATLAS detector. arXiv:1606.03833
2. CMS Collaboration, V. Khachatryan et al., Search for resonant production of high-mass photon pairs in proton–proton collisions at sqrt(s) = 8 and 13 TeV. arXiv:1606.04093
3. ATLAS Collaboration, T.A. collaboration, Search for scalar diphoton resonances with 15.4 fb^{-1} of data collected at $\sqrt{s}$ = 13 TeV in 2015 and 2016 with the ATLAS detector
4. CMS Collaboration, C. Collaboration, Search for resonant production of high mass photon pairs using 12.9 fb^{-1} of proton–proton collisions at $\sqrt{s}$ = 13 TeV and combined interpretation of searches at 8 and 13 TeV

5. S. Abel, V.V. Khoze, Photo-production of a 750 GeV di-photon resonance mediated by Kaluza–Klein leptons in the loop. arXiv:1601.07167
6. F. Abu-Ajamieh, R. Houtz, R. Zheng, Interpretation of 750 GeV diphoton resonance within the RS model and the associated radion phenomenology. arXiv:1607.01464
7. B. Agarwal, J. Isaacson, K.A. Mohan, Minimal dilaton model and the diphoton excess. arXiv:1604.05328
8. P. Agrawal, J. Fan, B. Heidenreich, M. Reece, M. Strassler, Experimental considerations motivated by the diphoton excess at the LHC. arXiv:1512.05775
9. A. Ahmed, B.M. Dillon, B. Grzadkowski, J.F. Gunion, Y. Jiang, Higgs-radion interpretation of 750 GeV di-photon excess at the LHC. arXiv:1512.05771
10. A. Ahriche, G. Faisel, S. Nasri, J. Tandean, Addressing the LHC 750 GeV diphoton excess without new colored states. arXiv:1603.01606
11. S. Alexander, L. Smolin, Enhanced color gauge invariance and a new di-photon state at the LHC. arXiv:1601.03091
12. B.C. Allanach, P.S.B. Dev, S.A. Renner, K. Sakurai, Di-photon excess explained by a resonant sneutrino in R-parity violating supersymmetry. arXiv:1512.07645
13. D. Aloni, K. Blum, A. Dery, A. Efrati, Y. Nir, On a possible large width 750 GeV diphoton resonance at ATLAS and CMS. arXiv:1512.05778
14. W. Altmannshofer, J. Galloway, S. Gori, A.L. Kagan, A. Martin, J. Zupan, On the 750 GeV di-photon excess. arXiv:1512.07616
15. E. Alvarez, L. Da Rold, J. Mazzitelli, A. Szynkman, A 750 GeV graviton and the Higgs as a pNGB. arXiv:1606.05326
16. A. Alves, A.G. Dias, K. Sinha, The 750 GeV S-cion: where else should we look for it? arXiv:1512.06091
17. A. Alves, A.G. Dias, K. Sinha, Diphotons at the Z-pole in models of the 750 GeV resonance decaying to axion-like particles. arXiv:1606.06375
18. H. An, C. Cheung, Y. Zhang, Broad diphotons from narrow states. arXiv:1512.08378
19. L.A. Anchordoqui, I. Antoniadis, H. Goldberg, X. Huang, D. Lust, T.R. Taylor, 750 GeV diphotons from closed string states. arXiv:1512.08502
20. L.A. Anchordoqui, H. Goldberg, X. Huang, Constraints on 750 GeV colorless Q-onia from running couplings. arXiv:1605.01937
21. L.A. Anchordoqui, I. Antoniadis, H. Goldberg, X. Huang, D. Lust, T.R. Taylor, Update on 750 GeV diphotons from closed string states. Phys. Lett. B **759**, 223–228 (2016). arXiv:1603.08294
22. O. Antipin, M. Mojaza, F. Sannino, A natural Coleman–Weinberg theory explains the diphoton excess. arXiv:1512.06708
23. O. Antipin, P. Culjak, K. Kumericki, I. Picek, Radiative neutrino models in light of diphoton signals. arXiv:1606.05163
24. L. Aparicio, A. Azatov, E. Hardy, A. Romanino, Diphotons from diaxions. arXiv:1602.00949
25. T. Appelquist, J. Ingoldby, M. Piai, J. Thompson, A spartan model for the LHC diphoton excess. arXiv:1606.00865
26. C. Arbelaez, A.E. Cárcamo Hernández, S. Kovalenko, I. Schmidt, Linking radiative seesaw-type mechanism of fermion masses and non-trivial quark mixing with the 750 GeV diphoton excess. arXiv:1602.03607
27. B.A. Arbuzov, I.V. Zaitsev, On a possibility of a consistent interpretation of diboson excesses at LHC. arXiv:1602.08293
28. G. Arcadi, P. Ghosh, Y. Mambrini, M. Pierre, Re-opening dark matter windows compatible with a diphoton excess. arXiv:1603.05601
29. M.T. Arun, P. Saha, Gravitons in multiply warped scenarios—at 750 GeV and beyond. arXiv:1512.06335
30. M.T. Arun, D. Choudhury, Bulk gauge and matter fields in nested warping: II. Symmetry breaking and phenomenological consequences. arXiv:1601.02321
31. J. Ashfaque, L. Delle Rose, A.E. Faraggi, C. Marzo, The LHC di-photon excess and gauge coupling unification in extra Z' heterotic-string derived models. arXiv:1606.01052
32. J.M. Ashfaque, The observed diphoton excess in F-theory inspired heterotic string-derived model. arXiv:1607.03076
33. U. Aydemir, T. Mandal, Interpretation of the 750 GeV diphoton excess with colored scalars in **SO(10)** grand unification. arXiv:1601.06761
34. U. Aydemir, D. Minic, C. Sun, T. Takeuchi, The 750 GeV diphoton excess in unified $SU(2)_L \times SU(2)_R \times SU(4)$ models from noncommutative geometry. Mod. Phys. Lett. A **31**(18), 1650101 (2016). arXiv:1603.01756
35. M. Backovic, A. Mariotti, D. Redigolo, Di-photon excess illuminates dark matter. arXiv:1512.04917
36. M. Badziak, Interpreting the 750 GeV diphoton excess in minimal extensions of two-Higgs-doublet models. arXiv:1512.07497
37. M. Badziak, M. Olechowski, S. Pokorski, K. Sakurai, Interpreting 750 GeV diphoton excess in plain NMSSM. arXiv:1603.02203
38. K.J. Bae, C.-R. Chen, K. Hamaguchi, I. Low, From the 750 GeV diphoton resonance to multilepton excesses. arXiv:1604.07941
39. K.J. Bae, K. Hamaguchi, T. Moroi, K. Yanagi, Probing the origin of 750 GeV diphoton excess with the precision measurements at the ILC. Phys. Lett. B **759**, 575–582 (2016). arXiv:1604.08307
40. K.J. Bae, M. Endo, K. Hamaguchi, T. Moroi, Diphoton excess and running couplings. arXiv:1602.03653
41. S. Baek, J.-H. Park, LHC 750 GeV diphoton excess and muon $(g-2)$. Phys. Lett. B **758**, 416–422 (2016). arXiv:1602.05588
42. Y. Bai, J. Berger, R. Lu, A 750 GeV dark pion: cousin of a dark G-parity-odd WIMP. arXiv:1512.05779
43. Y. Bai, V. Barger, J. Berger, Color-octet companions of a 750 GeV heavy pion. arXiv:1604.07835
44. Y. Bai, J. Berger, J. Osborne, B.A. Stefanek, A chiral composite model for the 750 GeV diphoton resonance. arXiv:1605.07183
45. S. Banerjee, D. Barducci, G. Bélanger, C. Delaunay, Implications of a high-mass diphoton resonance for heavy quark searches. arXiv:1606.09013
46. P. Baratella, J. Elias-Miro, J. Penedo, A. Romanino, A closer look to the sgoldstino interpretation of the diphoton excess. JHEP **06**, 086 (2016). arXiv:1603.05682
47. R. Barbieri, D. Buttazzo, L.J. Hall, D. Marzocca, Higgs mass and unified gauge coupling in the NMSSM with vector matter. arXiv:1603.00718
48. D. Bardhan, D. Bhatia, A. Chakraborty, U. Maitra, S. Raychaudhuri, T. Samui, Radion candidate for the LHC diphoton resonance. arXiv:1512.06674
49. D. Bardhan, P. Byakti, D. Ghosh, T. Sharma, The 750 GeV diphoton resonance as an sgoldstino: a reappraisal. JHEP **06**, 129 (2016). arXiv:1603.05251
50. D. Barducci, A. Goudelis, S. Kulkarni, D. Sengupta, One jet to rule them all: monojet constraints and invisible decays of a 750 GeV diphoton resonance. arXiv:1512.06842
51. N.D. Barrie, A. Kobakhidze, S. Liang, M. Talia, L. Wu, Heavy leptonium as the origin of the 750 GeV diphoton excess. arXiv:1604.02803
52. N.D. Barrie, A. Kobakhidze, M. Talia, L. Wu, 750 GeV composite axion as the LHC diphoton resonance. arXiv:1602.00475
53. M. Bauer, M. Neubert, Flavor anomalies, the diphoton excess and a dark matter candidate. arXiv:1512.06828
54. M. Bauer, C. Hoerner, M. Neubert, Diphoton resonance from a warped extra dimension. arXiv:1603.05978
55. M. Bauer, M. Neubert, A. Thamm, The "forgotten" decay $S \to Zh$ as a CP analyzer. arXiv:1606.01016
56. D. Becirevic, E. Bertuzzo, O. Sumensari, R.Z. Funchal, Can the new resonance at LHC be a CP-odd Higgs boson? arXiv:1512.05623

57. G. Bélanger, C. Delaunay, A dark aector for $g_\mu - 2$, R_K and a diphoton resonance. arXiv:1603.03333
58. A. Belhaj, S.-E. Ennadifi, On 750 GeV diphoton resonance in stringy standard-like models. arXiv:1606.02956
59. B. Bellazzini, R. Franceschini, F. Sala, J. Serra, Goldstones in diphotons. arXiv:1512.05330
60. A. Belyaev, G. Cacciapaglia, H. Cai, T. Flacke, A. Parolini, H. Serôdio, Singlets in composite Higgs models in light of the LHC di-photon searches. arXiv:1512.07242
61. K. Benakli, L. Darmé, M.D. Goodsell, J. Harz, The di-photon excess in a perturbative SUSY model. arXiv:1605.05313
62. R. Benbrik, C.-H. Chen, T. Nomura, Higgs singlet as a diphoton resonance in a vector-like quark model. arXiv:1512.06028
63. I. Ben-Dayan, R. Brustein, Hypercharge axion and the diphoton 750 GeV resonance. arXiv:1601.07564
64. A. Berlin, The diphoton and diboson excesses in a left-right symmetric theory of dark matter. arXiv:1601.01381
65. J. Bernon, C. Smith, Could the width of the diphoton anomaly signal a three-body decay? arXiv:1512.06113
66. J. Bernon, A. Goudelis, S. Kraml, K. Mawatari, D. Sengupta, Characterising the 750 GeV diphoton excess. JHEP **05**, 128 (2016). arXiv:1603.03421
67. L. Berthier, J.M. Cline, W. Shepherd, M. Trott, Effective interpretations of a diphoton excess. arXiv:1512.06799
68. E. Bertuzzo, P.A.N. Machado, M. Taoso, Di-photon excess in the 2HDM: hasting towards the instability and the non-perturbative regime. arXiv:1601.07508
69. A. Bharucha, A. Djouadi, A. Goudelis, Threshold enhancement of diphoton resonances. arXiv:1603.04464
70. S. Bhattacharya, S. Patra, N. Sahoo, N. Sahu, 750 GeV di-photon excess at CERN LHC from a dark sector assisted scalar decay. arXiv:1601.01569
71. X.-J. Bi, R. Ding, Y. Fan, L. Huang, C. Li, T. Li, S. Raza, X.-C. Wang, B. Zhu, A promising interpretation of diphoton resonance at 750 GeV. arXiv:1512.08497
72. X.-J. Bi, Q.-F. Xiang, P.-F. Yin, Z.-H. Yu, The 750 GeV diphoton excess at the LHC and dark matter constraints. arXiv:1512.06787
73. L. Bian, N. Chen, D. Liu, J. Shu, A hidden confining world on the 750 GeV diphoton excess. arXiv:1512.05759
74. N. Bizot, S. Davidson, M. Frigerio, J.L. Kneur, Two Higgs doublets to explain the excesses $pp \to \gamma\gamma(750\ \text{GeV})$ and $h \to \tau^{\pm}\mu^{\mp}$. arXiv:1512.08508
75. A. Bolaños, J.L. Diaz-Cruz, G. Hernández-Tomé, G. Tavares-Velasco, Has a Higgs-flavon with a 750 GeV mass been detected at the LHC13? arXiv:1604.04822
76. K. Bondarenko, A. Boyarsky, O. Ruchayskiy, M. Shaposhnikov, Features in the standard model diphoton background. arXiv:1606.09592
77. C. Bonilla, M. Nebot, R. Srivastava, J.W.F. Valle, Flavor physics scenario for the 750 GeV diphoton anomaly. Phys. Rev. D **93**(7), 073009 (2016). arXiv:1602.08092
78. E.E. Boos, V.E. Bunichev, I.P. Volobuev, Can the 750 GeV diphoton LHC excess be due to a radion-dominated state? arXiv:1603.04495
79. D. Borah, S. Patra, S. Sahoo, Subdominant left-right scalar dark matter as origin of the 750 GeV di-photon excess at LHC. arXiv:1601.01828
80. S.M. Boucenna, S. Morisi, A. Vicente, The LHC diphoton resonance from gauge symmetry. arXiv:1512.06878
81. M.R. Buckley, Wide or narrow? The phenomenology of 750 GeV diphotons. arXiv:1601.04751
82. D. Buttazzo, A. Greljo, D. Marzocca, Knocking on new physics' door with a scalar resonance. arXiv:1512.04929
83. D. Buttazzo, A. Greljo, G. Isidori, D. Marzocca, Toward a coherent solution of diphoton and flavor anomalies. arXiv:1604.03940
84. C. Cai, Z.-H. Yu, H.-H. Zhang, The 750 GeV diphoton resonance as a singlet scalar in an extra dimensional model. arXiv:1512.08440
85. X. Calmet, The dual standard model and the 750 GeV events at the LHC. arXiv:1604.06185
86. J. Cao, F. Wang, Y. Zhang, Interpreting the 750 GeV diphton excess within TopFlavor seesaw model. arXiv:1512.08392
87. Q.-H. Cao, Y. Liu, K.-P. Xie, B. Yan, D.-M. Zhang, A boost test of anomalous diphoton resonance at the LHC. arXiv:1512.05542
88. Q.-H. Cao, Y. Liu, K.-P. Xie, B. Yan, D.-M. Zhang, The diphoton excess, low energy theorem and the 331 model. arXiv:1512.08441
89. J. Cao, C. Han, L. Shang, W. Su, J. M. Yang, Y. Zhang, Interpreting the 750 GeV diphoton excess by the singlet extension of the Manohar–Wise model. arXiv:1512.06728
90. Q.-H. Cao, S.-L. Chen, P.-H. Gu, Strong CP problem, neutrino masses and the 750 GeV diphoton resonance. arXiv:1512.07541
91. Q.-H. Cao, Y.-Q. Gong, X. Wang, B. Yan, L.L. Yang, One bump or two peaks? The 750 GeV diphoton excess and dark matter with a complex mediator. arXiv:1601.06374
92. J. Cao, L. Shang, W. Su, Y. Zhang, J. Zhu, Interpreting the 750 GeV diphoton excess in the minimal dilaton model. arXiv:1601.02570
93. M. Carena, P. Huang, A. Ismail, I. Low, N.R. Shah, C.E.M. Wagner, A second peak in diphoton (or diboson) resonances. arXiv:1606.06733
94. A. Carmona, A 750 GeV graviton from holographic composite dark sectors. arXiv:1603.08913
95. A. Carmona, F. Goertz, A. Papaefstathiou, Uncovering the relation of a di-photon scalar resonance to the Higgs boson. arXiv:1606.02716
96. L.M. Carpenter, R. Colburn, J. Goodman, Supersoft SUSY models and the 750 GeV diphoton excess, beyond effective operators. arXiv:1512.06107
97. J.A. Casas, J.R. Espinosa, J.M. Moreno, The 750 GeV diphoton excess as a first light on supersymmetry breaking. arXiv:1512.07895
98. N. Chakrabarty, B. Mukhopadhyaya, S. SenGupta, Diphoton excess via Chern–Simons interaction in a warped geometry scenario. arXiv:1604.00885
99. J. Chakrabortty, A. Choudhury, P. Ghosh, S. Mondal, T. Srivastava, Di-photon resonance around 750 GeV: shedding light on the theory underneath. arXiv:1512.05767
100. S. Chakraborty, A. Chakraborty, S. Raychaudhuri, Diphoton resonance at 750 GeV in the broken MRSSM. arXiv:1512.07527
101. I. Chakraborty, A. Kundu, Diphoton excess at 750 GeV: singlet scalars confront naturalness. arXiv:1512.06508
102. M. Chala, M. Duerr, F. Kahlhoefer, K. Schmidt-Hoberg, Tricking Landau–Yang: how to obtain the diphoton excess from a vector resonance. arXiv:1512.06833
103. M. Chala, C. Grojean, M. Riembau, T. Vantalon, Deciphering the CP nature of the 750 GeV resonance. arXiv:1604.02029
104. S. Chang, A simple $U(1)$ gauge rheory explanation of the diphoton excess. arXiv:1512.06426
105. J. Chang, K. Cheung, C.-T. Lu, Interpreting the 750 GeV diphoton resonance using photon-jets in hidden-valley-like models. arXiv:1512.06671
106. W. Chao, Neutrino catalyzed diphoton excess. arXiv:1512.08484
107. W. Chao, Symmetries behind the 750 GeV diphoton excess. arXiv:1512.06297
108. W. Chao, R. Huo, J.-H. Yu, The minimal scalar-stealth top interpretation of the diphoton excess. arXiv:1512.05738
109. W. Chao, The diphoton excess inspired electroweak baryogenesis. arXiv:1601.04678
110. W. Chao, The diphoton excess from an exceptional supersymmetric standard model. arXiv:1601.00633
111. C.-Y. Chen, M. Lefebvre, M. Pospelov, Y.-M. Zhong, Diphoton excess through dark mediators. arXiv:1603.01256

112. C.-H. Chen, T. Nomura, 750 GeV diphoton resonance and the implications in an $SU(2)_1 \times SU(2)_2 \times U(1)_Y$ model. arXiv:1606.03804
113. K. Cheung, P. Ko, J.S. Lee, J. Park, P.-Y. Tseng, A Higgcision study on the 750 GeV di-photon resonance and 125 GeV SM Higgs boson with the Higgs-singlet mixing. arXiv:1512.07853
114. C.-W. Chiang, M. Ibe, T.T. Yanagida, Revisiting scalar quark hidden sector in light of 750-GeV diphoton resonance. arXiv:1512.08895
115. C.-W. Chiang, H. Fukuda, M. Ibe, T.T. Yanagida, 750 GeV diphoton resonance in a visible heavy QCD axion model. Phys. Rev. D **93**(9), 095016 (2016). arXiv:1602.07909
116. C.-W. Chiang, A.-L. Kuo, Can the 750-GeV diphoton resonance be the singlet Higgs boson of custodial Higgs triplet model? arXiv:1601.06394
117. R.S. Chivukula, A. Farzinnia, K. Mohan, E.H. Simmons, Diphoton resonances in the renormalizable coloron model. arXiv:1604.02157
118. W.S. Cho, D. Kim, K. Kong, S.H. Lim, K.T. Matchev, J.-C. Park, M. Park, The 750 GeV diphoton excess may not imply a 750 GeV resonance. arXiv:1512.06824
119. K. Choi, S.H. Im, H. Kim, D.Y. Mo, 750 GeV diphoton resonance and electric dipole moments. arXiv:1605.00206
120. D. Choudhury, K. Ghosh, The LHC diphoton excess at 750 GeV in the framework of the constrained minimal supersymmetric standard model. arXiv:1605.00013
121. D. Chway, R. Dermíšek, T.H. Jung, H.D. Kim, Glue to light signal of a new particle. arXiv:1512.08221
122. J.M. Cline, Z. Liu, LHC diphotons from electroweakly pair-produced composite pseudoscalars. arXiv:1512.06827
123. T. Cohen, G.D. Kribs, A.E. Nelson, B. Ostdiek, 750 GeV diphotons from supersymmetry with Dirac gauginos. arXiv:1605.04308
124. J.H. Collins, C. Csaki, J.A. Dror, S. Lombardo, Novel kinematics from a custodially protected diphoton resonance. Phys. Rev. D **93**(11), 115001 (2016). arXiv:1603.09350
125. P. Cox, A.D. Medina, T.S. Ray, A. Spray, Diphoton excess at 750 GeV from a radion in the bulk-Higgs scenario. arXiv:1512.05618
126. N. Craig, P. Draper, C. Kilic, S. Thomas, How the $\gamma\gamma$ resonance stole Christmas. arXiv:1512.07733
127. C. Csaki, J. Hubisz, J. Terning, The minimal model of a diphoton resonance: production without gluon couplings. arXiv:1512.05776
128. C. Csaki, L. Randall, A diphoton resonance from bulk RS. arXiv:1603.07303
129. C. Csaki, J. Hubisz, S. Lombardo, J. Terning, Gluon vs. photon production of a 750 GeV diphoton resonance. arXiv:1601.00638
130. Y. Cui, T. Okui, A. Yunesi, The 750 GeV diphoton casting the first light on baryogenesis. arXiv:1605.08736
131. D. Curtin, C.B. Verhaaren, Quirky explanations for the diphoton excess. arXiv:1512.05753
132. M. Cvetič, J. Halverson, P. Langacker, String consistency, heavy exotics, and the 750 GeV diphoton excess at the LHC. arXiv:1512.07622
133. G. Cynolter, J. Kovács, E. Lendvai, Diphoton excess and VV-scattering. Mod. Phys. Lett. A **31** (22), 1650133 (2016). arXiv:1604.01008
134. M. Dalchenko, B. Dutta, Y. Gao, T. Ghosh, T. Kamon, Exploring the jet multiplicity in the 750 GeV diphoton excess. arXiv:1606.03067
135. U. Danielsson, R. Enberg, G. Ingelman, T. Mandal, The force awakens—the 750 GeV diphoton excess at the LHC from a varying electromagnetic coupling. arXiv:1601.00624
136. K. Das, S. K. Rai, The 750 GeV diphoton excess in a $U(1)$ hidden symmetry model. arXiv:1512.07789
137. K. Das, T. Li, S. Nandi, S.K. Rai, A new proposal for diphoton resonance from E_6 motivated extra $U(1)$. arXiv:1607.00810
138. A. Dasgupta, M. Mitra, D. Borah, Minimal left-right symmetry confronted with the 750 GeV di-photon excess at LHC. arXiv:1512.09202
139. B. Dasgupta, J. Kopp, P. Schwaller, Photons, photon jets and dark photons at 750 GeV and beyond. arXiv:1602.04692
140. J.H. Davis, M. Fairbairn, J. Heal, P. Tunney, The significance of the 750 GeV fluctuation in the ATLAS Run 2 diphoton data. arXiv:1601.03153
141. H. Davoudiasl, C. Zhang, A 750 GeV messenger of dark conformal symmetry breaking. arXiv:1512.07672
142. H. Davoudiasl, P.P. Giardino, C. Zhang, Exo-Higgs at 750 GeV and genesis of baryons. arXiv:1605.00037
143. S. Dawson, I.M. Lewis, Singlet model interference effects and a 750 GeV diphoton resonance. arXiv:1605.04944
144. J. de Blas, J. Santiago, R. Vega-Morales, New vector bosons and the diphoton excess. arXiv:1512.07229
145. C. Delaunay, Y. Soreq, Probing new physics with isotope shift spectroscopy. arXiv:1602.04838
146. A. Delgado, M. Garcia-Pepin, M. Quiros, J. Santiago, R. Vega-Morales, Diphoton and diboson probes of fermiophobic Higgs bosons at the LHC. JHEP **06**, 042 (2016). arXiv:1603.00962
147. S.V. Demidov, D.S. Gorbunov, On sgoldstino interpretation of the diphoton excess. arXiv:1512.05723
148. F.F. Deppisch, S. Kulkarni, H. Päs, E. Schumacher, Leptoquark patterns unifying neutrino masses, flavor anomalies and the diphoton excess. arXiv:1603.07672
149. F.F. Deppisch, C. Hati, S. Patra, P. Pritimita, U. Sarkar, Implications of the diphoton excess on left-right models and gauge unification. arXiv:1601.00952
150. F. D'Eramo, J. de Vries, P. Panci, A 750 GeV portal: LHC phenomenology and dark matter candidates. arXiv:1601.01571
151. V. De Romeri, J.S. Kim, V. Martín-Lozano, K. Rolbiecki, R. Ruiz de Austri, Confronting dark matter with the diphoton excess from a parent resonance decay. Eur. Phys. J. C **76**(5), 262 (2016). arXiv:1603.04479
152. P.S.B. Dev, D. Teresi, Asymmetric dark matter in the Sun and the diphoton excess at the LHC. arXiv:1512.07243
153. P.S.B. Dev, R.N. Mohapatra, Y. Zhang, Quark seesaw vectorlike fermions and diphoton excess. arXiv:1512.08507
154. U.K. Dey, S. Mohanty, G. Tomar, 750 GeV resonance in the dark left-right model. arXiv:1512.07212
155. U.K. Dey, S. Mohanty, G. Tomar, Leptoquarks: 750 GeV diphoton resonance and IceCube events. arXiv:1606.07903
156. M. Dhuria, G. Goswami, Perturbativity, vacuum stability and inflation in the light of 750 GeV diphoton excess. arXiv:1512.06782
157. S. Di Chiara, L. Marzola, M. Raidal, First interpretation of the 750 GeV di-photon resonance at the LHC. arXiv:1512.04939
158. S. Di Chiara, A. Hektor, K. Kannike, L. Marzola, M. Raidal, Large loop-coupling enhancement of a 750 GeV pseudoscalar from a light dark sector. arXiv:1603.07263
159. A. Di Iura, J. Herrero-Garcia, D. Meloni, Phenomenology of SU(5) low-energy realizations: the diphoton excess and Higgs flavor violation. arXiv:1606.08785
160. B.M. Dillon, V. Sanz, A little KK graviton at 750 GeV. arXiv:1603.09550
161. B.M. Dillon, C. Han, H.M. Lee, M. Park, Confronting diphoton resonance with cascade decays in warped gravity. arXiv:1606.07171
162. L. Di Luzio, J.F. Kamenik, M. Nardecchia, Implications of perturbative unitarity for the $\gamma\gamma$ resonance at 750 GeV. arXiv:1604.05746
163. S. Dimopoulos, A. Hook, J. Huang, G. Marques-Tavares, A 750 GeV QCD axion. arXiv:1606.03097
164. K. Dimopoulos, C. Owen, How the diphoton excess may save minimal hybrid inflation in supergravity. arXiv:1606.06677

165. R. Ding, L. Huang, T. Li, B. Zhu, Interpreting 750 GeV diphoton excess with R-parity violation supersymmetry. arXiv:1512.06560
166. R. Ding, Z.-L. Han, Y. Liao, X.-D. Ma, Interpretation of 750 GeV diphoton excess at LHC in singlet extension of color-octet neutrino mass model. arXiv:1601.02714
167. R. Ding, Y. Fan, L. Huang, C. Li, T. Li, S. Raza, B. Zhu, Systematic study of diphoton resonance at 750 GeV from sgoldstino. arXiv:1602.00977
168. D.N. Dinh, N.A. Ky, P.Q. Văn, N.T.H. Vân, A see-saw scenario of an A_4 flavour symmetric standard model. arXiv:1602.07437
169. A. Djouadi, J. Ellis, J. Quevillon, Interference effects in the decays of 750 GeV states into $\gamma\gamma$ and $t\bar{t}$. arXiv:1605.00542
170. A. Djouadi, J. Ellis, R. Godbole, J. Quevillon, Future collider signatures of the possible 750 GeV state. arXiv:1601.03696
171. A. Djouadi, A. Pilaftsis, The 750 GeV diphoton resonance in the MSSM. arXiv:1605.01040
172. B.A. Dobrescu, P.J. Fox, J. Kearney, Multi-step production of a diphoton resonance. arXiv:1605.08772
173. F. Domingo, S. Heinemeyer, J.S. Kim, K. Rolbiecki, The NMSSM lives: with the 750 GeV diphoton excess. Eur. Phys. J. C **76**(5), 249 (2016). arXiv:1602.07691
174. I. Dorsner, S. Fajfer, N. Kosnik, Is symmetry breaking of SU(5) theory responsible for the diphoton excess? arXiv:1601.03267
175. P. Draper, D. McKeen, Diphotons, new vacuum angles, and strong CP. arXiv:1602.03604
176. H.K. Dreiner, M.E. Krauss, B. O'Leary, T. Opferkuch, F. Staub, Validity of the CMSSM interpretation of the diphoton excess. Phys. Rev. D **94** (5), 055013 (2016). arXiv:1606.08811
177. M. Duerr, P. Fileviez Perez, J. Smirnov, New forces and the 750 GeV resonance. arXiv:1604.05319
178. B. Dutta, Y. Gao, T. Ghosh, I. Gogoladze, T. Li, Interpretation of the diphoton excess at CMS and ATLAS. arXiv:1512.05439
179. B. Dutta, Y. Gao, T. Ghosh, I. Gogoladze, T. Li, J.W. Walker, An SU(6) GUT origin of the TeV-scale vector-like particles associated with the 750 GeV diphoton resonance. arXiv:1604.07838
180. B. Dutta, Y. Gao, T. Ghosh, I. Gogoladze, T. Li, Q. Shafi, J. W. Walker, Diphoton excess in consistent supersymmetric SU(5) models with vector-like particles. arXiv:1601.00866
181. A. Efrati, J.F. Kamenik, Y. Nir, The phenomenology of the diphoton excess and $h \to \tau\mu$ within 2HDM. arXiv:1606.07082
182. J. Ellis, S.A.R. Ellis, J. Quevillon, V. Sanz, T. You, On the interpretation of a possible $\sim$ 750 GeV particle decaying into $\gamma\gamma$. arXiv:1512.05327
183. U. Ellwanger, C. Hugonie, A 750 GeV diphoton signal from a very light pseudoscalar in the NMSSM. arXiv:1602.03344
184. M. Fabbrichesi, A. Urbano, The breaking of the $SU(2)_L \times U(1)_Y$ symmetry: the 750 GeV resonance at the LHC and perturbative unitarity. arXiv:1601.02447
185. M. Fabbrichesi, M. Pinamonti, A. Urbano, Telling the spin of the di-photon resonance. arXiv:1604.06948
186. A. Falkowski, O. Slone, T. Volansky, Phenomenology of a 750 GeV singlet. arXiv:1512.05777
187. A. Falkowski, J.F. Kamenik, Di-photon portal to warped gravity. arXiv:1603.06980
188. A.E. Faraggi, J. Rizos, The 750 GeV diphoton LHC excess and Extra Z's in heterotic-string derived models. arXiv:1601.03604
189. T.-F. Feng, X.-Q. Li, H.-B. Zhang, S.-M. Zhao, The LHC 750 GeV diphoton excess in supersymmetry with gauged baryon and lepton numbers. arXiv:1512.06696
190. S. Fichet, G. von Gersdorff, C. Royon, Scattering light by light at 750 GeV at the LHC. arXiv:1512.05751
191. S. Fichet, G. von Gersdorff, C. Royon, Measuring the diphoton coupling of a 750 GeV resonance. arXiv:1601.01712
192. R. Franceschini, G.F. Giudice, J.F. Kamenik, M. McCullough, A. Pomarol, R. Rattazzi, M. Redi, F. Riva, A. Strumia, R. Torre, What is the gamma gamma resonance at 750 GeV? arXiv:1512.04933
193. R. Franceschini, G.F. Giudice, J.F. Kamenik, M. McCullough, F. Riva, A. Strumia, R. Torre, Digamma, what next? arXiv:1604.06446
194. M.T. Frandsen, I.M. Shoemaker, Asymmetric dark matter models and the LHC diphoton excess. JCAP **1605**(05), 064 (2016). arXiv:1603.09354
195. D.B. Franzosi, M.T. Frandsen, Symmetries and composite dynamics for the 750 GeV diphoton excess. arXiv:1601.05357
196. C.D. Froggatt, H.B. Nielsen, Production and decay of 750 Gev state of 6 top and 6 anti top quarks. arXiv:1605.03909
197. C. Frugiuele, E. Fuchs, G. Perez, M. Schlaffer, Atomic probes of new physics. arXiv:1602.04822
198. H. Fukuda, M. Ibe, O. Jinnouchi, M. Nojiri, Cracking down on fake photons—a case of 750 GeV diphoton resonance. arXiv:1607.01936
199. E. Gabrielli, K. Kannike, B. Mele, M. Raidal, C. Spethmann, H. Veermäe, A SUSY inspired simplified model for the 750 GeV diphoton excess. arXiv:1512.05961
200. J. Gao, H. Zhang, H.X. Zhu, Diphoton excess at 750 GeV: gluon–gluon fusion or quark-antiquark annihilation? arXiv:1512.08478
201. C. Garcia-Cely, J. Heeck, Polynomial spectral features from dark matter and connection to the diphoton resonance. arXiv:1605.08049
202. S.-F. Ge, H.-J. He, J. Ren, Z.-Z. Xianyu, Realizing dark matter and Higgs inflation in light of LHC diphoton excess. arXiv:1602.01801
203. C.-Q. Geng, D. Huang, Note on Spin-2 particle interpretation of the 750 GeV diphoton excess. arXiv:1601.07385
204. H. Georgi, Y. Nakai, Diboson excess from a new strong force. arXiv:1606.05865
205. D.M. Ghilencea, H.M. Lee, Diphoton resonance at 750 GeV in supersymmetry. arXiv:1606.04131
206. T. Gherghetta, N. Nagata, M. Shifman, A visible QCD axion from an enlarged color group. Phys. Rev. D **93**(11), 115010 (2016). arXiv:1604.01127
207. K. Ghorbani, H. Ghorbani, The 750 GeV diphoton excess from a pseudoscalar in fermionic dark matter scenario. arXiv:1601.00602
208. K. Ghosh, S. Jana, S. Nandi, Neutrino mass generation and 750 GeV diphoton excess via photon–photon fusion at the large hadron collider. arXiv:1607.01910
209. A. Ghoshal, On electroweak phase transition and di-photon excess with a 750 GeV scalar resonance. arXiv:1601.04291
210. S.B. Giddings, H. Zhang, Kaluza–Klein graviton phenomenology for warped compactifications, and the 750 GeV diphoton excess. arXiv:1602.02793
211. S.I. Godunov, A.N. Rozanov, M.I. Vysotsky, E.V. Zhemchugov, New physics at 1 TeV? arXiv:1602.02380
212. F. Goertz, J.F. Kamenik, A. Katz, M. Nardecchia, Indirect constraints on the scalar di-photon resonance at the LHC. arXiv:1512.08500
213. S. Gopalakrishna, T.S. Mukherjee, The 750 GeV diphoton excess in a two Higgs doublet model and a singlet scalar model, with vector-like fermions, unitarity constraints, and dark matter implications. arXiv:1604.05774
214. B. Gripaios, M. Nardecchia, T. You, An anomalous composite Higgs and the 750 GeV di-gamma resonance. arXiv:1605.09647
215. B. Gripaios, D. Sutherland, An operator basis for the standard model with an added scalar singlet. arXiv:1604.07365
216. C. Gross, O. Lebedev, J.M. No, Drell–Yan constraints on new electroweak states and the di-photon anomaly. arXiv:1602.03877
217. J. Gu, Z. Liu, Running after diphoton. arXiv:1512.07624
218. Y.-C. Guo, C.-X. Yue, Z.-H. Zhao, 750 GeV diphoton excess confronted with a top-pion in the TTM model. Int. J. Mod. Phys. A **31**(16), 1650086 (2016). arXiv:1605.08183

219. R.S. Gupta, S. Jaeger, Y. Kats, G. Perez, E. Stamou, Interpreting a 750 GeV diphoton resonance. arXiv:1512.05332
220. L.J. Hall, K. Harigaya, Y. Nomura, 750 GeV diphotons: implications for supersymmetric unification. arXiv:1512.07904
221. L.J. Hall, K. Harigaya, Y. Nomura, 750 GeV diphotons: implications for supersymmetric unification II. arXiv:1605.03585
222. Y. Hamada, T. Noumi, S. Sun, G. Shiu, An O(750) GeV resonance and inflation. arXiv:1512.08984
223. Y. Hamada, H. Kawai, K. Kawana, K. Tsumura, Models of LHC diphoton excesses valid up to the Planck scale. arXiv:1602.04170
224. K. Hamaguchi, S.P. Liew, Models of 750 GeV quarkonium and the LHC excesses. arXiv:1604.07828
225. C. Han, H.M. Lee, M. Park, V. Sanz, The diphoton resonance as a gravity mediator of dark matter. arXiv:1512.06376
226. H. Han, S. Wang, S. Zheng, Scalar explanation of diphoton excess at LHC. arXiv:1512.06562
227. X.-F. Han, L. Wang, Implication of the 750 GeV diphoton resonance on two-Higgs-doublet model and its extensions with Higgs field. arXiv:1512.06587
228. H. Han, S. Wang, S. Zheng, Dark matter theories in the light of diphoton excess. arXiv:1512.07992
229. X.-F. Han, L. Wang, L. Wu, J.M. Yang, M. Zhang, Explaining 750 GeV diphoton excess from top/bottom partner cascade decay in two-Higgs-doublet model extension. arXiv:1601.00534
230. X.-F. Han, L. Wang, J.M. Yang, An extension of two-Higgs-doublet model and the excesses of 750 GeV diphoton, muon g-2 and $h \to \mu\tau$. arXiv:1601.04954
231. C. Han, T.T. Yanagida, N. Yokozaki, Implications of the 750 GeV diphoton excess in gaugino mediation. arXiv:1602.04204
232. C. Han, K. Ichikawa, S. Matsumoto, M.M. Nojiri, M. Takeuchi, Heavy fermion bound states for diphoton excess at 750 GeV—collider and cosmological constraints. JHEP **04**, 159 (2016). arXiv:1602.08100
233. K. Harigaya, Y. Nomura, Composite models for the 750 GeV diphoton excess. arXiv:1512.04850
234. K. Harigaya, Y. Nomura, Hidden pion varieties in composite models for diphoton resonances. arXiv:1603.05774
235. K. Harigaya, Y. Nomura, A composite model for the 750 GeV diphoton excess. arXiv:1602.01092
236. L.A. Harland-Lang, V.A. Khoze, M.G. Ryskin, The photon PDF in events with rapidity gaps. arXiv:1601.03772
237. L.A. Harland-Lang, V.A. Khoze, M.G. Ryskin, The production of a diphoton resonance via photon–photon fusion. arXiv:1601.07187
238. C. Hati, Explaining the diphoton excess in alternative left-right symmetric model. arXiv:1601.02457
239. M. He, X.-G. He, Y. Tang, A $\gamma\gamma$ collider for the 750 GeV resonant state. Phys. Lett. B **759**, 166–170 (2016). arXiv:1603.00287
240. J.J. Heckman, 750 GeV diphotons from a D3-brane. arXiv:1512.06773
241. A. Hektor, L. Marzola, Di-photon excess at LHC and the gamma ray excess at the Galactic Centre. arXiv:1602.00004
242. A.E. Cárcamo Hernández, The 750 GeV diphoton resonance can cause the SM fermion mass and mixing pattern. arXiv:1512.09092
243. A.E. Cárcamo Hernández, I. Nisandzic, LHC diphoton 750 GeV resonance as an indication of $SU(3)_c \times SU(3)_L \times U(1)_X$ gauge symmetry. arXiv:1512.07165
244. A.E. Cárcamo Hernández, I. de Medeiros Varzielas, E. Schumacher, The 750 GeV diphoton resonance in the light of a 2HDM with S_3 flavour symmetry. arXiv:1601.00661
245. J.L. Hewett, T.G. Rizzo, 750 GeV diphoton resonance in warped geometries. arXiv:1603.08250
246. T. Higaki, K.S. Jeong, N. Kitajima, F. Takahashi, The QCD axion from aligned axions and diphoton excess. arXiv:1512.05295
247. B. Holdom, M. Ratzlaff, Heavy Higgs decay to $t\bar{t}Z$ and constraints on a 750 GeV pseudoscalar. arXiv:1605.08411
248. K. Howe, S. Knapen, D.J. Robinson, Diphotons from an electroweak triplet-singlet. arXiv:1603.08932
249. F.P. Huang, C.S. Li, Z.L. Liu, Y. Wang, 750 GeV diphoton excess from cascade decay. arXiv:1512.06732
250. W.-C. Huang, Y.-L.S. Tsai, T.-C. Yuan, Gauged two Higgs doublet model confronts the LHC 750 GeV di-photon anomaly. arXiv:1512.07268
251. X.-J. Huang, W.-H. Zhang, Y.-F. Zhou, A 750 GeV dark matter messenger at the Galactic Center. arXiv:1512.08992
252. X.-J. Huang, W.-H. Zhang, Y.-F. Zhou, Connecting the LHC diphoton excess to the Galatic center gamma-ray excess. arXiv:1605.09018
253. D.T. Huong, P.V. Dong, Left-right asymmetry and 750 GeV diphoton excess. Phys. Rev. D **93**(9), 095019 (2016). arXiv:1603.05146
254. L.E. Ibanez, V. Martin-Lozano, A megaxion at 750 GeV as a first hint of low scale string theory. arXiv:1512.08777
255. H. Ito, T. Moroi, Y. Takaesu, Studying 750 GeV di-photon resonance at photon–photon collider. arXiv:1601.01144
256. S. Iwamoto, G. Lee, Y. Shadmi, R. Ziegler, Diphoton signals from colorless hidden quarkonia. arXiv:1604.07776
257. S. Jain, F. Margaroli, S. Moretti, L. Panizzi, The 750 GeV threshold to a new particle world. arXiv:1605.08741
258. Y. Jiang, Y.-Y. Li, T. Liu, 750 GeV resonance in the gauged $U(1)'$-extended MSSM. arXiv:1512.09127
259. Y. Jiang, L. Li, R. Zheng, Boosted scalar confronting 750 GeV di-photon excess. arXiv:1605.01898
260. S. Jung, J. Song, Y.W. Yoon, How resonance-continuum interference changes 750 GeV diphoton excess: signal enhancement and peak shift. arXiv:1601.00006
261. J.F. Kamenik, M. Redi, Back to 1974: the $\mathcal{Q}$-onium. arXiv:1603.07719
262. J.F. Kamenik, B.R. Safdi, Y. Soreq, J. Zupan, Comments on the diphoton excess: critical reappraisal of effective field theory interpretations. arXiv:1603.06566
263. A.Y. Kamenshchik, A.A. Starobinsky, A. Tronconi, G.P. Vacca, G. Venturi, Vacuum energy, standard model physics and the 750 GeV diphoton excess at the LHC. arXiv:1604.02371
264. S. Kanemura, K. Nishiwaki, H. Okada, Y. Orikasa, S.C. Park, R. Watanabe, LHC 750 GeV diphoton excess in a radiative seesaw model. arXiv:1512.09048
265. S. Kanemura, N. Machida, S. Odori, T. Shindou, Diphoton excess at 750 GeV in an extended scalar sector. arXiv:1512.09053
266. K. Kaneta, S. Kang, H.-S. Lee, Diphoton excess at the LHC Run 2 and its implications for a new heavy gauge boson. arXiv:1512.09129
267. S.K. Kang, J. Song, Top-phobic heavy Higgs boson as the 750 GeV diphoton resonance. arXiv:1512.08963
268. K. Kannike, G.M. Pelaggi, A. Salvio, A. Strumia, The diphoton as the Higgs of the Higgs. arXiv:1605.08681
269. A. Karozas, S.F. King, G.K. Leontaris, A.K. Meadowcroft, Diphoton excess from E_6 in F-theory GUTs. arXiv:1601.00640
270. B.J. Kavanagh, Re-examining the significance of the 750 GeV diphoton excess at ATLAS. arXiv:1601.07330
271. J. Kawamura, Y. Omura, Diphoton excess at 750 GeV and LHC constraints in models with vector-like particles. arXiv:1601.07396
272. J.S. Kim, K. Rolbiecki, R.R. de Austri, Model-independent combination of diphoton constraints at 750 GeV. arXiv:1512.06797
273. J.S. Kim, J. Reuter, K. Rolbiecki, R.R. de Austri, A resonance without resonance: scrutinizing the diphoton excess at 750 GeV. arXiv:1512.06083
274. J.E. Kim, Is an axizilla possible for di-photon resonance? arXiv:1512.08467
275. S.F. King, R. Nevzorov, 750 GeV diphoton resonance from singlets in an exceptional supersymmetric standard model. arXiv:1601.07242

276. S. Knapen, T. Melia, M. Papucci, K. Zurek, Rays of light from the LHC. arXiv:1512.04928
277. P. Ko, Y. Omura, C. Yu, Diphoton excess at 750 GeV in leptophobic U(1)′ model inspired by E_6 GUT. arXiv:1601.00586
278. P. Ko, C. Yu, T.-C. Yuan, 750 GeV diphoton excess as a composite (pseudo)scalar boson from new strong interaction. arXiv:1603.08802
279. P. Ko, T. Nomura, H. Okada, Y. Orikasa, Confronting a new three-loop seesaw model with the 750 GeV diphoton excess. arXiv:1602.07214
280. P. Ko, T. Nomura, Dark sector shining through 750 GeV dark Higgs boson at the LHC. arXiv:1601.02490
281. A. Kobakhidze, F. Wang, L. Wu, J.M. Yang, M. Zhang, LHC 750 GeV diphoton resonance explained as a heavy scalar in top-seesaw model. arXiv:1512.05585
282. M.E. Krauss, T. Opferkuch, F. Staub, M.W. Winkler, Soft Gamma Rays from Heavy WIMPs. Phys. Dark Univ. **14**, 29–34 (2016). arXiv:1605.05327
283. K. Kulkarni, Extension of ν MSM model and possible explanations of recent astronomical and collider observations. arXiv:1512.06836
284. A. Kusenko, L. Pearce, L. Yang, Leptogenesis via the 750 GeV pseudoscalar. Phys. Rev. D **93**(11), 115005 (2016). arXiv:1604.02382
285. L.V. Laperashvili, H.B. Nielsen, C.R. Das, New results at LHC confirming the vacuum stability and multiple point principle. arXiv:1601.03231
286. G. Lazarides, Q. Shafi, Diphoton resonances in a $\mathrm{U}(1)_{B-L}$ extension of the minimal supersymmetric standard model. Phys. Rev. D **93**(11), 111702 (2016). arXiv:1602.07866
287. P. Lebiedowicz, M. Luszczak, R. Pasechnik, A. Szczurek, Can the diphoton enhancement at 750 GeV be due to a neutral technipion? arXiv:1604.02037
288. G.K. Leontaris, Q. Shafi, Diphoton resonance in F-theory inspired flipped SO(10). arXiv:1603.06962
289. G. Li, Y.-N. Mao, Y.-L. Tang, C. Zhang, Y. Zhou, S.-H. Zhu, A Pseudoscalar Decaying Only via Loops as an Explanation for the 750 GeV Diphoton Excess. Phys. Rev. Lett. **116**(15), 151803 (2016). arXiv:1512.08255
290. W. Li, J.N. Ng, Doubly charged vector leptons and the 750 GeV diphoton resonance. arXiv:1605.04885
291. T. Li, J.A. Maxin, V.E. Mayes, D.V. Nanopoulos, The 750 GeV diphoton excesses in a realistic D-brane model. arXiv:1602.09099
292. T. Li, J.A. Maxin, V.E. Mayes, D.V. Nanopoulos, A flippon related singlet at the LHC II. arXiv:1602.01377
293. W. Liao, H.-Q. Zheng, Scalar resonance at 750 GeV as composite of heavy vector-like fermions. Commun. Theor. Phys. **66**(2), 219–223 (2016). arXiv:1512.06741
294. J. Liu, X.-P. Wang, W. Xue, LHC diphoton excess from colorful resonances. arXiv:1512.07885
295. N. Liu, W. Wang, M. Zhang, R. Zheng, 750 GeV diphoton resonance in a vector-like extension of Hill model. arXiv:1604.00728
296. X. Liu, H. Zhang, RG-improved prediction for 750 GeV resonance production at the LHC. arXiv:1603.07190
297. M. Low, A. Tesi, L.-T. Wang, A pseudoscalar decaying to photon pairs in the early LHC run 2 data. arXiv:1512.05328
298. I. Low, J. Lykken, Implications of gauge invariance on a heavy diphoton resonance. arXiv:1512.09089
299. M.-X. Luo, K. Wang, T. Xu, L. Zhang, G. Zhu, Squarkonium, diquarkonium and octetonium at the LHC and their di-photon decays. Phys. Rev. D **93**(5), 055042 (2016). arXiv:1512.06670
300. E. Ma, N. Pollard, O. Popov, M. Zakeri, Gauge $B-L$ model of radiative neutrino mass with multipartite dark matter. arXiv:1605.00991
301. Y. Mambrini, G. Arcadi, A. Djouadi, The LHC diphoton resonance and dark matter. arXiv:1512.04913
302. S.F. Mantilla, R. Martinez, F. Ochoa, C.F. Sierra, Diphoton decay for a 750 GeV scalar boson in a $SU(6) \otimes U(1)_X$ model. arXiv:1602.05216
303. A.D. Martin, M.G. Ryskin, Advantages of exclusive $\gamma\gamma$ production to probe high mass systems. arXiv:1601.07774
304. R. Martinez, F. Ochoa, C.F. Sierra, Diphoton decay for a 750 GeV scalar boson in an $U(1)'$ model. arXiv:1512.05617
305. R. Martinez, F. Ochoa, C.F. Sierra, $\boldsymbol{SU(3)_C \otimes SU(3)_L \otimes U(1)_X}$ models in view of the 750 GeV diphoton signal. arXiv:1606.03415
306. A. Martini, K. Mawatari, D. Sengupta, Diphoton excess in phenomenological spin-2 resonance scenarios. arXiv:1601.05729
307. L. Marzola, A. Racioppi, M. Raidal, F.R. Urban, H. Veermäe, Non-minimal CW inflation, electroweak symmetry breaking and the 750 GeV anomaly. arXiv:1512.09136
308. S. Matsuzaki, K. Yamawaki, 750 GeV diphoton signal from one-family walking technipion. arXiv:1512.05564
309. S. Matsuzaki, K. Yamawaki, Walking from 750 GeV to 950 GeV in the technipion zoo. Phys. Rev. D **93**(11), 115027 (2016). arXiv:1605.04667
310. S.D. McDermott, P. Meade, H. Ramani, Singlet scalar resonances and the diphoton excess. arXiv:1512.05326
311. J. McDonald, The 750 GeV resonance as non-minimally coupled inflaton: unitarity violation and why the resonance is a real singlet scalar. arXiv:1604.01711
312. E. Megias, O. Pujolas, M. Quiros, On dilatons and the LHC diphoton excess. arXiv:1512.06106
313. T. Modak, S. Sadhukhan, R. Srivastava, 750 GeV diphoton excess from gauged $B-L$ symmetry. arXiv:1601.00836
314. J.W. Moffat, A composite model of quarks and bosons and the 750 GeV resonance. arXiv:1605.09404
315. E. Molinaro, F. Sannino, N. Vignaroli, Minimal composite dynamics versus axion origin of the diphoton excess. arXiv:1512.05334
316. E. Molinaro, F. Sannino, N. Vignaroli, Collider tests of (composite) diphoton resonances. arXiv:1602.07574
317. S. Moretti, K. Yagyu, The 750 GeV diphoton excess and its explanation in 2-Higgs doublet models with a real inert scalar multiplet. arXiv:1512.07462
318. E. Morgante, D. Racco, M. Rameez, A. Riotto, The 750 GeV diphoton excess, dark matter and constraints from the IceCube experiment. arXiv:1603.05592
319. C.W. Murphy, Vector leptoquarks and the 750 GeV diphoton resonance at the LHC. arXiv:1512.06976
320. Y. Nakai, R. Sato, K. Tobioka, Footprints of new strong dynamics via anomaly. arXiv:1512.04924
321. R. Nevzorov, A.W. Thomas, Diphoton signature of neutral pseudo-Goldstone boson in the E6CHM at the CERN LHC. arXiv:1605.07313
322. H.P. Nilles, M.W. Winkler, 750 GeV diphotons and supersymmetric grand unification. JHEP **05**, 182 (2016). arXiv:1604.03598
323. J.M. No, V. Sanz, J. Setford, See-saw composite Higgses at the LHC: linking Naturalness to the 750 GeV di-photon resonance. arXiv:1512.05700
324. J.M. No, Is it $SU(2)_{\mathrm{L}}$ or just $U(1)_{\mathrm{Y}}$? 750 GeV di-photon probes of the electroweak nature of new states. arXiv:1605.05900
325. T. Nomura, H. Okada, Four-loop neutrino model Inspired by diphoton excess at 750 GeV. arXiv:1601.00386
326. T. Nomura, H. Okada, Generalized Zee-Babu model with 750 GeV diphoton resonance. arXiv:1601.07339
327. T. Nomura, H. Okada, Four-loop radiative seesaw model with 750 GeV diphoton resonance. arXiv:1601.04516
328. H. Okada, K. Yagyu, Renormalizable model for neutrino mass, dark matter, muon $g-2$ and 750 GeV diphoton excess. arXiv:1601.05038
329. D. Palle, On the possible new 750 GeV heavy boson resonance at the LHC. arXiv:1601.00618

330. E. Palti, Vector-like exotics in F-theory and 750 GeV diphotons. arXiv:1601.00285
331. J.-C. Park, S. C. Park, Indirect signature of dark matter with the diphoton resonance at 750 GeV. arXiv:1512.08117
332. K.M. Patel, P. Sharma, Interpreting 750 GeV diphoton excess in SU(5) grand unified theory. arXiv:1512.07468
333. G.M. Pelaggi, A. Strumia, E. Vigiani, Trinification can explain the di-photon and di-boson LHC anomalies. arXiv:1512.07225
334. M. Perelstein, Y.-D. Tsai, 750 GeV di-photon excess and strongly first-order electroweak phase transition. arXiv:1603.04488
335. C. Petersson, R. Torre, The 750 GeV diphoton excess from the goldstino superpartner. arXiv:1512.05333
336. A. Pilaftsis, Diphoton signatures from heavy axion decays at LHC. arXiv:1512.04931
337. C.T. Potter, Pseudoscalar gluinonia to diphotons at the LHC. arXiv:1601.00240
338. M. Redi, A. Strumia, A. Tesi, E. Vigiani, Di-photon resonance and dark matter as heavy pions. JHEP **05**, 078 (2016). arXiv:1602.07297
339. J. Ren, J.-H. Yu, SU(2) x SU(2) x U(1) interpretation on the 750 GeV diphoton excess. arXiv:1602.07708
340. P. Roig, J.J. Sanz-Cillero, A broad 750 GeV diphoton resonance? Not alone. arXiv:1605.03831
341. I. Sahin, Semi-elastic cross section for a scalar resonance of mass 750 GeV. arXiv:1601.01676
342. A. Salvio, A. Mazumdar, Higgs stability and the 750 GeV diphoton excess. arXiv:1512.08184
343. A. Salvio, F. Staub, A. Strumia, A. Urbano, On the maximal diphoton width. arXiv:1602.01460
344. V. Sanz, Theoretical interpretation of a spin-two diphoton excess. arXiv:1603.05574
345. R. Sato, K. Tobioka, LHC future prospects of the 750 GeV resonance. arXiv:1605.05366
346. M. Son, A. Urbano, A new scalar resonance at 750 GeV: towards a proof of concept in favor of strongly interacting theories. arXiv:1512.08307
347. D. Stolarski, R. Vega-Morales, The virtual diphoton excess. arXiv:1601.02004
348. A. Strumia, Interpreting the 750 GeV digamma excess: a review (2016). arXiv:1605.09401
349. F. Takahashi, M. Yamada, N. Yokozaki, Diphoton excess from hidden U(1) gauge symmetry with large kinetic mixing. arXiv:1604.07145
350. Y.-L. Tang, S.-H. Zhu, NMSSM extended with vector-like particles and the diphoton excess on the LHC. arXiv:1512.08323
351. Y. Tsai, L.-T. Wang, Y. Zhao, Faking the diphoton excess by displaced dark photon decays. arXiv:1603.00024
352. F. Wang, L. Wu, J.M. Yang, M. Zhang, 750 GeV diphoton resonance, 125 GeV Higgs and muon g-2 anomaly in deflected anomaly mediation SUSY breaking scenario. arXiv:1512.06715
353. F. Wang, W. Wang, L. Wu, J.M. Yang, M. Zhang, Interpreting 750 GeV diphoton resonance in the NMSSM with vector-like particles. arXiv:1512.08434
354. M. Yamada, T.T. Yanagida, K. Yonekura, Diphoton excess as a hidden monopole. Phys. Lett. B **759**, 459–463 (2016). arXiv:1604.07203
355. J.-H. Yu, Hidden gauged U(1) model: unifying scotogenic neutrino and flavor dark matter. arXiv:1601.02609
356. J. Zhang, S. Zhou, Electroweak vacuum stability and diphoton excess at 750 GeV. arXiv:1512.07889
357. H. Zhang, The 750 GeV diphoton excess: who introduces it? arXiv:1601.01355
358. Y.-J. Zhang, B.-B. Zhou, J.-J. Sun, The fourth generation quark and the 750 GeV diphoton excess. arXiv:1602.05539
359. C. Zhang, M.-Y. Cui, L. Feng, Y.-Z. Fan, Z.-Z. Ren, γ-ray line signal in the 750 GeV-diphoton-excess-motivated gravity mediator dark matter model. arXiv:1606.00557
360. A. Angelescu, A. Djouadi, G. Moreau, Scenarii for interpretations of the LHC diphoton excess: two Higgs doublets and vector-like quarks and leptons. arXiv:1512.04921
361. F. Staub, SARAH. arXiv:0806.0538
362. F. Staub, From superpotential to model files for FeynArts and CalcHep/CompHep. Comput. Phys. Commun. **181**, 1077–1086 (2010). arXiv:0909.2863
363. F. Staub, Automatic calculation of supersymmetric renormalization group equations and self energies. Comput. Phys. Commun. **182**, 808–833 (2011). arXiv:1002.0840
364. F. Staub, SARAH 3.2: Dirac gauginos, UFO output, and more. Comput. Phys. Commun. **184**, 1792–1809 (2013). arXiv:1207.0906
365. F. Staub, SARAH 4: a tool for (not only SUSY) model builders. Comput. Phys. Commun. **185**, 1773–1790 (2014). arXiv:1309.7223
366. F. Staub, Exploring new models in all detail with SARAH. Adv. High Energy Phys. **2015**, 840780 (2015). arXiv:1503.04200
367. W. Porod, SPheno, a program for calculating supersymmetric spectra, SUSY particle decays and SUSY particle production at e+ e− colliders. Comput. Phys. Commun. **153**, 275–315 (2003). arXiv:hep-ph/0301101
368. W. Porod, F. Staub, SPheno 3.1: extensions including flavour, CP-phases and models beyond the MSSM. Comput. Phys. Commun. **183**, 2458–2469 (2012). arXiv:1104.1573
369. P. Athron, J.-H. Park, D. Stöckinger, A. Voigt, FlexibleSUSY—a spectrum generator generator for supersymmetric models. Comput. Phys. Commun. **190**, 139–172 (2015). arXiv:1406.2319
370. F. Staub, P. Athron, U. Ellwanger, R. Grober, M. Muhlleitner, P. Slavich, A. Voigt, Higgs mass predictions of public NMSSM spectrum generators. arXiv:1507.05093
371. G. Degrassi, P. Slavich, F. Zwirner, On the neutral Higgs boson masses in the MSSM for arbitrary stop mixing. Nucl. Phys. B **611**, 403–422 (2001). arXiv:hep-ph/0105096
372. A. Brignole, G. Degrassi, P. Slavich, F. Zwirner, On the O(alpha(t)**2) two loop corrections to the neutral Higgs boson masses in the MSSM. Nucl. Phys. B **631**, 195–218 (2002). arXiv:hep-ph/0112177
373. A. Dedes, P. Slavich, Two loop corrections to radiative electroweak symmetry breaking in the MSSM. Nucl. Phys. B **657**, 333–354 (2003). arXiv:hep-ph/0212132
374. A. Brignole, G. Degrassi, P. Slavich, F. Zwirner, On the two loop sbottom corrections to the neutral Higgs boson masses in the MSSM. Nucl. Phys. B **643**, 79–92 (2002). arXiv:hep-ph/0206101
375. A. Dedes, G. Degrassi, P. Slavich, On the two loop Yukawa corrections to the MSSM Higgs boson masses at large tan beta. Nucl. Phys. B **672**, 144–162 (2003). arXiv:hep-ph/0305127
376. G. Degrassi, P. Slavich, On the radiative corrections to the neutral Higgs boson masses in the NMSSM. Nucl. Phys. B **825**, 119–150 (2010). arXiv:0907.4682
377. M.D. Goodsell, K. Nickel, F. Staub, Two-loop Higgs mass calculations in supersymmetric models beyond the MSSM with SARAH and SPheno. Eur. Phys. J. C **75**(1), 32 (2015). arXiv:1411.0675
378. M. Goodsell, K. Nickel, F. Staub, Generic two-loop Higgs mass calculation from a diagrammatic approach. Eur. Phys. J. C **75**(6), 290 (2015). arXiv:1503.03098
379. A. Pukhov, CalcHEP 2.3: MSSM, structure functions, event generation, batchs, and generation of matrix elements for other packages. arXiv:hep-ph/0412191
380. E.E. Boos, M.N. Dubinin, V.A. Ilyin, A.E. Pukhov, V.I. Savrin, CompHEP: specialized package for automatic calculations of elementary particle decays and collisions (1994). arXiv:hep-ph/9503280

381. J. Alwall, M. Herquet, F. Maltoni, O. Mattelaer, T. Stelzer, MadGraph 5: going beyond. JHEP **06**, 128 (2011). arXiv:1106.0522
382. J. Alwall, R. Frederix, S. Frixione, V. Hirschi, F. Maltoni, O. Mattelaer, H.S. Shao, T. Stelzer, P. Torrielli, M. Zaro, The automated computation of tree-level and next-to-leading order differential cross sections, and their matching to parton shower simulations. JHEP **07**, 079 (2014). arXiv:1405.0301
383. G. Belanger, F. Boudjema, A. Pukhov, micrOMEGAs: a code for the calculation of dark matter properties in generic models of particle interaction, in *The Dark Secrets of the Terascale*, pp. 739–790 (2013). arXiv:1402.0787
384. P. Bechtle, O. Brein, S. Heinemeyer, G. Weiglein, K.E. Williams, HiggsBounds: confronting arbitrary Higgs sectors with exclusion bounds from LEP and the Tevatron. Comput. Phys. Commun. **181**, 138–167 (2010). arXiv:0811.4169
385. P. Bechtle, O. Brein, S. Heinemeyer, G. Weiglein, K.E. Williams, HiggsBounds 2.0.0: confronting neutral and charged Higgs sector predictions with exclusion bounds from LEP and the Tevatron. Comput. Phys. Commun. **182**, 2605–2631 (2011). arXiv:1102.1898
386. P. Bechtle, S. Heinemeyer, O. Stål, T. Stefaniak, G. Weiglein, HiggsSignals: confronting arbitrary Higgs sectors with measurements at the Tevatron and the LHC. Eur. Phys. J. C **74**(2), 2711 (2014). arXiv:1305.1933
387. J.E. Camargo-Molina, B. O'Leary, W. Porod, F. Staub, **Vevacious**: a tool for finding the global minima of one-loop effective potentials with many scalars. Eur. Phys. J. C **73**(10), 2588 (2013). arXiv:1307.1477
388. M. Bahr et al., Herwig++ physics and manual. Eur. Phys. J. C **58**, 639–707 (2008). arXiv:0803.0883
389. J. Bellm et al., Herwig 7.0/Herwig++ 3.0 release note. arXiv:1512.01178
390. T. Sjostrand, S. Mrenna, P.Z. Skands, PYTHIA 6.4 physics and manual. JHEP **05**, 026 (2006). arXiv:hep-ph/0603175
391. T. Sjöstrand, S. Ask, J.R. Christiansen, R. Corke, N. Desai, P. Ilten, S. Mrenna, S. Prestel, C.O. Rasmussen, P.Z. Skands, An introduction to PYTHIA 8.2. Comput. Phys. Commun. **191**, 159–177 (2015). arXiv:1410.3012
392. T. Gleisberg, S. Hoeche, F. Krauss, M. Schonherr, S. Schumann, F. Siegert, J. Winter, Event generation with SHERPA 1.1. JHEP **02**, 007 (2009). arXiv:0811.4622
393. S. Höche, F. Krauss, M. Schönherr, F. Siegert, W+ n-jet predictions at the large hadron collider at next-to-leading order matched with a parton shower. Phys. Rev. Lett. **110**(5), 052001 (2013). arXiv:1201.5882
394. B.C. Allanach, SOFTSUSY: a program for calculating supersymmetric spectra. Comput. Phys. Commun. **143**, 305–331 (2002). arXiv:hep-ph/0104145
395. B.C. Allanach, P. Athron, L.C. Tunstall, A. Voigt, A.G. Williams, Next-to-minimal SOFTSUSY. Comput. Phys. Commun. **185**, 2322–2339 (2014). arXiv:1311.7659
396. B.C. Allanach, M.A. Bernhardt, Including R-parity violation in the numerical computation of the spectrum of the minimal supersymmetric standard model: SOFTSUSY. Comput. Phys. Commun. **181**, 232–245 (2010). arXiv:0903.1805
397. B.C. Allanach, C.H. Kom, M. Hanussek, Computation of neutrino masses in R-parity violating supersymmetry: SOFTSUSY3.2. Comput. Phys. Commun. **183**, 785–793 (2012). arXiv:1109.3735
398. B.C. Allanach, A. Bednyakov, R.R. de Austri, Higher order corrections and unification in the minimal supersymmetric standard model: SOFTSUSY3.5. Comput. Phys. Commun. **189**, 192–206 (2015). arXiv:1407.6130
399. B.C. Allanach, A. Bednyakov, R. Ruiz de Austri, The inclusion of two-loop SUSYQCD corrections to gluino and squark pole masses in the minimal and next-to-minimal supersymmetric standard model: SOFTSUSY3.7. arXiv:1601.06657
400. A. Djouadi, J.-L. Kneur, G. Moultaka, SuSpect: a Fortran code for the supersymmetric and Higgs particle spectrum in the MSSM. Comput. Phys. Commun. **176**, 426–455 (2007). arXiv:hep-ph/0211331
401. S. Heinemeyer, W. Hollik, G. Weiglein, FeynHiggs: a program for the calculation of the masses of the neutral CP even Higgs bosons in the MSSM. Comput. Phys. Commun. **124**, 76–89 (2000). arXiv:hep-ph/9812320
402. P. Drechsel, L. Galeta, S. Heinemeyer, G. Weiglein, Precise predictions for the Higgs-boson masses in the NMSSM. arXiv:1601.08100
403. U. Ellwanger, C. Hugonie, NMSPEC: a Fortran code for the sparticle and Higgs masses in the NMSSM with GUT scale boundary conditions. Comput. Phys. Commun. **177**, 399–407 (2007). arXiv:hep-ph/0612134
404. J. Baglio, R. Gröber, M. Mühlleitner, D.T. Nhung, H. Rzehak, M. Spira, J. Streicher, K. Walz, NMSSMCALC: a program package for the calculation of loop-corrected Higgs boson masses and decay Widths in the (complex) NMSSM. Comput. Phys. Commun. **185**(12), 3372–3391 (2014). arXiv:1312.4788
405. J.P. Vega, G. Villadoro, SusyHD: Higgs mass determination in supersymmetry. JHEP **07**, 159 (2015). arXiv:1504.05200
406. A. Djouadi, J. Kalinowski, M. Spira, HDECAY: a program for Higgs boson decays in the standard model and its supersymmetric extension. Comput. Phys. Commun. **108**, 56–74 (1998). arXiv:hep-ph/9704448
407. W. Frisch, H. Eberl, H. Hlucha, HFOLD—a program package for calculating two-body MSSM Higgs decays at full one-loop level. Comput. Phys. Commun. **182**, 2219–2226 (2011). arXiv:1012.5025
408. U. Ellwanger, J.F. Gunion, C. Hugonie, NMHDECAY: a Fortran code for the Higgs masses, couplings and decay widths in the NMSSM. JHEP **02**, 066 (2005). arXiv:hep-ph/0406215
409. U. Ellwanger, C. Hugonie, NMHDECAY 2.0: an updated program for sparticle masses, Higgs masses, couplings and decay widths in the NMSSM. Comput. Phys. Commun. **175**, 290–303 (2006). arXiv:hep-ph/0508022
410. M. Muhlleitner, A. Djouadi, Y. Mambrini, SDECAY: a Fortran code for the decays of the supersymmetric particles in the MSSM. Comput. Phys. Commun. **168**, 46–70 (2005). arXiv:hep-ph/0311167
411. H. Hlucha, H. Eberl, W. Frisch, SFOLD—a program package for calculating two-body sfermion decays at full one-loop level in the MSSM. Comput. Phys. Commun. **183**, 2307–2312 (2012). arXiv:1104.2151
412. D. Das, U. Ellwanger, A.M. Teixeira, NMSDECAY: a Fortran code for supersymmetric particle decays in the next-to-minimal supersymmetric standard model. Comput. Phys. Commun. **183**, 774–779 (2012). arXiv:1106.5633
413. G. Degrassi, P. Gambino, P. Slavich, SusyBSG: a Fortran code for BR[B –> X(s) gamma] in the MSSM with minimal flavor violation. Comput. Phys. Commun. **179**, 759–771 (2008). arXiv:0712.3265
414. F. Mahmoudi, SuperIso v2.3: a program for calculating flavor physics observables in supersymmetry. Comput. Phys. Commun. **180**, 1579–1613 (2009). arXiv:0808.3144
415. J. Rosiek, P. Chankowski, A. Dedes, S. Jager, P. Tanedo, SUSY_FLAVOR: a computational tool for FCNC and CP-violating processes in the MSSM. Comput. Phys. Commun. **181**, 2180–2205 (2010). arXiv:1003.4260
416. A. Crivellin, J. Rosiek, P.H. Chankowski, A. Dedes, S. Jaeger, P. Tanedo, SUSY_FLAVOR v2: a computational tool for FCNC and CP-violating processes in the MSSM. Comput. Phys. Commun. **184**, 1004–1032 (2013). arXiv:1203.5023
417. J.S. Lee, M. Carena, J. Ellis, A. Pilaftsis, C.E.M. Wagner, CPsuperH2.3: an updated tool for phenomenology in the MSSM with

explicit CP violation. Comput. Phys. Commun. **184**, 1220–1233 (2013). arXiv:1208.2212
418. P. Athron, M. Bach, H.G. Fargnoli, C. Gnendiger, R. Greifenhagen, J.-H. Park, S. Paßehr, D. Stöckinger, H. Stöckinger-Kim, A. Voigt, GM2Calc: precise MSSM prediction for $(g-2)$ of the muon. arXiv:1510.08071
419. M. Spira, A. Djouadi, D. Graudenz, P.M. Zerwas, Higgs boson production at the LHC. Nucl. Phys. B **453**, 17–82 (1995). arXiv:hep-ph/9504378
420. C. Hartmann, M. Trott, On one-loop corrections in the standard model effective field theory; the $\Gamma(h \to \gamma\,\gamma)$ case. JHEP **07**, 151 (2015). arXiv:1505.02646
421. F. Goertz, A. Katz, M. Son, A. Urbano, Precision Drell–Yan measurements at the LHC and implications for the diphoton excess. arXiv:1602.04801
422. LHC Higgs Cross Section Working Group Collaboration, S. Dittmaier et al., Handbook of LHC Higgs cross sections: 1. Inclusive observables. arXiv:1101.0593
423. ATLAS Collaboration, G. Aad et al., Search for new phenomena in the dijet mass distribution using $p-p$ collision data at $\sqrt{s}=8$ TeV with the ATLAS detector. Phys. Rev. D **91**(5), 052007 (2015). arXiv:1407.1376
424. H. Georgi, M. Machacek, Doubly charged Higgs bosons. Nucl. Phys. B **262**, 463 (1985)
425. P. Kant, R.V. Harlander, L. Mihaila, M. Steinhauser, Light MSSM Higgs boson mass to three-loop accuracy. JHEP **08**, 104 (2010). arXiv:1005.5709
426. K. Nickel, F. Staub, Precise determination of the Higgs mass in supersymmetric models with vectorlike tops and the impact on naturalness in minimal GMSB. JHEP **07**, 139 (2015). arXiv:1505.06077
427. M.E. Machacek, M.T. Vaughn, Two loop renormalization group equations in a general quantum field theory. 1. Wave function renormalization. Nucl. Phys. B **222**, 83 (1983)
428. M.E. Machacek, M.T. Vaughn, Two loop renormalization group equations in a general quantum field theory. 2. Yukawa couplings. Nucl. Phys. B **236**, 221 (1984)
429. M.E. Machacek, M.T. Vaughn, Two loop renormalization group equations in a general quantum field theory. 3. Scalar quartic couplings. Nucl. Phys. B **249**, 70 (1985)
430. M. Luo, H. Wang, Y. Xiao, Two loop renormalization group equations in general gauge field theories. Phys. Rev. D **67**, 065019 (2003). arXiv:hep-ph/0211440
431. S.P. Martin, M.T. Vaughn, Two loop renormalization group equations for soft supersymmetry breaking couplings. Phys. Rev. D **50**, 2282 (1994). arXiv:hep-ph/9311340. [Erratum: Phys. Rev.D78,039903(2008)]
432. R.M. Fonseca, M. Malinsky, W. Porod, F. Staub, Running soft parameters in SUSY models with multiple U(1) gauge factors. Nucl. Phys. B **854**, 28–53 (2012). arXiv:1107.2670
433. M.D. Goodsell, Two-loop RGEs with Dirac gaugino masses. JHEP **01**, 066 (2013). arXiv:1206.6697
434. R.M. Fonseca, M. Malinský, F. Staub, Renormalization group equations and matching in a general quantum field theory with kinetic mixing. Phys. Lett. B **726**, 882–886 (2013). arXiv:1308.1674
435. M. Sperling, D. Stöckinger, A. Voigt, Renormalization of vacuum expectation values in spontaneously broken gauge theories. JHEP **07**, 132 (2013). arXiv:1305.1548
436. M. Sperling, D. Stöckinger, A. Voigt, Renormalization of vacuum expectation values in spontaneously broken gauge theories: two-loop results. JHEP **01**, 068 (2014). arXiv:1310.7629
437. A. Djouadi, The anatomy of electro-weak symmetry breaking. I: the Higgs boson in the standard model. Phys. Rep. **457**, 1–216 (2008). arXiv:hep-ph/0503172
438. M. Kramer, E. Laenen, M. Spira, Soft gluon radiation in Higgs boson production at the LHC. Nucl. Phys. B **511**, 523–549 (1998). arXiv:hep-ph/9611272
439. K.G. Chetyrkin, B.A. Kniehl, M. Steinhauser, Hadronic Higgs decay to order alpha-s**4. Phys. Rev. Lett. **79**, 353–356 (1997). arXiv:hep-ph/9705240
440. K.G. Chetyrkin, J.H. Kuhn, C. Sturm, QCD decoupling at four loops. Nucl. Phys. B **744**, 121–135 (2006). arXiv:hep-ph/0512060
441. Y. Schroder, M. Steinhauser, Four-loop decoupling relations for the strong coupling. JHEP **01**, 051 (2006). arXiv:hep-ph/0512058
442. P.A. Baikov, K.G. Chetyrkin, Top quark mediated Higgs boson decay into hadrons to order α_s^5. Phys. Rev. Lett. **97**, 061803 (2006). arXiv:hep-ph/0604194
443. S. Dawson, A. Djouadi, M. Spira, QCD corrections to SUSY Higgs production: the role of squark loops. Phys. Rev. Lett. **77**, 16–19 (1996). arXiv:hep-ph/9603423
444. LHC Higgs Cross Section Working Group Collaboration, J.R. Andersen et al., Handbook of LHC Higgs cross sections: 3. Higgs properties. arXiv:1307.1347
445. M. Spira, HIGLU: a program for the calculation of the total Higgs production cross-section at hadron colliders via gluon fusion including QCD corrections. arXiv:hep-ph/9510347
446. R.V. Harlander, S. Liebler, H. Mantler, SusHi: a program for the calculation of Higgs production in gluon fusion and bottom-quark annihilation in the standard model and the MSSM. Comput. Phys. Commun. **184**, 1605–1617 (2013). arXiv:1212.3249
447. ATLAS collaboration, Search for production of vector-like quark pairs and of four top quarks in the lepton plus jets final state in pp collisions at $\sqrt{s}=8$ TeV with the ATLAS detector. Tech. Rep. ATLAS-CONF-2015-012, CERN, Geneva, Mar, 2015
448. C. Anastasiou, C. Duhr, F. Dulat, E. Furlan, T. Gehrmann, F. Herzog, A. Lazopoulos, B. Mistlberger, CP-even scalar boson production via gluon fusion at the LHC. arXiv:1605.05761
449. H. An, T. Liu, L.-T. Wang, 125 GeV Higgs boson, enhanced diphoton rate, and gauged $U(1)_P Q$-extended MSSM. Phys. Rev. D **86**, 075030 (2012). arXiv:1207.2473
450. A.V. Manohar, M.B. Wise, Flavor changing neutral currents, an extended scalar sector, and the Higgs production rate at the CERN LHC. Phys. Rev. D **74**, 035009 (2006). arXiv:hep-ph/0606172
451. M. Singer, J.W.F. Valle, J. Schechter, Canonical neutral current predictions from the weak electromagnetic gauge group SU(3) X $u(1)$. Phys. Rev. D **22**, 738 (1980)
452. J.W.F. Valle, M. Singer, Lepton number violation with quasi Dirac neutrinos. Phys. Rev. D **28**, 540 (1983)
453. F. Pisano, V. Pleitez, An SU(3) x U(1) model for electroweak interactions. Phys. Rev. D **46**, 410–417 (1992). arXiv:hep-ph/9206242
454. P.H. Frampton, Chiral dilepton model and the flavor question. Phys. Rev. Lett. **69**, 2889–2891 (1992)
455. R. Foot, O.F. Hernandez, F. Pisano, V. Pleitez, Lepton masses in an SU(3)-L x U(1)-N gauge model. Phys. Rev. D **47**, 4158–4161 (1993). arXiv:hep-ph/9207264
456. J.C. Montero, F. Pisano, V. Pleitez, Neutral currents and GIM mechanism in SU(3)-L x U(1)-N models for electroweak interactions. Phys. Rev. D **47**, 2918–2929 (1993). arXiv:hep-ph/9212271
457. V. Pleitez, M.D. Tonasse, Heavy charged leptons in an SU(3)-L x U(1)-N model. Phys. Rev. D **48**, 2353–2355 (1993). arXiv:hep-ph/9301232
458. A.J. Buras, F. De Fazio, J. Girrbach, M.V. Carlucci, The anatomy of quark flavour observables in 331 models in the flavour precision era. JHEP **02**, 023 (2013). arXiv:1211.1237
459. P.V. Dong, N.T.K. Ngan, Phenomenology of the simple 3-3-1 model with inert scalars. arXiv:1512.09073
460. R.M. Fonseca, Calculating the renormalisation group equations of a SUSY model with Susyno. Comput. Phys. Commun. **183**, 2298–2306 (2012). arXiv:1106.5016

461. R.N. Mohapatra, J.W.F. Valle, Neutrino mass and baryon number nonconservation in superstring models. Phys. Rev. D **34**, 1642 (1986)
462. S.M. Boucenna, J.W.F. Valle, A. Vicente, Predicting charged lepton flavor violation from 3-3-1 gauge symmetry. Phys. Rev. D **92**(5), 053001 (2015). arXiv:1502.07546
463. E. Ma, Diphoton revelation of the utilitarian supersymmetric standard model. arXiv:1512.09159
464. S.F. King, S. Moretti, R. Nevzorov, Theory and phenomenology of an exceptional supersymmetric standard model. Phys. Rev. D **73**, 035009 (2006). arXiv:hep-ph/0510419
465. S.F. King, S. Moretti, R. Nevzorov, Exceptional supersymmetric standard model. Phys. Lett. B **634**, 278–284 (2006). arXiv:hep-ph/0511256
466. E. Ma, Compendium of models from a gauge U(1) framework. arXiv:1601.01400
467. R.M. Capdevilla, A. Delgado, A. Martin, Light stops in a minimal U(1)x extension of the MSSM. Phys. Rev. D **92**(11), 115020 (2015). arXiv:1509.02472
468. B. O'Leary, W. Porod, F. Staub, Mass spectrum of the minimal SUSY B-L model. JHEP **05**, 042 (2012). arXiv:1112.4600
469. F. Staub, T. Ohl, W. Porod, C. Speckner, A tool box for implementing supersymmetric models. Comput. Phys. Commun. **183**, 2165–2206 (2012). arXiv:1109.5147
470. M. Hirsch, M. Malinsky, W. Porod, L. Reichert, F. Staub, Hefty MSSM-like light Higgs in extended gauge models. JHEP **02**, 084 (2012). arXiv:1110.3037
471. M. Hirsch, W. Porod, L. Reichert, F. Staub, Phenomenology of the minimal supersymmetric $U(1)_{B-L} \times U(1)_R$ extension of the standard model. Phys. Rev. D **86**, 093018 (2012). arXiv:1206.3516
472. J.E. Camargo-Molina, B. O'Leary, W. Porod, F. Staub, The stability Of R-parity in supersymmetric models extended By $U(1)_{B-L}$. Phys. Rev. D **88**, 015033 (2013). arXiv:1212.4146
473. C.L. Wainwright, CosmoTransitions: computing cosmological phase transition temperatures and bubble profiles with multiple fields. Comput. Phys. Commun. **183**, 2006–2013 (2012). arXiv:1109.4189
474. S.P. Martin, Taming the Goldstone contributions to the effective potential. Phys. Rev. D **90**(1), 016013 (2014). arXiv:1406.2355
475. J. Elias-Miro, J.R. Espinosa, T. Konstandin, Taming infrared divergences in the effective potential. JHEP **08**, 034 (2014). arXiv:1406.2652
476. Planck Collaboration, P.A.R. Ade et al., Planck 2013 results. XVI. Cosmological parameters. Astron. Astrophys. **571**, A16 (2014). arXiv:1303.5076
477. L. Basso, B. O'Leary, W. Porod, F. Staub, Dark matter scenarios in the minimal SUSY B-L model. JHEP **09**, 054 (2012). arXiv:1207.0507
478. SINDRUM Collaboration, U. Bellgardt et al., Search for the decay mu+ —> e+ e+ e−. Nucl. Phys. B **299**, 1 (1988)
479. K. Hayasaka et al., Search for lepton flavor violating Tau decays into three leptons with 719 million produced Tau+Tau− pairs. Phys. Lett. B **687**, 139–143 (2010). arXiv:1001.3221
480. SINDRUM II Collaboration, C. Dohmen et al., Test of lepton flavor conservation in mu –> e conversion on titanium. Phys. Lett. B **317**, 631–636 (1993)
481. SINDRUM II Collaboration, W.H. Bertl et al., A search for muon to electron conversion in muonic gold. Eur. Phys. J. C **47**, 337–346 (2006)
482. ATLAS collaboration, Search for new phenomena in the dilepton final state using proton–proton collisions at $\sqrt{s} = 13$ TeV with the ATLAS detector
483. M.E. Krauss, B. O'Leary, W. Porod, F. Staub, Implications of gauge kinetic mixing on Z' and slepton production at the LHC. Phys. Rev. D **86**, 055017 (2012). arXiv:1206.3513
484. L. Basso, B. Fuks, M.E. Krauss, W. Porod, Doubly-charged Higgs and vacuum stability in left-right supersymmetry. JHEP **07**, 147 (2015). arXiv:1503.08211